Modulation of ATF7IP in Huntington's disease patient-derived iPSCs prevents neural gene expression changes induced by H3K9 trimethylation

Inaugural-Dissertation

zur

Erlangung des Doktorgrades

der Mathematisch-Naturwissenschaftlichen Fakultät

der Universität zu Köln

vorgelegt von

Dilber Irmak

aus Bielefeld, Deutschland

Köln 2018

Berichterstatter: Dr. David Vilchez

Prof. Dr. Aleksandra Trifunovic

Tag der mündlichen Prüfung: 11.06.2018

Isolation is the gift,

all the others are a test of your endurance,
of how much you really want to do it
and you'll do it.
despite rejection
and the worst odds
and it will be better
than anything else you can imagine.

If you're going to try,
go all the way.
there is no other feeling like that.
you will be alone with the gods
and the nights will flame with fire.

do it, do it, do it.
do it.
all the way
all the way.

- Charles Bukowski

Table of contents

List of figures

List of tables

Abstract

Huntington's disease (HD) is an autosomal dominant neurodegenerative disorder caused by mutations in the huntingtin gene (HTT). These mutations expand the CAG triplet repeat region resulting in an unstable polyglutamine stretch (polyQ) in the N-terminal domain of the protein. Epigenetic marks such as histone methylation are significantly altered in HD patients as well as HD cellular and organismal models. Specifically, H3K9 trimethylation (H3K9me3) is markedly increased in HD patients and HD mouse models, which correlates with transcriptional repression. In this study we make use of induced pluripotent stem cells (iPSCs) as they present a unique tool for disease modeling and hold a great promise for regenerative medicine. We use iPSCs from patients with HD (HD-iPSCs) and induce their differentiation into neuronal HD-IPSCs (HD-NPCs) to identify mechanisms that can correct HD disease-related changes. Therefore, in a first step we asked for the normal function of HTT. We show for the first time that HTT interacts with chromatin factor ATF7IP and its specific H3K9 methyltransferase SETDB1. In addition, we observed that loss of HTT increased the levels of ATF7IP and global H3K9me3 in hESCs. In pluripotent stem cells the levels of heterochromatin-associated histone modifications such as H3K9me3 are usually reduced which indicates that HTT regulates H3K9me3 levels in hESCs. Next, we show that knockdown of ATF7IP in HD-iPSCs and their neuronal differentiated counterparts results in a decrease of H3K9me3. As with HTT, upon knockdown of huntingtin interacting protein 2 (UBE2K) we observed increased H3K9me3 in hESCs, probably through the histone methyltransferase regulator JARID2, an interactor of UBE2K found firstly in this study. However, UBE2K KD came with a dramatic dysfunctional phenotype towards the neural differentiation abilities of the cells. Therefore, UBE2K and the normal function of HTT could be required within a bigger complex of epigenetic regulators to maintain the H3K9me3 landscape of hESCs and HD-iPSCs.

Zusammenfassung

Die Huntington-Krankheit (HD) ist eine autosomal dominante neurodegenerative Erkrankung, die durch Mutationen im Huntingtin-Gen (HTT) verursacht wird. Diese Mutationen erweitern den CAG-Triplett-Wiederholungsbereich, was zu einem instabilen Polyglutamin-Stretch (polyQ) in der N-terminalen Domäne des Proteins führt. Epigenetische Marker wie die Histonmethylierung sind bei HD-Patienten sowie bei zellulären und organismischen HD-Modellen signifikant verändert. Insbesondere die H3K9-Trimethylierung (H3K9me3) ist bei HD-Patienten und HD-Mausmodellen deutlich erhöht, was mit einer transkriptionellen Repression korreliert. In dieser Studie verwenden wir induzierte pluripotente Stammzellen (iPSCs), da sie ein einzigartiges Werkzeug zur Modellierung von Krankheiten darstellen und ein großes Potenzial für die regenerative Medizin bieten. Wir verwenden iPSCs von Patienten mit HD (HD-iPSCs) und induzieren deren Differenzierung in neuronale HD-IPSCs (HD-NPCs), um Mechanismen zu identifizieren, die krankheitsbedingte Veränderungen bei HD korrigieren können. Daher haben wir in einem ersten Schritt nach der normalen Funktion von HTT gefragt. Wir zeigen hier zum ersten Mal, dass HTT mit dem Chromatinfaktor ATF7IP und seiner spezifischen H3K9-Methyltransferase SETDB1 interagiert. Darüber hinaus beobachteten wir, dass der Verlust von HTT das Ausmaß von ATF7IP und globalem H3K9me3 in hESCs erhöhte. In pluripotenten Stammzellen sind die Werte von Heterochromatin-assoziierten Histon-Modifikationen wie H3K9me3 in der Regel reduziert, was darauf hindeutet, dass HTT den Gehalt an H3K9me3 in hESCs reguliert. Als nächstes zeigen wir, dass der Knockdown von ATF7IP bei HD-iPSCs und ihren neuronal differenzierten Gegenstücken zu einem Rückgang von H3K9me3 führt. Wie bei HTT beobachteten wir beim Knockdown des mit Huntingtin interagierenden Proteins 2 (UBE2K) einen Anstieg von H3K9me3 in hESCs, vermutlich mit Hilfe des Histon-Methyltransferase-Regulators JARID2, einem Interaktor von UBE2K, der erstmals in dieser Studie gefunden wurde. Der UBE2K KD hatte jedoch einen drastisch dysfunktionalen Phänotyp in Bezug auf die neuronalen Differenzierungsfähigkeiten der Zellen. Daher könnten UBE2K und die normale Funktion von HTT in einem größeren Komplex epigenetischer Regulatoren erforderlich sein, um den H3K9me3-Spiegel aus hESCs und HD-iPSCs zu erhalten.

1 Introduction

1.1 Huntington's disease

Huntington's disease (HD) is an autosomal dominant neurodegenerative disorder caused by mutations in the *huntingtin* gene (*HTT*). The characteristic symptoms of the HD which entail abnormal movements (chorea), cognitive decline (dementia) and psychosis, manifest usually from the age of 35 to 50[1,2]. The disease leads to death approximately 20 years after onset of first symptoms[3]. The mutations of the *HTT* gene expand a CAG triplet repeat region in exon 1 resulting in an unstable polyglutamine stretch (polyQ) in the N-terminal domain of the protein. In its wild-type form, HTT contains 6-35 glutamine residues. However, in individuals affected by HD, it contains greater than 35 polyQ repeats[4]. Although HTT is ubiquitously expressed[5,6], mHTT particularly leads to neuronal dysfunction and death in many brain regions with the striatum undergoing the greatest neurodegeneration[7]. Extensive data and the dominant inheritance pattern of HD indicate that gain-of-function of mHTT is toxic and triggers neurodegeneration[4,8,9], especially in the striatal medium-sized spiny neurons[10]. However, growing evidence suggests that loss of normal HTT function also contributes to HD[5,6]. For instance, loss of wild-type HTT induces HD-related changes such as progressive neurodegeneration and motor dysfunction or hastens these changes in human and mouse HD models[11–15]. Moreover, ectopic expression of wild-type HTT improves brain cell survival and ameliorates the deleterious effects of the mutant protein[12, 16–22] .

1.2 Huntingtin

The HTT gene is well conserved from flies to mammals and has no sequence homology with other proteins. It probably appeared millions of years ago, before the seperation of the protostoma (origin of insects) and deuterostoma (mammals) branches[5,6]. HTT is a completely soluble high-molecular-weight protein of 348 kDa (3,144 amino acids) and is ubiquitously expressed.

In HTT protein structure, the region of highest interest in HD-research is the expandable polyQ region. The polyQ tract starts at the eighteenth amino acid and contains up to 34 glutamine residues in healthy individuals. Moreover, there are also other proteins such as transcription factors which contain a polyQ region[23]. A study showed

that the polyQ tract forms a three-dimensional protein motif that forms interactions with polar residues (Polar Zipper) and thus might have its physiological function in the binding of these proteins[24]. A region found only in higher vertebrates is the polyproline stretch, which is assumed to aid in the solubility of the HTT[25]. The protein also contains several HEAT domains of ~40 amino acids which enable protein-protein interactions[26,27]. In HTT around 37 HEAT repeats were discovered[28], of which three key clusters were identified[27].

Further downstream, a carboxy (C)-terminal nuclear export signal (NES) sequence and a nuclear localization signal (NLS) are localized. The NLS was found to be less active than the NES. This indicates that this location of the protein is responsible for molecular transportation from the nucleus to the cytoplasm[29]. In addition, the widespread distribution of HTT within the cell nucleus and other cell compartments supports this idea. In more detail studies showed, that HTT functions as a nuclear export protein through its interaction with the nuclear pore protein TPR (translocated promoter region). In support of this role was the observation that HTT accumulates in the nucleus, when the amino acids of the interacting region were deleted[30].

The three protease cleavage sites split the protein into normal and mutant HTT (mHTT) fragments[31–33], which are found in the nucleus and cytoplasm[34–38]. Caspase and calpain family members have a proteolytic role for mHTT[36,38–40]. HTT has several consensus caspase[38] and calpain cleavage sites[40], also known as cysteine proteases. Calpains, however are Ca^{2+}-dependant intracellular cysteine proteases[41]. It should be noted that excessive glutamatergic signaling and impaired excessive Ca^{2+} influx in the brain striatum, lead to mitochondrial dysfunction and cell death[42]. This pathway is an activator of cysteine proteases like caspases and calpains[41]. Caspase cleavage is activated by proteolytic processes such as apoptosis[41] and is a common process, as this event was observed in control human brains as well as in HD-brains in the early stage of disease, or in WT and HD transgenic mouse brains before neurodegeneration commenced[38]. It is known that HTT is a substrate of calpain to induce cleavage. The activation of calpain cleavage is initiated by programmed cell death in the cell[43] and also targets other polyQ containing proteins causing neurodegenerative diseases[32].

HTT fragments resulting from caspase-and calpain proteolysis tend to accumulate in the nucleus. This is because mHTT cleavage only releases the polyQ containing N-terminal fragments, which are prone for aggregation and are toxic in the cell[32,39].

Interestingly, reducing the activity of calpain and caspase cleavage sites decreased the cleavage of the mHTT and thus delayed the onset of the disease[33,39,44].

The post-translational modifications of HTT include sumoylation, ubiquitination, phosphorylation and palmitoylation. The amino (N)-terminal lysines K6, K9 and K15 get either ubiquitinated[45] or sumoylated[25]. Further, the serines 421 and 434 get phosphorylated, which influences the cleavage and toxicity of mHTT. Studies showed that phosphorylation of these serines is reduced in the HD[46–49]. The palmytoylation of huntintin is done by the HTT-interacting protein 14 (HIP14) which is a palmitoyl transferase[50]. Proteins which are palmitoylated are known to regulate components which control vesicle trafficking and thus support the role of HTT in vesicle trafficking[50,51].

HTT is capable of binding to its numerous interactors in both its wild-type and mutant form[52,53]. This feature indicates that it has a flexible structure which adapts its conformation and function depending on the current subcellular location, state of maturation or cell type[54,52,28,55,56]. For example, the expanded polyQ region is capable of changing the three-dimensional structure of the HTT, making it accessible to different interacting proteins[24,52]. The protein epitopes presented by HTT are supposedly differentially accessible by the same antibodies, depending on the intracellular compartment the HTT is found in[57,58].

In humans and rodents HTT is found mainly in the cytoplasm[51], with the highest levels in the CNS neurons and the testes[59–61]. Within the cell it is found in several organelles including the nucleus, endoplasmic reticulum and golgi complex[51,62–65] . HTT has many binding partners and the most important ones are involved in transcriptional regulation, intracellular trafficking and cytoskeletal organization. Interestingly many of the known interactors of HTT have functions in endocytosis and only a few in exocytosis[66]. HTT has been associated with synaptic vesicles[51,62], microtubule-based axonal transport, endosomal structures and clathrin-coated vesicles[63]. Taken together, an important function of normal HTT seems to lie in membrane trafficking. HTT also facilitates tri-methylation of H3K27 by the chromatin regulator polycomb repressive complex 2 (PRC2) in mouse embryonic stem cells (mESCs), a mechanism further induced by a gain of function of the mHTT[67].

1.3 The role of HTT in development and cell differentiation.

Remarkably, conditional knockout of *Htt* in mice at embryonic day 14.5 causes progressive neurodegeneration that mimics HD phenotypes[11]. At earlier stages, complete depletion of HTT results in severe neural developmental defects and embryonic lethality[68–70], providing a link between normal function of HTT and development. Mice with reduced levels of HTT to below 50% bypass the lethality phenotype but display aberrant brain development, suggesting a role of HTT in neurogenesis[71]. Loss of HTT during embryonic neurogenesis decreases the pool of cortical progenitors by accelerating their differentiation, a process that results in altered cell fate decisions[72]. *In vitro*, neural progenitor cells (NPCs) derived from *Htt*$^{-/-}$ mouse ESCs (mESCs) can be terminally differentiated into neurons. However, a study demonstrated that their neuronal differentiation efficiency is altered as they tend to give rise to more astrocytes compared with wild-type NPCs[73]. Another study finds even earlier phenotypes such as decreased self-renewal, increased cell death and alterations in the lineage potential of NPCs derived from *Htt*$^{-/-}$ mESCs[74]. Although patients with HD and disease mouse models do not exhibit striking developmental phenotypes as HTT knockout models[5,71,75,76], cumulative evidence indicates developmental deficits in HD mouse models and human pathological specimens[77–80]. For instance, polyQ-expanded HTT induces deficits such as impairment in the maintenance of striatal neural stem cells and their specification into medium spiny neurons[80]. Furthermore, both HD patients and mouse models exhibit abnormalities in brain morphology and synaptic plasticity before the onset of apparent clinical deficits[81–87]. It is also known that HTT improves brain cell survival when it is overexpressed[18,19,21,22,88].

Research showed that HTT has anti-apoptotic effects, both in vitro[19,46,89] and in vivo[17,88] and protects neurons from excitotoxicity in vivo[18]. These cell-autonomous activities originate from the 548 amino acid terminus (N548) of the HTT protein and affect neuronal and non-neuronal cells[5]. An important function of HTT, which is more specific to neurons, is the stimulation of brain-derived neurotrophic factor (BDNF) gene transcription. It controls the transcription of the gene by inhibiting the silencer element "Repressor element 1" (RE1), or "neuron-restrictive silencer element" (NRSE) on the BDNF gene promoter[21,22], but also of many other genes which carry these silencer elements on their promoters. Besides, HTT is responsible for vesicle and BDNF transport,

and the regulation of many processes important to normal brain function, such as fast axonal trafficking and synaptic transmission[5]. When mESCs are genetically modified to express polyQ-expanded HTT, they maintain their ability to form NPCs. Upon neuronal induction, these cells exhibit a higher percentage of neuronal cell death resulting in a decreased percentage of neurons remaining at the end of the differentiation process[73]. Although HD-iPSCs from patients and control iPSCs differentiate into NPCs with indistinguishable efficiency, HD-NPCs exhibit abnormalities in cytoskeleton, cell adhesion and energetics[90]. Moreover, HD-NPCs present HD-related transcriptional dysregulation in genes involved in cell cycle, signaling, axonal guidance and neuronal development[90]. HD-NPCs can be terminally differentiated into neurons that exhibit HD-related changes such as alterations in calcium homeostasis, electrophysiology, increased vulnerability to excitotoxic stressors and cumulative risk of death over time[37]. Altogether, these findings suggest a role of HTT during development whereas its potential dysregulation by mutant polyQ could predispose neurons to degeneration and/or other HD-related changes.

1.4 Stem cells and their epigenetic landscape

Given the role of HTT in neuronal development, it is of importance to understand its regulatory function in embryonic stem cells (ESCs). Human embryonic stem cells (hESCs) are derived from the inner cell mass of blastocysts. These cells replicate continuously in the absence of senescence while maintaining their ability to differentiate into all cell lineages[91,92] .

One essential mechanism in order to maintain stem cell identity is the maintenance of the proteome via the ubiquitin-proteasome system (UPS). The UPS administers selective protein degradation by covalent ligation to a 76-amino-acid-residue protein called ubiquitin[93]. There are numerous targets for the ubiquitin-mediated degradation, such as regulatory proteins, which control cell-cycle progression, signal transduction or transcriptional regulation among many other important processes[93,94]. Importantly, the UPS was found to coordinate pluripotency in embryonic stem cells and induced pluripotent stem cells[95]. Furthermore, ubiquitin-mediated degradation is known for its important role in development and programmed cell death[93,94]. In eukaryotic cells the degradation of proteins is usually accomplished through a multi-step ubiquitination

process, which includes the reversible covalent conjugation of polypeptides to its substrates in an adenosine triphosphate (ATP)-dependent manner. The synthesized polyubiquitin chain, linked mostly through lysine 48 of the ubiquitin peptide, is recognized and hydrolyzed into short peptides by the 26S (2000 kDa) proteasome. The released ubiquitin molecules are then re-used[94,96]. As a first step a ubiquitin polypeptide is adenylated by the ubiquitin activating enzyme (E1). Next a sulfhydryl group of the proteasome is added to build a E1–ubiquitin thiolester and the activated ubiquitin is directed to one of the many E2 enzymes via transthiolation. As a last step the protein ubitquitination is catalyzed by the E2 enzyme, either alone or with an E3 ligase[97].

Extensive progress has been made in characterizing the transcriptional network that regulates self-renewal and differentiation of hESCs, including transcription factors such as OCT4, NANOG and SOX2[98]. Likewise, epigenetic modifiers regulate hESC pluripotency and cell reprogramming[99,100]. In comparison with their differentiated counterparts, hESCs have a unique nuclear and chromatin architecture such as fewer condensed heterochromatin foci[101]. This less compact chromatin pattern facilitates its dynamic reorganization during development. The chromatin state is modulated by DNA methylation and dynamic assembly/disassembly of histones as well as other related proteins. hESCs have a specific signature of DNA methylation, a key epigenetic regulatory mechanism to modulate gene expression[102]. Whereas differentiated cells exhibit more DNA methylation genome-wide suggesting a less active chromatin structure, hESCs have less DNA methylation reflecting a more open and dynamic architecture of chromatin[103,104]. Furthermore, ESCs exhibit a specific histone modification pattern, named bivalent domains, consisting of large regions of H3K27me3 repressive marks harboring smaller regions of H3K4me4 activation marks[105]. These bivalent domains could have a function to silence developmental genes in ESC while keep them poised for activation. Moreover, the levels of heterochromatin-associated histone modifications such as H3K9me3 are usually reduced whereas the levels of transcriptional activations marks such as acetylated histones are generally increased in hESCs[106,107]. A complex network of proteins such as the polycomb repressive complex 2 (PRC2) regulates histone modifications. In ESCs, PRC2 forms a complex with the Jumonji and ARID-domain-containing protein (JARID2) maintaining H3K27me3 chromatin marks[108]. Although the histone code has a critical role in chromatin and gene regulation, the molecular mechanisms that modulate the unique chromatin pattern of hESCs remain largely

unknown. Given their specific chromatin structure signature, hESCs could provide a different paradigm to discover novel epigenetic regulatory mechanisms and their impact on differentiation. Moreover, a better understanding of chromatin regulation in hESCs could lead to novel pathways to facilitate cell reprogramming of somatic cells. Thus, a firm understanding of the epigenetic machinery involved in hESC self-renewal and cell fate decisions is central importance.

Importantly, NPCs and neurons derived from HD-iPSCs show transcriptional changes consistent with those observed in HD brain, including dysregulation of genes involved in cell cycle, cell signaling, neuronal development and axonal guidance[90]. Transcriptional dysregulation is a prominent defect observed in postmortem HD brains and distinct HD mouse models[6,109]. Epigenetic marks such as DNA methylation and post-translational modifications of histone proteins are significantly altered in HD patients as well as HD cellular and organismal models[110]. Thus, epigenetic alterations could contribute to transcriptional abnormalities in HD[110]. Among these epigenetic changes, H3K9 trimethylation (H3K9me3) is robustly increased in HD patients and HD mouse models[111–114]. H3K9 hypermethylation is accompanied by upregulation of its specific methyltransferase SETDB1[113]. SETDB1 activity is regulated by ATF7IP. H3K9me3 is associated with heterochromatin and correlates with transcriptional repression[115].

ATF7IP regulates chromatin formation by binding and directing transcriptional factors to the general transcriptional machinery. Depending on the subcellular conditions the protein can operate either as an activator or a repressor[116–119]. In particular, ATF7IP has an effect on histone methylation that is essential for chromatin structure and function. In particular, the histone methyltransferase (HMTase) activity of Histone-lysine N-methyltransferase SETDB1 (SETDB1) depends on the assistance of ATF7IP. It triggers the transformation of the dimethyl (H3K9me2) to the trimethyl state (H3K9me3) by increasing the turnover rate of the reaction, both in vitro and in vivo.

To conclude, pluripotent stem cells are an invaluable resource for disease modeling and hold a great promise for regenerative medicine, in particular for understanding disease mechanisms in neurodegenerative diseases. The observations raise an intriguing question: does HTT regulate H3K9me3 levels in pluripotent stem cells via the described ATF7IP/SETDB mechanisms? In this thesis, I use human embryonic

stem cells (hESCs) and induced pluripotent stem cells (iPSCs) from HD-patients (HD-iPSCs) to identify epigenetic mechanisms that can correct disease-related changes.

1.5 The role of the HTT interacting protein 2 "UBE2K"

As described above, HTT has many binding partners. One of the first described interactors of HTT is the HTT interacting protein 2 (UBE2K or HIP2). UBE2K is a member of the E2 ubiquitin ligase family, which consists of approximately 35 enzymes. E2 ligases are essential for the proper functioning of the UPS. Briefly, as an E2 ubiquitin conjugating enzyme, UBE2K accepts ubiquitin from the E1 complex and catalyzes its covalent attachment to other protein lysine residues via E3 ubiquitin ligases[120]. Although it is known that HTT is ubiquitinated it is not known whether UBE2K targets HTT for ubiquitination[45]. The 22 kDa protein was discovered as an HTT interactor in a yeast two-hybrid system study. They found that the human protein consisted of an amino acid sequence identical to the bovine ubiquitin-conjugating enzyme (E2-25K), and was further described to interact with the amino terminus of the HD protein. Specifically, by using an anti-E2-25K polyclonal antibody, a protein slightly bigger than UBE2K was bound and exclusively located in HD-affected brain regions[45]. Further studies showed that UBE2K is highly expressed in the frontal cortex and striatum of the brain[121].

Like HTT, mRNA expression of the mouse UBE2K homolog (mHIP-2) was shown to increase with maturation of neurons, and thus, both are likely to have an impact brain development. Also, both HTT and mHIP-2 have the same regional mRNA distribution pattern. This indicates a common transcriptional regulation for the two proteins, although the mHIP-2 expression started earlier than HTT expression[122].

A different study using the yeast two-hybrid system identified UBE2K as one of six E2's interacting with the human heterodimeric RING E3 BRCA1-BARD1 ubiquitin-protein ligase complex. UBE2K binds to the BRCA1 RING and mediates the synthesis of Lys63- or Lys48-linked polyubiquitin chains on BRCA1[123]. Moreover, UBE2K could be a involved in the pathogenesis of Alzheimer's disease, by suppressing the proteasome activity and causing aggregation of ubiquitin conjugates in neurons, also referred to as amyloid-β peptide (Aβ) neurotoxicity[124,125]. It is known that protein aggregation is a hallmark of

neurodegenerative diseases such as HD and that the protein modification molecule ubiquitin aids in the localization and degradation of toxic aggregates[125]. Another study looked at the subcellular localization in neuronally differentiated cells and showed positive staining of UBE2K primarily co-aggregates with expanded polyglutamine proteins in apoptotic cells. This finding is in line with staining experiments in postmortem brain cells from HD patients[126].

UBE2K might be involved also in other biological systems, for instance in the ubiquitination of proteins in atherosclerosis, caused by macrophages and human monocytes. The aggregated low-density lipoprotein (agLDL) hinders the apoptosis of atherosclerosis causing, lipid-bearing macrophages, leading to unwanted foam cell formation. One of the genes induced by agLDL, termed low-density lipoprotein (LDL)-inducible gene (LIG) contained the coding sequence for UBE2K. This anti-apoptotic function could be revoked in the presence of proteasome inhibitor[127]. In mice, the SUMOylation of UBE2K ortholog E2-25K protects against neuronal cell death during oxidative stress. By SUMOylation the proteasome activity of subunit S5a is downregulated means of protection against cell death. UBE2K also interacts with a regulatory protein named cyclin B1, which is involved in mitosis. It thereby ameliorates cyclin B1-induced apoptosis by regulating the stability of the cyclin B1 protein[121]. In the model organism *C. elegans* knockdown of RNAi mediated ubiquitin-conjugating enzymes (UBC's) showed severe effects on aggregates. Especially, after the knockdown of *ubc-1, ubc-13, or uev-1*, aggregates could not be localized by the ubiquitin molecule, suggesting that these ubc enzymes are necessary for aggregate ubiquitination[125].

It is currently unclear if UBE2K plays a role in the abundant modifications of histone lysine residues during epigenetic changes (methylation, acetylation, ubiquitylation) in stem cell differentiation. Therefore, the aim of this thesis was to dissect the role of Huntington and UBE2K on the epigenetic landscape and on the function of neuronal differentiation in hESCs.

2 Material and Methods

2.1 Materials

Table 1: Cell lines

NAME	DESCRIPTION	SOURCE
H9 (WA09)	hESC	WiCell Research Institute
H1 (WA01)	hESC	WiCell Research Institute
HFIB2-IPS4	iPSCs control	(Park, Zhao et al. 2008) [128]
HD-IPSC#1	iPSC Q71	(Park, Arora et al. 2008) [129]
ND42242	iPSC Q21 control	Coriell Institute
ND36997	iPSC Q33 control	Coriell Institute
ND42229	HD iPSC Q71	Coriell Institute
ND36999	HD iPSC Q180	Coriell Institute

Table 2: hESC Culture and chemicals

NAME	COMPANY
1X PBS, W/O CA/MG	Life technologies
2-MERCAPTOETHANOL	Sigma
2-PROPANOL	Sigma
2,4,6-TRICHLORANISOL (TCA)	Sigma
4X LAEMMLI SAMPLE BUFFER	BioRad
4X500ML ACRYLAMIDE/BIS SOLUTION 37,5:1	Serva
5-BROMO-2`DEOXYURIDINE	Sigma
10X DPBS	Life technologies
10X TRIS BUFFERED SALINE	BioRad
10X TRIS/BORIC ACID/EDTA	BioRad
10X TRIS/GLYCINE	BioRad
10X TRIS/GLYCINE/SDS	BioRad
ACCUTASE 100 ML	Stem Cell Technologies
ACETON	Sigma
ADENOSINE 5′ -TRIPHOSPHATE DISODIUM SALT HYDRATE	Sigma
AGAROSE, ULTRAPURE 500G	Life technologies
ALBUMINE FROM BOVINE SERUM	Sigma
AMMONIUM BICARBONATE	Roche
AMMONIUMSULFATE	Carl Roth
AMMONIUM PERSULFATE, 10 G	BioRad
ASCORBIC ACID	Sigma
APROTININ FROM BOVINE LUNG	Sigma
B27 SERUMFREE SUPPLEMENT	Life technologies
BDNF	Peprotech
BFGF	Joint Protein Central
CHLOROFORM	Sigma

CITRIC ACID	Sigma
CF-1 MEFS	Amsbio
CLARITY WESTERN ECL SUBSTRATE	BioRad
COLLAGENASE TYPE IV	Life technologies
CYCLOHEXIMIDE	Sigma
D-(+)-GALACTOSE	Sigma
D-(+)-GLUCOSE	Sigma
DAPI (4,6 DIAMINIDO-2-PHENYLIN)	Life technologies
DEPC-TREATED WATER	Life technologies
DEOXYCHOLIC ACID SODIUM	Sigma
DIBUTYRYL-CYCLIC AMP	Sigma
DL-DITHIOTHREITOL (DTT)	Sigma
DISPASE	Stem Cell Technologies
DMEM, NO GLUCOSE	Life technologies
DMEM/F-12, HEPES	Life technologies
DMEM/F:12	Life technologies
DMSO	Sigma
DNA POLYMERASE I	Promega
DYNABEADS PROTEIN G	ThermoFisher
EDTA	Sigma (Roche Prot.)
EDTA SOLUTION PH 8,0	VWR
EGTA	Sigma
EPIDERMAL GROWTH FACTOR	Sigma
ETHANOL 99,5% (DENAT. 1% MEK)	VWR
ETHANOL PURE	Sigma
FBS SOUTH AMERICAN HI	Life technologies
FGF-BASIC HUMAN 1000MG	Peprotech
FLUORSAVE REAGENT	Merck
FORMALDEHYDE, 10%, METHANOL FREE	Polyscience
FORMIC ACID	Sigma
GDNF HUMAN	Peprotech
GELATIN FROM PORCINE SKIN	Sigma
GELTREX LDEV	Life technologies
GENTLE DISSOCIATION REAGENT	Stem Cell Technologies
GLACIAL ACETIC ACID	Sigma
GLUTAMAX 1	Life technologies
GLYCEROL, 500 ML	LifeTechnologies
GLYCOGEN	Life technologies
GLYCIN	Sigma
HEPES STERIL 1M PH7.3	VWR
HI-MARK PRE-STAINED PROTEIN LADDER	Life technologies
HOECHST	LifeTechnologies
HYDROCHLORIC ACID	Sigma
HYDROGEN PEROXIDE 30%	Sigma
IGEPAL CA-630	Sigma
IMMOBILON WESTERN CHEMILUM HRP SUBSTRATE	Merck
INCUWATER-CLEAN	VWR

IODACETAMIDE (IAA)	Sigma
ISOPROPANOL	Sigma
KALIUMHYDROGENPHOSPAT	Roth
KNOCKOUT SERUM REPLACEMENT	ThermoFisher Scientific
LAMININ	Life technologies
L-ASCORBIC ACID	Sigma
L-GLUTAMINE	Joint Protein Central
LITHIUMCHLORID (LICL)	Sigma
MAGNESIUM CHLORIDE HEXAHYDRATE	Millipore
METHANOL	Sigma
MTESR1	Stem Cell Technologies
MOWIOL	Carl Roth
N2 SUPPLEMENT	ThermoFisher Scientific
N-LAUROYLSARCOSINE	Sigma
N-ETHYLMALEIMIDE	Sigma
NEUROBASAL MEDIUM	Life technologies
NITROCELLULOSE MEMBRANE 45MM	Bio-Rad
N,N-DIMETHYLFORMAMID	Sigma
NON-ESSENTIAL AMINO ACIDS	Life technologies
NONFAT-DRIED MILK FROM BOVINE	Sigma
NP-40	Sigma
PBS, W/O CA/MG (10X)	Life technologies
PENICILIN/STREPTOMYCIN	Life technologies
PHENOL CHLOROFORM	BD
PHENOL:CHLOROFORM:ISOAMYL ALCOHOL	Sigma-Aldrich
PHENYLMETHYLSULFONYL FLUORIDE (PMSF)	Sigma
POLY-L-ORNITHINE HYDROBROMIDE	Sigma
PONCEAU S SOLUTION	Sigma
POTASSIUM ACETATE	Sigma
POTASSIUM CHLORIDE	Sigma
POTASSIUM DIHYDROGEN PHOSPHATE	Fisher
POTASSIUM HYDROGEN PHOSPHATE DIBASIC	ALFA
POTASSIUM HYDROXIDE	ALFA
PRECISION PLUS PROTEIN DUAL COLOR STANDARDS, 5X	BioRad
PROTEIN A BEADS	Miltenyi
PROTEIN ASSAY DYE REAGENT CONCENTRATE, 450 ML	BioRad
PROTEINASE K, RECOMBINANT	Sigma
PROTEASE INHIBITOR (25 TABL.)	Sigma
PUROMYCIN 10X1ML	Life technologies
PVDF.45UM IMMOBILON	Merck
RANDOM PRIMERS	ThermoFisher Scientific
RESOLVING GEL BUFFER, 1.5 M TRIS-HCL, PH 8.8, 1	BioRad
RNABEE	Tel-Test Inc.
RNASE A	Peqlab

RNASE H	Peqlab
ROCK INHIBITOR (Y-27632 DIHYDROCHLORIDE)	Abcam
SDS- SODIUM DODECYL SULFATE	Sigma
SDS SOLUTION 20% (W/V)	BioRad
SODIUM 4-PHENYLBUTYRATE	Sigma
SODIUM ACETATE, ANHYDROUS	VWR
SODIUM ACETYL-L-CYSTEINE	Sigma
SODIUM AZIDE	Sigma
SODIUM BICARBONATE	Life technologies
SODIUM CHLORIDE	VWR
SODIUM DEOXYCHOLATE	Sigma
SODIUM FLUORIDE	Sigma
SODIUM HYDROGEN PHOSPHATE DIBASIC	ALFA
SODIUM HYPOCHLORITE SOLUTION	Sigma
SODIUM ORTHOVANADATE	Sigma
SODIUM SELENITE	Sigma
SUCROSE	Sigma
STACKING GEL BUFFER	BioRad
STEMDIFF DEFINITIVE ENDODERM KIT	Stem Cell Technologies
STEMDIFF NEURAL INDUCTION MEDIUM	Stem Cell Technologies
STEMDIFF NEURAL PROGENITOR MEDIUM	Stemcell Technologies
TEMED	BioRad
TETRAETHYLAMMONIUM BOROHYDRIDE (TEAB)	Sigma
TRIS 1M PH 7,5	VWR
TRIS–HCL	Sigma, Roth
TRITON X-100	Sigma
TRYPSIN 0.25 EDTA	Life technologies
TWEEN® 20	Biochemica
ULTRAPURE DNASE/RNASE-FREE WATER	Life technologies
UREA	Roche

Table 3: Antibodies & chemicals protein biochemistry

ANTIBODY	COMPANY
ALEXA FLUOR 488 GOAT ANTI MOUSE IGG (H+L)	Life technologies
ALEXA FLUOR 488 GOAT ANTI RABBIT IGG (H+L)	Life technologies
ALEXA FLUOR 546 GOAT ANTI MOUSE IGM	Life technologies
ANTI-ATF7IP	Proteintech 1:500 WB
ANTI-BETA ACTIN	Abcam 1:1,000 WB
ANTI-H3	Cell Signaling Technologies, 1:10,000 WB

ANTI-H3K9ME3	Abcam, 1:1000 WB
ANTI-HTT	Cell Signaling Technologies, 1:1000 WB
ANTI-HTT-POLYQ (MW1-S)	from DSHB, 1:500 WB
ANTI-MAP2	Sigma 1:500 WB
ANTI-NESTIN	Stem Cell Technologies, 1:1,000
ANTI-OCT4	Stem Cell Technologies, 1:500
ANTI-PAX6	Stem Cell Technologies, 1:200
ANTI-SETDB1	Abcam, 1:500
ANTI-SOX2	Abcam, 1:1,000
HRP AP DONKEY ANTI-MOUSE IGG (H+L)	Jackson Immuno Research
HRP AP DONKEY ANTI-RABBIT IGG (H+L)	Jackson Immuno Research
STEMDIFF NEURAL PROGENITOR ANTIBODYPANEL	Stemcell Technologies
ANTI-FLAG	Sigma

Table 4: Lentiviral vectors. in pLKO.1-puro vector Mission shRNA

NAME	COMPANY
LENTIVIRUS (LV)-NON-TARGETING SHRNA CONTROL	Sigma
LV-HTT SHRNA#1 (TRCN0000322961)	Sigma
LV-HTT SHRNA#2 (TRCN0000019869)	Sigma
LV- ATF7IP SHRNA#1(TRCN0000020827)	Sigma
LV-ATF7IP SHRNA#2 (TRCN0000338504)	Sigma
LV-UBE2K SHRNA#1 (TRCN0000237896)	Sigma
LV-UBE2K SHRNA#2 (TRCN0000237893)	Sigma

Table 5: Kits

NAME	COMPANY
ADDGENE FIRELAB KIT	Addgene
FUGENE	Promega
NORMOCIN	InvivoGen
PIERCE BCA PROETIN ASSAY KIT	Fisher Sientific
QIAGEN LONGRANGE 2STEP RT-PCR KIT	Quiagen
QIAGEN-TIP 20	Quiagen
QUANTA Q FLEX REVERSE TRANSCRIPTION KIT	VWR
RNA BEE	Gentaur
SSOADVANCED SYBR GREEN SUPERMIX	Bio-Rad
TMTSIXPLEX ISOBARIC MASS TAG KIT PROTOCOL	Thermo Scientific

Table 6: qRT-PCR Primers

GENE	FORWARD	REVERSE
ACTB	CTGGCACCCAGCACAATG	CCGATCCACACGGAGTACTTG
GAPDH	GCACCGTCAAGGCTGAGAAC	GGATCTCGCTCCTGGAAGATG
HTT F	TGCAGCCCTGTCCTTTCAAG	CTCCAAGGCTTCTTCTTCTCCTAA
ATF7IP F	CACTGAACTACAGGCCAAGATAGC	GGTGGATGTTCATGTCTTTTCTTAAG
OCT4 F	GGAGGAAGCTGACAACAATGAAA	GGCCTGCACGAGGGTTT
NANOG F	AAATCTAAGAGGTGGCAGAAAAACA	GCCTTCTGCGTCACACCATT
DPPA4 F	CTGGTGCCAACAATTGAAGCT	AGGCACACAGGCGCTTATATG
SOX2 F	TGCGAGCGCTGCACAT	TCATGAGCGTCTTGGTTTTCC
PAX6 F	CATACCAAGCGTGTCATCAATAAAC	TGCGCCCATCTGTTGCT
NESTIN F	TGAAGGGCAATCACAACAGG	TGACCCCAACATGACCTCTG
MAP2	AAAGAAGCTCAACATAAAGACCAGACT	GTGGAGAAGGAGGCAGATTAGC
FGF5 F	ACGAGGAGTTTTCAGCAACAAAT	TTGGCACTTGCATGGAGTTTT
MSX1 F	CTCCGCAAACACAAGACGAAC	CACATGGGCCGTGTAGAGTC
ALB F	TGAGGTTGCTCATCGGTTTAAA	GCAATCAACACCAAGGCTTTG
GATA4 F	TCCGTGTCCCAGACGTTCTC	GAGAGGACAGGGTGGATGGA
GATA6 F	AGCGCGTGCCTTCATCA	GTGGTAGTTGTGGTGTGACAGTTG
ASCL2	CGCGCGATCACATTCTGTAA	TCGCAGATTTCGCCAGTTG
GBX1	TTTCTTCCCTCTGTTCGCCT	GGAAGGCCGAAAGAAAGCAA
SMC1B	GAGTGAGGGCAGAGAACAGG	CCTTCATCTCAGGGGCTCC
ADGRB1	TTGTGATGGTGTTGGTGCTG	ACCATCATCACCACCACCAT
UBE2K	CGCGGTGCAGCGAATC	TTGCTCGTCTCCTCGCTCTT
ZFP42	CCTGCAGGCGGAAATAGAAC	GCACACATAGCCATCACATAAGG
AADC	GGACCCCACTTACCTGAAGCA	CTGCCAATGCCGGTAGTCA
TH+	TGTCCACGCTGTACTGGTTCAC	CGGCACCATAGGCCTTCA
TUJ1	GGCCAAGTTCTGGGAAGTCA	CGAGTCGCCCACGTAGTTG
SYN	CGCAGTGGAAGCGCTACA	CCCACCACCTCAATGATGTG
NEUN	ACCAACGGCTGGAAGCTAAA	GCATAGAATTCAGGCCCGTAGA
GABAR	TGCGAAGGACAGTGGAGAAGT	GAGGGCGGATGGAGATATCC
NEFL	GCTATGCAGGACACGATCAACA	TTAGGTATCGTGCCATTTCACTCTT
NEFM	CAGGACCTCCTCAACGTCAAG	CCTGCAAATGTGCTAAATCTAGTCTCT
SOX1	GCTGACACCAGACTTGGGTT	GTGCTTGGACCTGCCTTACT

Table 7: Electrical devices

DEVICE	COMPANY
ACHRO-PLAN 10X	ZEISS
AGILENT 2100	Bioanalyzer
AXIOCAM 506 MONO	ZEISS
AXIO ZOOM.V16	ZEISS
BINDER CB-150	BINDER GmbH
BIORUPTOR SONICATOR	Diagenode
C1000 TOUCH THERMAL CYCLER	Bio-Rad
CFC384 REAL-TIME SYSTEM	Bio-Rad
DRI-BLOCK DB-2D	Techne
EC-PLAN-NEOFLUAR 20X-40X	ZEISS
ENSPIRE MULTIMODE PLATE READER 2300	Perkin Elmer
EPPENDORF 5430R, 5424, 5810R	Eppendorf
FUSION SOLO	Vilber Lourmat
HANNA INSTRUMENTS HI3220	HANNA Instruments GmbH
HEIDOLPH UNIMAX 1010	Heidolph Instruments GmbH
ILLUMINA HISEQ 4000 SEQUENCER	Illumina
IMAGER. Z1	ZEISS
INCUCELL MMM	MMM group
MINI TRANS-BLOT CELL	Bio-Rad
MINI-PROTEAN TGX, 10% ;10W; 10	Bio-Rad
MINI-PROTEAN TETRA CELL	Bio-Rad
MINI-SUB CELL GT SYSTEM W/ 7X7	Bio-Rad
MINI-TRANS-BLOT MODULE	Bio-Rad
NANODROP 8000	ThermoFisher Scientific
POWERPAC BASIC HC	Bio-Rad
PRECISA XB4200C	Precisa Gravimetrics AG
S1000 THERMAL CYCLER	Bio-Rad
SCANLAF CLASS 2 MARS	Labogene
SHAKING PLATFORM RM S-30V	M. Zipper GmbH
STEREO DISCOVERY.V8	ZEISS
THERMOMIXER COMFORT	Eppendorf
VTX-3000L MIXER UZUSIO	LMS Co., Ltd
ZEISS APOTOME .2	ZEISS
ZEN IMAGING SOFTWARE	ZEISS

2.2 Methods

2.2.1 Cell Culture

2.2.1.1 hESC culture and differentiation

hESC/iPSC lines were maintained on Geltrex (ThermoFisher Scientific) coated plates using mTeSR1 (Stem Cell Technologies). Undifferentiated colonies were passaged using dispase (2 mg ml^{-1}), and colonies were scraped with a glass pipette. Genetic identity of H9 and H1 hESCs was assessed by short tandem repeat (STR) analysis using the Promega PowerPlex 21 system (Promega Corporation) by Eurofins Genomics (Germany). The H9 and H1 hESC lines used in this study match exactly the known STR profile of these cells across the 8 STR loci analyzed. All the cell lines used in this study were tested for mycoplasma contamination at least once every three weeks and no mycoplasma contamination was detected. Research involving hESC lines was performed with approval of the German Federal competent authority (Robert Koch Institute).

Neural differentiation of hESCs/iPSCs was performed following the monolayer culture method with STEMdiff Neural Induction Medium (Stem Cell Technologies) based on Chambers, S. M. et al.[130].

The hESCs were rinsed once with PBS and 1 ml Gentle Dissociation Reagent (Stem Cell Technologies) was added. After 10 min at 37°C the pluripotent stem cells were gently dislodged using a p1000 pipette and 2ml of Dulbecco's Modified Eagle Medium (DMEM)-F12 + 10 µM ROCK inhibitor (Abcam) were added. Accordingly, cells were centrifuged at 300*g* for 5 min in a 15 ml falcon. Cells were re-suspended on STEMdiff Neural Induction Medium + 10 µM ROCK inhibitor and plated on polyornithine (15 µg ml^{-1})/laminin (10 µg ml^{-1})-coated plates (200,000 cells cm^{-2}). Following this protocol, we were able to induce neural differentiation of H9, H1 and iPSCs.

For pan-neuronal differentiation, NPCs were dissociated with 1 ml Accutase (Stem Cell Technologies) and plated on polyornithine (15 µg ml^{-1})/laminin (10 µg ml^{-1})-coated plates in neuronal differentiation medium consisting of Dulbecco's Modified Eagle Medium (DMEM)/F12, B27, N2 (ThermoFisher Scientific), 1 µg ml^{-1} laminin (ThermoFisher Scientific), 20 ng ml^{-1} GDNF (Peprotech), 20 ng ml^{-1} BDNF (Peprotech), 200 nM ascorbic acid (Sigma) and 1 mM dibutyryl-cyclic AMP (Sigma). Cells were

differentiated for 1 month (otherwise the time is indicated in the respective figures), with weekly feeding of neuronal differentiation medium.

Endoderm differentiation of H9 hESCs was performed using STEMdiff Definitive Endoderm Kit (Stem Cell Technologies).

2.2.1.2 Lentiviral infection of hESCs.

Transient infection experiments for shRNA screen were performed as follows. hESC colonies growing on Geltrex were incubated with mTesR1 medium containing 10 μM ROCK inhibitor (Abcam) for 2 h. For de-attaching the cells 1 l Accutase per well were added for 5 min at 37°C and centrifuged at 300*g* for 5 min in a 15 ml falcon. Cells were then re-suspended with a p1000 pipette in order to produce single cells. Hundred thousand cells per well were seeded on Geltrex coated W12 plates and incubated with mTesR1 medium containing 10 μM ROCK inhibitor. The next day cells were infected with 5 μl of concentrated lentivirus. Plates were centrifuged at 800*g* for 1 h at 30 °C. Cells were fed with fresh media on day 2 after infection to remove virus. On day 3 cells were selected for lentiviral integration using 2 μg ml^{-1} puromycin (ThermoFisher Scientific). Cells were then collected for qPCR experiments after 4–6 days of infection.

For UBE2K shRNA experiments we generated stable transfected hESCs. To obtain shRNA stable lines, hESC colonies growing on Geltrex coated plates were incubated with mTesR1 medium containing 10 μM ROCK inhibitor for 1 h. For dislodging the cells 1 ml Accutase per well were added for 5 min at 37°C and centrifuged at 300*g* for 5 min in a 15 ml falcon. Cells were then re-suspended with a p1000 pipette to obtain single cells. Fifty thousand cells were infected with 20 μl of concentrated lentivirus in the presence of 10 μM ROCK inhibitor for 1 h. Cell suspension was centrifuged to remove virus, pipetted up and down to obtain individual cells, and plated on a feeder layer of mitotically inactive mouse embryonic fibroblasts (MEFs) in hESC media (DMEM/F12, 20% knockout serum replacement (ThermoFisher Scientific), 0.1 mM non-essential amino acids, 1 mM L-glutamine, β-mercaptoethanol and 10 ng ml^{-1} bFGF (Joint Protein Central)) supplemented with 10 μM ROCK inhibitor. After a few days in culture, allowing small hESC colonies to grow, knockdown cells were selected by 1 μg ml^{-1} puromycin treatment for 2 days. Colonies were then passaged onto Geltrex coated plates to establish new hESC lines.

2.2.1.3 Immunocytochemistry.

Human cells were fixed with paraformaldehyde (4% in PBS) for 15 min, followed by permeabilization (0.2% Triton X-100 in PBS for 10 min) and blocking (3% BSA in 0.2% Triton X-100 in PBS for 10 min). Human cells were incubated in primary antibody for 2 h at room temperature (Rabbit anti-HTT (Cell Signaling Technologies #5656, 1:100), Mouse anti-OCT4 (Stem Cell Technologies, #60093, 1:200), Rabbit anti-PAX6 (Stem Cell Technologies, #60094, 1:300), Mouse anti-MAP2 (Sigma, #1406, 1:500), Rabbit anti-H3K9me3 (Abcam #8898, 1:500), Mouse anti-SETDB1 (Abcam, #107225, 1:200) and Rabbit anti-ATF7IP (Proteintech #14699-1-AP, 1:500)). Then, cells were washed with 0.2% Triton-X/PBS and incubated with secondary antibody (Alexa Fluor 488 goat anti-mouse (ThermoFisher Scientific, A-11029, 1:500), Alexa Fluor 568 goat anti-rabbit (ThermoFisher Scientific, A-11011, 1:500), and 2 μg ml^{-1} Hoechst 33342 (Life Technologies, #1656104) for 1 h at room temperature. The cover slips were washed with 0.2% Triton-X/PBS and distilled water before mounting.

2.2.2 Gene expression analysis

RNA isolation and quantitative RT–PCR. For human cell samples, total RNA was extracted using RNAbee (Tel-Test Inc.). cDNA was generated using qScript Flex cDNA synthesis kit (Quantabio). SybrGreen real-time qPCR experiments were performed with a 1:20 dilution of cDNA using a CFC384 Real-Time System (Bio-Rad) following the manufacturer's instructions. Data were analyzed with the comparative 2ΔΔCt method using the geometric mean of ACTB and GAPDH as housekeeping genes.

2.2.3 Biochemistry

2.2.3.1 Sample preparation for quantitative proteomics and analysis

For the comparison between Non-targeting control and HTT KD H9 hESCs, we performed label-free quantitative (LFQ) proteomics. Cells were collected in urea buffer (8 M urea, 50 mM ammonium bicarbonate and 1x complete protease inhibitor mix with EDTA (Roche)), homogenized with a syringe and cleared using centrifugation (16,000*g*, 20 min). Supernatants were reduced (1 mM DTT, 30 min), alkylated (5 mM iodoacetamide (IAA), 45 min) and digested with trypsin at a 1:100 w/w ratio after diluting urea concentration to 2 M. The next day samples were cleared (16,000*g*, 20 min) and supernatant was acidified. Peptides were cleaned up using stage tip extraction[131]. The liquid chromatography tandem mass spectrometry (LC-MS/MS) equipment consisted out of an EASY nLC 1000 coupled to the quadruple based QExactive instrument (Thermo Scientific) via a nano-spray electroionization source. Peptides were separated on an in-house packed 50 cm column (1.9 µm C18 beads, Dr.Maisch) using a binary buffer system: A) 0.1% formic acid and B) 0.1% formic acid in ACN. The content of buffer B was raised from 7% to 23 % within 120 min and followed by an increase to 45% within 10 min. Then, within 5 min buffer B fraction was raised to 80% and held for further 5 min after which it was decreased to 5% within 2 min and held there for further 3 min before the next sample was loaded on the column. Eluted peptides were ionized by an applied voltage of 2.2 kV. The capillary temperature was 275°C and the S-lens RF level was set to 60. MS1 spectra were acquired using a resolution of 70,000 (at 200 *m/z*), an Automatic Gain Control (AGC) target of 3e6 and a maximum injection time of 20 ms in a scan range of 300–1750 Th. In a data dependent mode, the 10 most intense peaks were selected for isolation and

fragmentation in the HCD cell using normalized collision energy of 25 at an isolation window of 2.1 Th. Dynamic exclusion was enabled and set to 20 s. The MS/MS scan properties were: 17,500 resolution at 200 *m/z*, an AGC target of 5e5 and a maximum injection time of 60 ms. All label-free proteomics data sets were analyzed with the MaxQuant software (release 1.5.3.8). We employed the LFQ mode[132] and used MaxQuant default settings for protein identification and LFQ quantification. All downstream analyzes were carried out on LFQ values with Perseus (v. 1.5.2.4)[133].

2.2.3.2 Western blot

Cells were washed twice with PBS, then scraped from tissue culture plates and lysed in protein cell lysis buffer (10 mM Tris–HCl, pH 7.4, 150 mM NaCl, 10 EDTA, 50 mM NaF, 1% Triton X-100, 0.1% SDS supplemented with 20 μg ml^{-1} Aprotinin, 2 mM sodium orthovanadate, 1 mM phenylmethylsulphonyl fluoride and protease inhibitor (Roche)) by incubating samples for 10 min on ice and homogenization through syringe needle (27G). Cell lysates were centrifuged at 10,000*g* for 10 min at 4°C and the supernatant was collected. Protein concentrations were determined with a standard BCA protein assay (Thermo Scientific). Approximately 10–20 μg of total protein were separated by SDS–PAGE, transferred to PVDF membranes (Millipore) and subjected to immunoblotting.

2.2.3.3 Protein immunoprecipitation for interactome analysis.

hESCs were lysed in modified RIPA buffer (50 mM Tris-HCl (pH 7.4), 150 M NaCl, 1% IgPal, 0.25% sodium deoxycholate, 1 mM EDTA, 1 mM PMSF) supplemented with protease inhibitor (Roche). Lysates were centrifuged at 10,000*g* for 10 min at 4°C. Then, the supernatant was collected and incubated with HTT antibody (Cell Signaling Technology, #5656, 1:50) for 30 min and subsequently with 100 µl Protein A beads (Miltenyi) for 1 h on the overhead shaker at 4°C. As a control, the same amount of protein was incubated with anti-FLAG antibody (SIGMA, F7425, 1:100) in parallel. After this incubation, supernatants were subjected to magnetic column purification. Three washes were performed using wash buffer 1 (containing 50 mM Tris–HCl (pH 7.4), 150 mM NaCl, 5% glycerol and 0.05% IgPal). Next, columns were washed five times with wash buffer 2 (containing 50 mM Tris–HCl (pH 7.4), 150 mM NaCl). Then, columns were subjected to in-column tryptic digestion containing 7.5 mM ammonium bicarbonate, 2 M urea, 1 mM DTT and 5 ng ml^{-1} trypsin. Digested peptides were eluted using two times 50 µl of elution

buffer 1 containing 2 M urea, 7.5 mM Ambic, and 5 mM IAA. Digests were incubated over night at room temperature with mild shaking in the dark. Samples were stage-tipped the next day for label-free quantitative proteomics and analyzed with MaxQuant software. The downstream analyzes were carried out on LFQ values with Perseus (v. 1.5.2.4).

2.2.3.4 RNA sequencing.

Total RNA was extracted using RNAbee (Tel-Test Inc.). Libraries were prepared using the TruSeq Stranded mRNA Library Prep Kit. Library preparation started with 1 µg total RNA. After selection (using poly-T oligo-attached magnetic beads), mRNA was purified and fragmented using divalent cations under elevated temperature. The RNA fragments underwent reverse transcription using random primers followed by second strand cDNA synthesis with DNA Polymerase I and RNase H. After end repair and A-tailing, indexing adapters were ligated. The products were then purified and amplified (20 µl template, 14 PCR cycles) to create the final cDNA libraries. After library validation and quantification (Agilent 2100 Bioanalyzer), equimolar amounts of library were pooled. The pool was quantified by using the Peqlab KAPA Library Quantification Kit and the Applied Biosystems 7900HT Sequence Detection System. The pool was sequenced on an Illumina HiSeq 4000 sequencer with a paired- end (2x 75bp) protocol. We used the human genome sequence and annotation (EnsEMBL79) together with the splice-aware STAR read aligner[134] (release 2.5.1b) to map and assemble our reference transcriptome. Subsequent transcriptome analyzes on differential gene and transcript abundance were carried out with the cufflinks package[135] cuffdiff program (version 2.2.1). Transcripts showing a log2-fold change at a FDR < 0.05 were retained as significantly differentially expressed.

2.2.3.5 Chromatin Immunoprecipitation ChIP-sequencing

Cells were cross linked by adding 1% formaldehyde to the medium on the tissue culture dish and incubated on balancer for 10 min at RT. Cross linked cells were quenched with 0,125 M glycine on a balancer for 10 min at RT and then scraped and transferred to a 15 ml falcon on ice. Centrifugation at 1200 rpm for 5 min at 4°C and afterwards 2 washing steps with 5 ml PBS 1x / PMSF 1 mM followed. The pellets were re-suspended with 5 ml lysis buffer 1 (50 mM Hepes, 140 mM NaCL, 1 mM EDTA, 10% glycerol, 0.5% NP-40, 0.25% TX-100 and protease inhibitor (Roche)) and rotated vertically at 4°C for 10

min. Cell suspensions were centrifuged at 4°C and 1350*g* for 5 min. The pellets were re-suspended with 5 ml lysis buffer 2 (10 mM Tris, 200 mM NaCL, 1 mM EDTA, 0.5 mM EGTA) and rotated vertically at RT for 10 min. Again, cell suspensions were centrifuged at 4°C and 1350*g* for 5 min with a re-suspension step of the pellets with 1.5 ml lysis buffer 3 (10 mM Tris, 100 mM NaCL, 1 mM EDTA, 0.5 mM EGTA, 0.1% Na-Deoxycholate, 0.5% N-Lauroylsarcosine) and a p1000 to obtain single cells. Then, cells were sonicated at 4°C and centrifuged for 10 min at 16.000*g* at 4°C. The sonicated lysate was treated with 1% Triton X-100 and 75 µl were taken and stored as an input at -20°C. 750 µl were incubated with 10 µg antibody rotating vertically ON at 4°C. The next day, magnetic Dynabeads G (ThermoFisher) at 10x volume of Antibody were aliquoted into a new microtube. The beads were washed 3 times in cold blocking solution (0,5% BSA, 1 PBS) and with the tubes placed on the magnetholder. 1 ml of antibody-chromatin mix were added to the beads and rotated vertically for at least 2 h at 4°C. Then the beads were washed 5x with cold RIPA wash buffer (50 mM Hepes, 500 mM LiCl, 1 mM EDTA, 1% NP-40, 0.7% Na-Deoxycholate) with the tubes placed on the magnetholder. Afterwards, the beads were washed 1x with 1 ml TE+ 50 mM NaCl on ice and samples were centrifuged for 3 min at 950*g* and 4°C. After removing all liquid from the beads, 210 µl elution buffer (50 mM Tris, 10 mM EDTA, 1% SDS) were added and mixed by flicking the tube. The proteins bound to the antibodies were eluted for 15 min at 65°C. Finally, beads were centrifuged for 1 min at 1600*g* at RT and placed on a magnetholder to settle and supernatants were transferred into a new tube. To reverse crosslinking, 3x volume of the elution buffer were added to the input and were incubated with the ChIP samples at 65°C ON. The next day, 1x volume of TE buffer and 0.2 mg ml^{-1} RNase were added and incubated for 1h at 37°C. Afterwards 0.2 mg ml^{-1} Proteinase K were added and left for 2 h at 55°C to digest proteins. The DNA was phenol-chloroform extracted at RT with 1x volume of 25:24:1 phenol-chloroform-isoamyl alcohol and centrifuged for 5 min, at maximum speed at RT, to separate layers, 1x volume chloroform were added to extract the DNA and centrifuged again. The upper layer containing the DNA, was transferred to a new tube for ethanol precipitation as follows: 1/10 of NaOAc 3 M, 1 µl 20 mg ml^{-1} glycogen, 2x volume of ice cold ethanol were added on ice and incubated for 30 min at -80°C to precipitate DNA. A centrifugation at max speed at 4°C was performed for 30 min to pellet the DNA. Supernatants were removed and 0.5 ml ice cold 70% ethanol were added to the pellets and centrifuged at 7500 rpm for 5 min. After removing the remaining ethanol, the pellets were air dried at RT and re-suspended in 40 µl dH2O and concentration of DNA determined.

2.2.3.6 Bioinformatic analysis of ChIP-sequencing

ChIP-Seq data was analyzed by using QuickNGS (Next-Generation Sequencing) pipeline. ChIP-Seq reads was mapped to the Homo Sapiens (Ensembl database version 87) using BWA[136]. Quality check of the sequencing data were performed with FastQC (version 0.10.1.). For peak calling used MACS2 (version 2.0.10)[137]. QuickNGS pipeline identifies all genes that are 2000 bp up- or downstream from the MACS2 peaks. The peak sequences are analyzed for enrichment of transcription factor binding motifs using MEME-ChIP (Version 4.10.0)[138]. The results comprise lists of significant peaks and reports for motif enrichment. The result was uploaded into MySQL database. Basic QC statistics and password-protected track hubs for the UCSC Genome Browser with direct hyperlinks for visualization were used.

2.2.4 Statistics

PRISM 6 software was used for statistical analysis to determine median and percentiles. P-values were calculated using the log-rank (Mantel–Cox) method. The P-values refer to a single experiment. For the rest of experiments, unless stated otherwise, two-tailed unpaired students't-test was used to check for statistical significance. Error bars represent standard error of the mean (S.E.M.). (*p<0.05 **p<0.01 ***p<0.001)

3 Results

3.1 The role of HTT in epigenetic control of embryonic stem cell differentiation

3.1.1 HTT interacts with the chromatin regulator ATF7IP

In order to find out about the potential role of HTT as an epigenetic regulator in hESCs, in a first attempt we assessed its expression levels and abundance in hESCs compared to differentiated cells. Strikingly, we found that hESCs exhibit higher expression of HTT than their differentiated neuronal counterparts at both protein and mRNA levels (Figure 1A-B), supporting a role of HTT in hESC identity.

To determine the protein binding partners of HTT in hESCs, we performed co-immunoprecipitation experiments followed by a single shot label-free proteomic approach. We quantified approximately 2000 proteins and compared protein abundance in HTT antibody pulldowns with control FLAG antibody pulldowns in both hESCs and terminally differentiated neurons. Although HTT was the most enriched protein in both hESCs and neurons (Figure 1C-D), hierarchical clustering revealed a clear separation in HTT-interacting proteins between these cells (Figure 2).

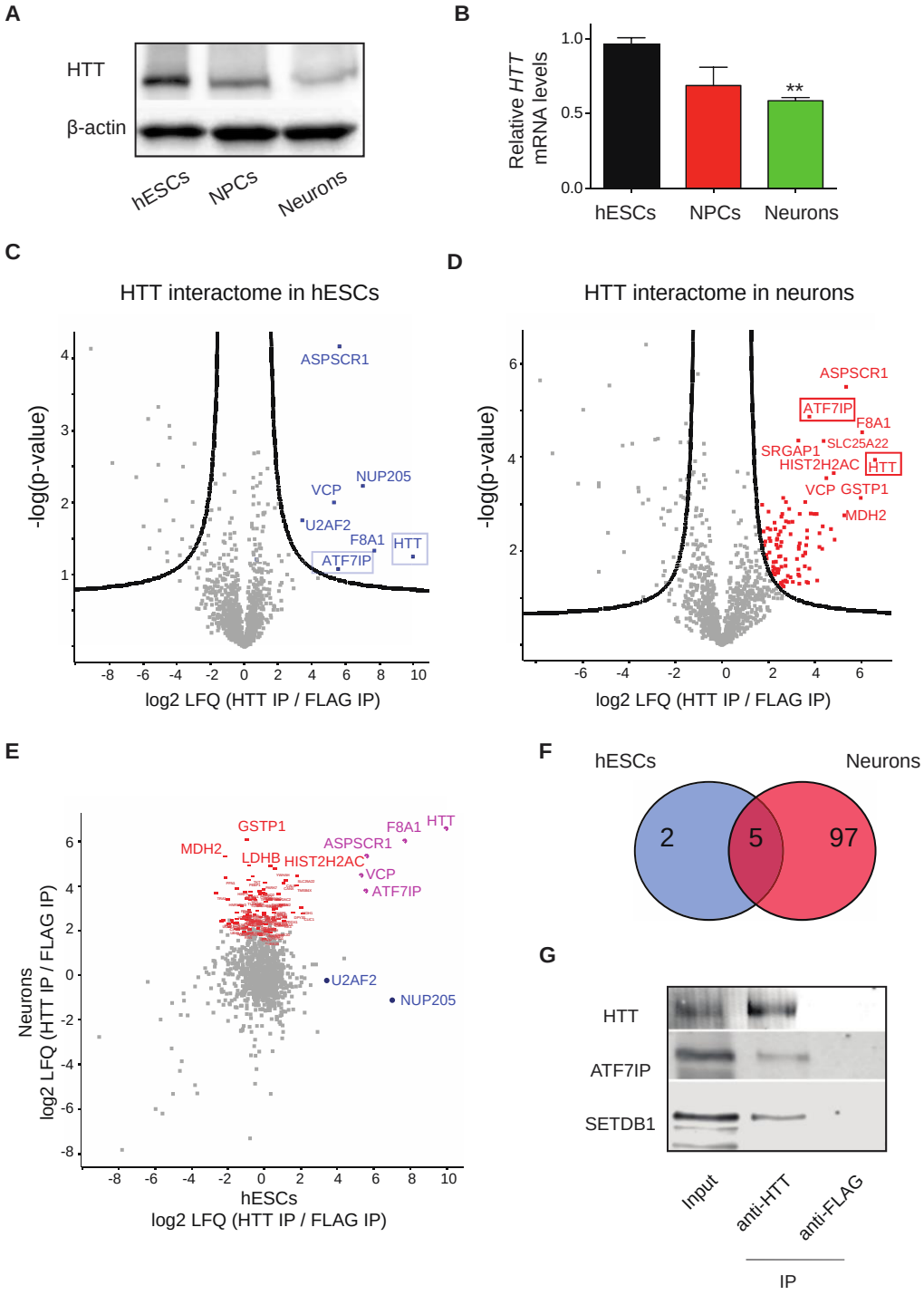

Figure 1. HTT interacts with the chromatin factor ATF7IP in both hESCs and neurons. A, Western blot analysis of H9 hESCs and their differentiated counterparts with antibody to HTT. β-actin is the loading control. B, HTT relative expression to H9 hESCs represents the mean ± s.e.m. (n= 3 independent experiments). Statistical comparisons were made by Student's t-test for unpaired samples. p-value: **(p< 0.01). C, Volcano plot of HTT interactome in H9 hESCs (n= 3). –log (p-value) of a two-tailed t-test is plotted against the log2 ratio of protein label-free quantification (LFQ) values from co-immunoprecipitation (co-IP) experiments using HTT antibody compared to control co-IP with FLAG antibody. Blue coloured dots beyond the curved lines indicate significance after correction for multiple testing. D, Volcano plot of HTT interactome in neurons (n= 4). Red coloured dots beyond the curved lines demonstrate significance after correction for multiple testing. E, Scatterplot of protein enrichments in HTT co-IP from hESCs and neuronal cells. Significant intrinsic interactors in neurons, hESCs as well as common interactors in both cell types are indicated in red, blue and magenta, respectively. F, Venn diagram represents the number of specific and common co-immunoprecipitated proteins with HTT antibody in hESCs and neurons. G, Co-immunoprecipitation with HTT and FLAG antibodies in H9 hESCs followed by western blot with antibodies to HTT, SETDB1 and ATF7IP. The images are representative of two independent experiments.

Immunoprecipitation of HTT itself was more effective in hESCs when compared with neurons (Figure 1 E), consistent with increased HTT expression in hESCs (Figure 1 A). On the contrary, a major population of proteins specifically interacted with HTT in neurons, but not in hESCs (Figure 1 E-F).

Protein names	T-test difference	-log P-value
HTT	9.96	1.25
F8A1	7.69	1.33
NUP205	7.00	2.23
ASPSCR1	5.61	4.17
ATF7IP	5.55	1.08
VCP	5.30	2.01
U2AF2	1.76	3.42

Table 8. Protein interactors of HTT in H9 hESCs. Protein label-free quantification (LFQ) values from co-immunoprecipitation (co-IP) experiments using HTT antibody compared to control co-IP with FLAG antibody. (Student's t-test, n= 3, FDR< 0.05).

Whereas 102 proteins passed the criterions for significant interaction with HTT in neurons (Figure 1 D), only 7 proteins were significantly detected in hESCs (Figure 1 C,E and Table 8). Among them, NUP205 and U2AF2 were exclusively co-immunoprecipitated in hESCs whereas the other 5 proteins were also detected in neurons (Figure 1 F), including HTT itself and its known interactors F8A1[139] and VCP[140]. In both hESCs and neurons, we found a novel interaction of HTT with ATF7IP (Figure 1 C-D), a factor that binds the H3K9 methyltransferase SETDB1 to regulate heterochromatin formation[116,141,142–144]. Notably, co-immunoprecipitation experiments followed by western blot indicated that HTT could form a complex with ATF7IP and SETDB1 (Figure 1 G).

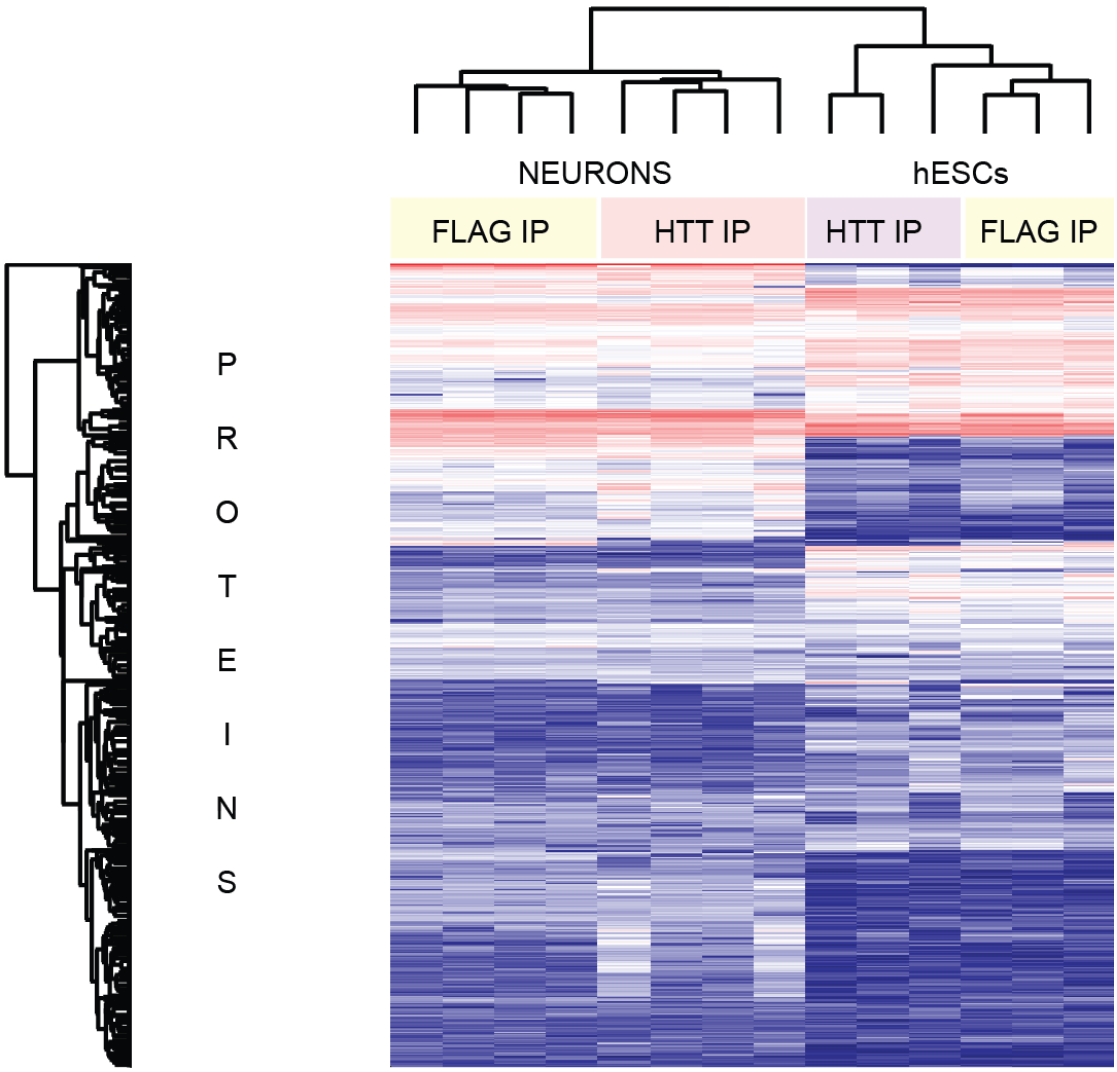

Figure 2. Proteomic analysis of co-immunoprecipitation (Co-IP) experiments with HTT and control FLAG antibodies in H9 hESCs and neurons. Protein label-free quantification (LFQ) intensities indicating protein amounts are indicated by color code (red= high, blue= low abundance). Proteins (rows) and samples (columns) were clustered by Euclidean distance (neurons (n= 4), hESCs (n= 3). A clear separation of sample types and pulldowns was observable.

3.1.2 Loss of HTT induces trimethylation of H3K9 in hESCs

ATF7IP stimulates the H3K9 methyltransferase activity of SETDB1, facilitating H3K9 trimethylation and concomitant heterochromatin formation[116,141]. Knockdown of ATF7IP dramatically diminished nuclear SETDB1 levels as well as trimethylation of H3K9 in hESCs (Figure 3 A-B), indicating that ATF7IP also regulates H3K9me3 in these cells. Interestingly, reduction of H3K9 trimethylation upon loss of ATF7IP did not affect the expression of pluripotency markers (Figure 3 C).

Given that HTT interacted with ATF7IP (Figure 1 C-G), we assessed whether modulation of HTT impairs H3K9 trimethylation in hESCs. Indeed, we observed a dramatic increase in H3K9me3 levels upon HTT knockdown (Figure 3 D-E). Since hESCs

can vary in their characteristics, we analyzed an independent hESC line and obtained similar results (Figure 4 A-B). With the role of HTT in brain development[72], we asked whether alterations in H3K9me3 levels of hESCs are transmitted to their NPC counterparts. For this purpose, we performed neural induction and found that the expression of the early neuroectodermal marker PAX6[145] as well as other neural markers were triggered at the same extent in both control and HTT KD cells (Figure 5 A-C). These results indicate that HTT is not required for hESC commitment into NPCs. However, NPCs-derived from HTT KD hESCs maintained high levels of H3K9me3 compared with control NPCs (Figure 3 F-G).

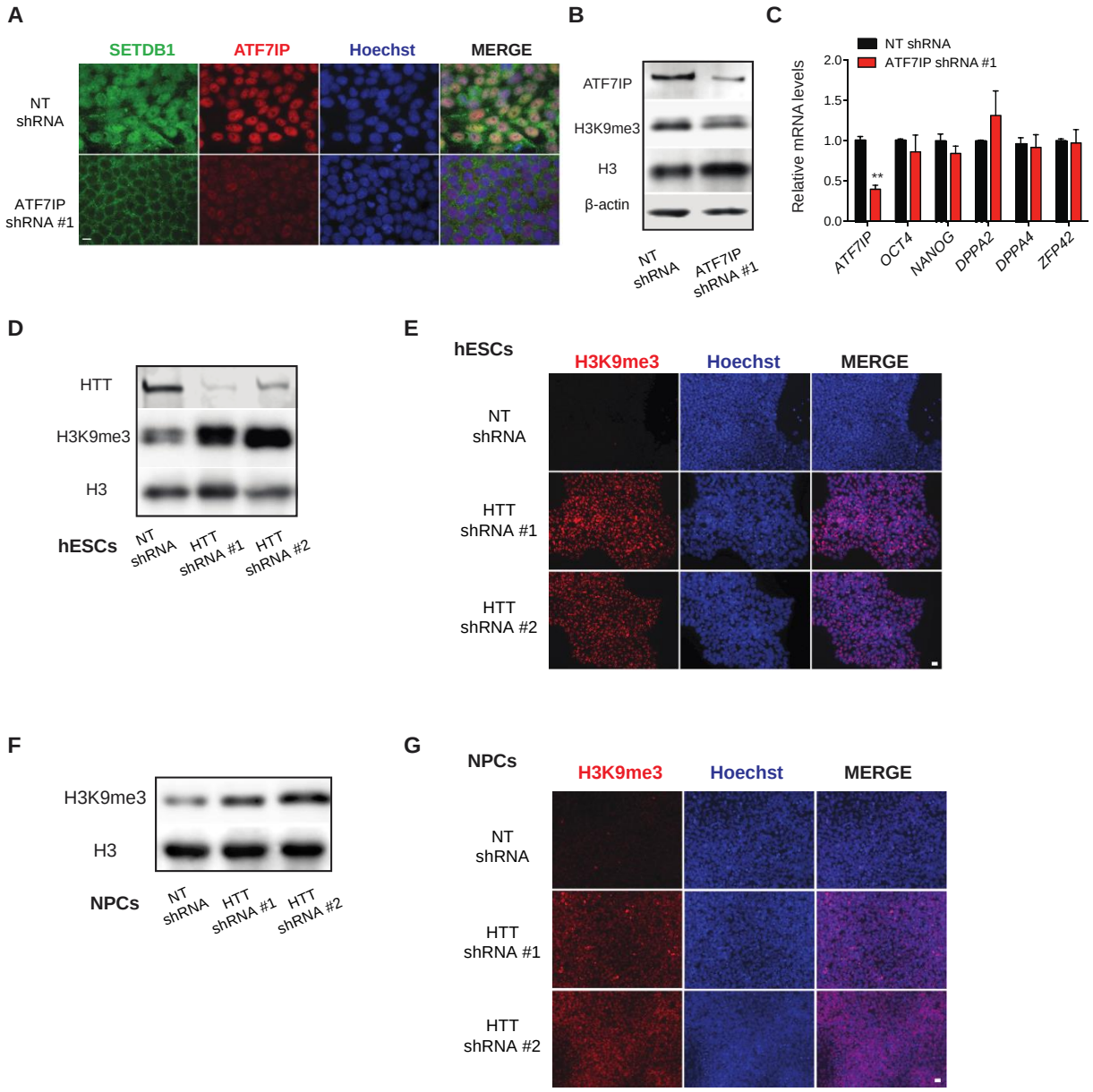

Figure 3. Loss of HTT induces trimethylation of H3K9me3. A, Immunocytochemistry of H9 hESCs with antibodies to ATF7IP and SETDB1. Hoechst staining was used as a marker of nuclei. Scale bar represents 10 μm. B, Western blot analysis of H9 hESC lysates with antibodies to ATF7IP, H3K9me3, and total H3. β-actin is the loading control. C, qPCR analysis of pluripotency markers. Graph (relative expression to NT shRNA H9 hESCs) represents the mean ± s.e.m. of three independent experiments. D, Western blot analysis of H9 hESC lysates with antibodies to HTT, H3K9me3 and total

H3. E, Immunocytochemistry of H9 hESCs with antibody to H3K9me3. Hoechst staining was used as a marker of nuclei. Scale bar represents 20 μm. F, Western blot analysis of H9 NPC lysates with antibody to H3K9me3 and total H3. G, Immunocytochemistry of H9 NPC with antibody to H3K9me3. Hoechst staining was used as a marker of nuclei. Scale bar represents 20 μm. All the statistical comparisons were made by Student's t-test for unpaired samples. P-value: *(P<0.05), **(P<0.01), ***(P<0.001), **** (P<0.0001).

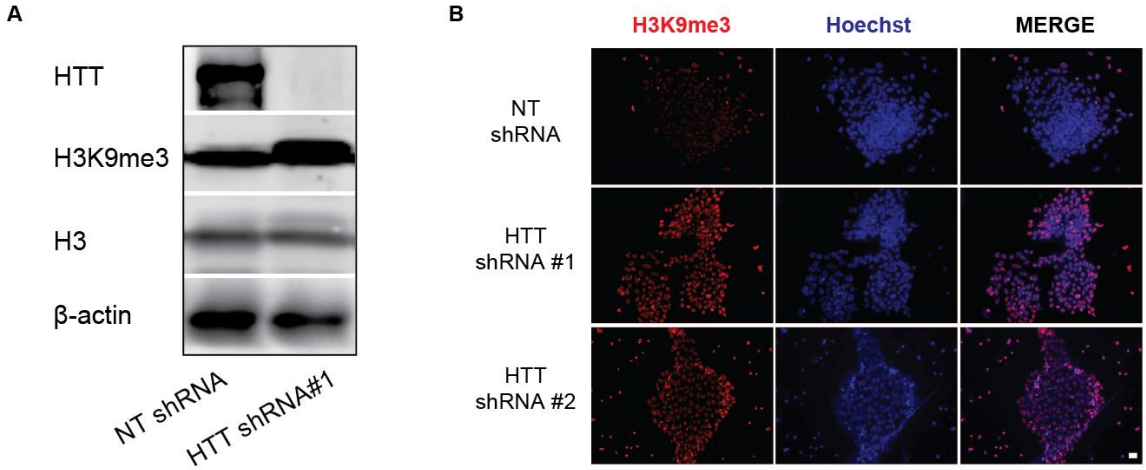

Figure 4. Loss of HTT induces trimethylation of H3K9me3 in H1 hESCs. A, Western blot analysis with antibody to HTT, H3K9me3 and total H3. β-actin is the loading control. B, Immunocytochemistry of H1 hESCs with antibody to H3K9me3. Hoechst staining was used as a marker of pluripotency of nuclei. Scale bar represents 20 μm.

Loss of HTT did not affect the total levels of ATF7IP (Figure 6 A). However, loss of HTT changed the nuclear distribution of ATF7IP, which markedly concentrated in specific areas in contrast to the diffused pattern characteristic of control hESCs (Figure 6 A).

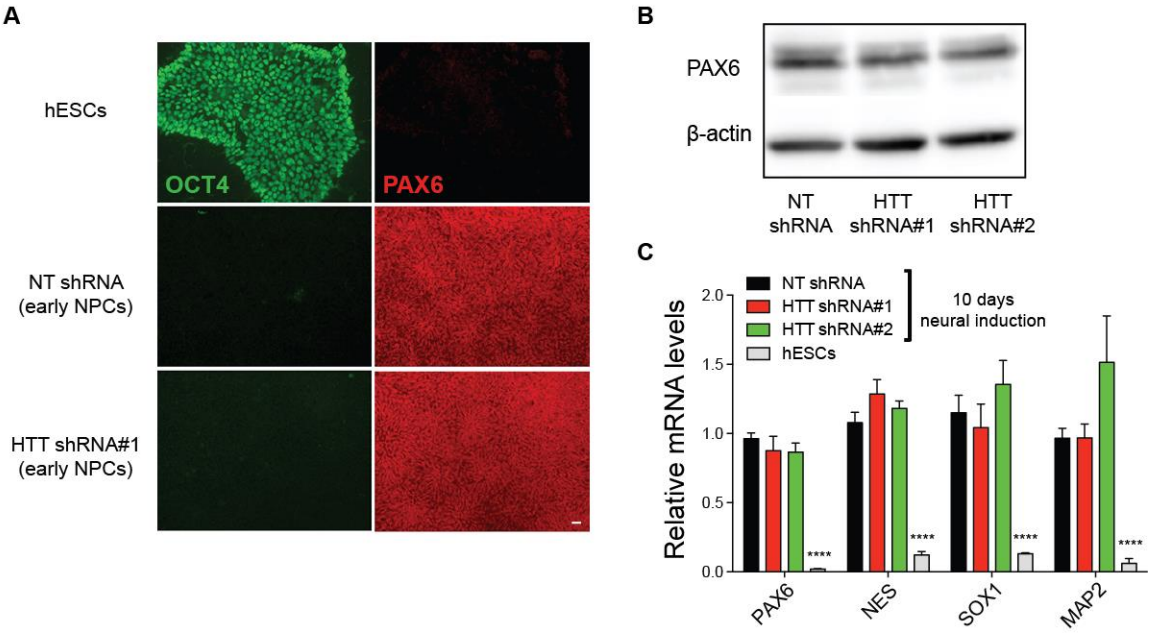

Figure 5. HTT KD hESCs retain their ability to differentiate into NPCs. A, Immunocytochemistry after 10 days of neural differentiation assay. OCT4, PAX6, and DAPI staining were used as markers of pluripotency, neuroectodermal differentiation, and nuclei, respectively. Scale bar represents 20 μm. B, Western blot analysis with antibody to PAX6 in early NPCs (10 days after neural induction). β-actin is the loading control. C, Data represent the mean ± s.e.m. of relative expression levels to NT shRNA early NPCs (n= 9).

Notably, loss of HTT induced the interaction of ATF7IP with SETDB1 as well as other alterations in the interactome of ATFTIP (Figure 6 B). Taken together, these preliminary results indicate that HTT modulates the interaction of SETDB1 with its activator ATF7IP to control trimethylation of H3K9.

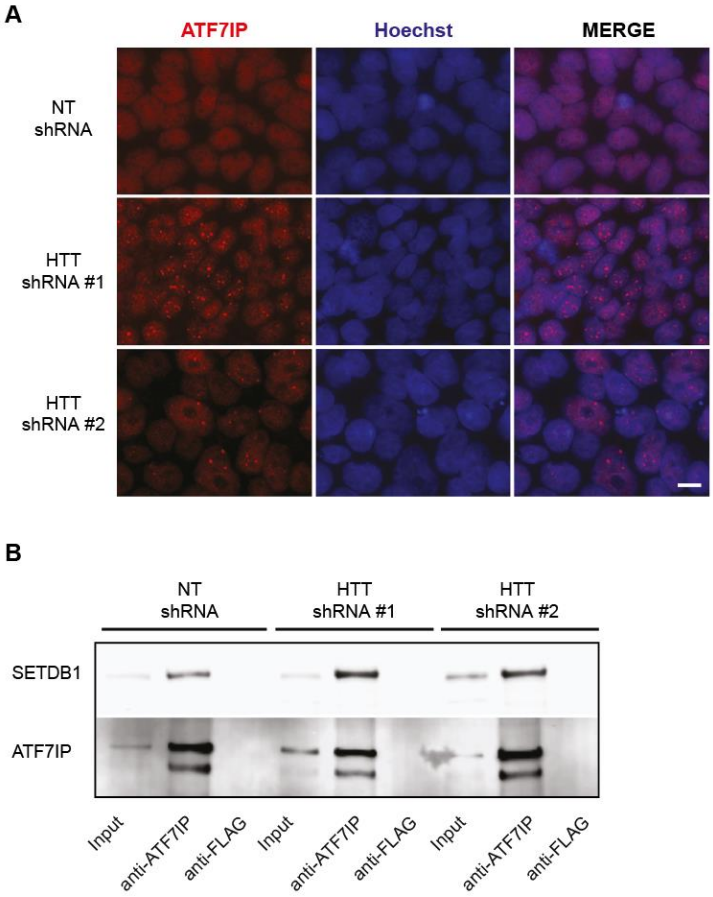

Figure 6. HTT modulates ATF7IP and its interaction with SETDB1. A, Immunocytochemistry of H9 hESCs with antibody to ATF7IP. Hoechst staining was used as a marker of nuclei. Scale bar represents 10 µm. B, Co-immunoprecipitation with ATF7IP and FLAG antibodies in H9 hESCs followed by western blot with antibodies to SETDB1 and ATF7IP. The images are representative of two independent experiments.

3.1.3 Aberrant H3K9me3 marks upon HTT knockdown impairs induction of distinct neural genes

Next, we asked whether the knockdown of HTT would alter the expression of marker proteins of pluripotency and neuronal differentiation. Knockdown of HTT did not impair the levels of pluripotency markers of hESCs (Figure 7 A-B). Moreover, we found no differences in the markers of the distinct germ layers (Figure 7 C).

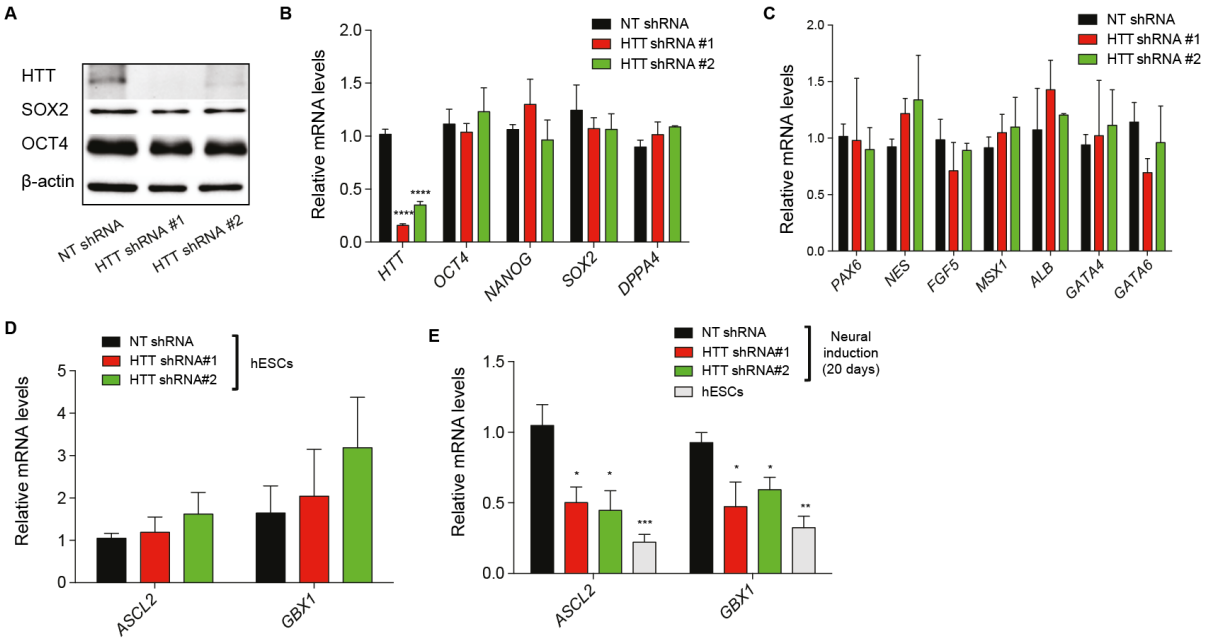

Figure 7. Altered H3K9me3 marks upon HTT knockdown impairs the induction of distinct neural genes. A, Western blot analysis of H9 hESC lysates with antibodies to HTT, OCT4 and SOX2. β-actin is the loading control. B, Knockdown of HTT does not change the mRNA levels of pluripotency markers. Graph (relative expression to non-targeting (NT) shRNA H9 hESCs) represents the mean ± s.e.m. (n= 9). C, qPCR analysis of ectodermal (PAX6, NES, FGF5), mesodermal (MSX1) and endodermal (ALB, GATA4, GATA6) germ layer markers. Graph (relative expression to NT shRNA hESCs) represents the mean ± s.e.m. (n= 8). E, qPCR analysis of H9 hESCs. Graph (relative expression to NT shRNA) represents the mean ± s.e.m. of three independent experiments with two biological replicates. F, qPCR analysis after 20 days of neural induction. Data (relative expression to NT shRNA cells) represent three independent experiments. All the statistical comparisons were made by Student's t-test for unpaired samples. P-value: *(P<0.05), **(P<0.01), ***(P<0.001), **** (P<0.0001).

To further assess changes induced by loss of HTT, we analyzed the proteome of hESCs. In quintuplicate analysis, we identified 6610 proteins, of which we quantified 4820 in all samples. Hierarchical clustering revealed separation of HTT knockdown and NT samples based on global protein expression profiles (Figure 8 A). The quantitative analysis revealed that 186 of proteins were changed in HTT shRNA#1 hESCs as compared to NT control, whereas 64 of proteins were changed in HTT shRNA#2 hESCs as compared to NT hESCs (Figure 8 B). Correlational analysis revealed a moderate, but significant correlation between HTT shRNA #1 and HTT shRNA #2 KD hESC lines (Figure 8 C). To examine the function of these proteins altered on HTT KD, we performed 2D Gene Ontology (GO) enrichment (Figure 8 D).

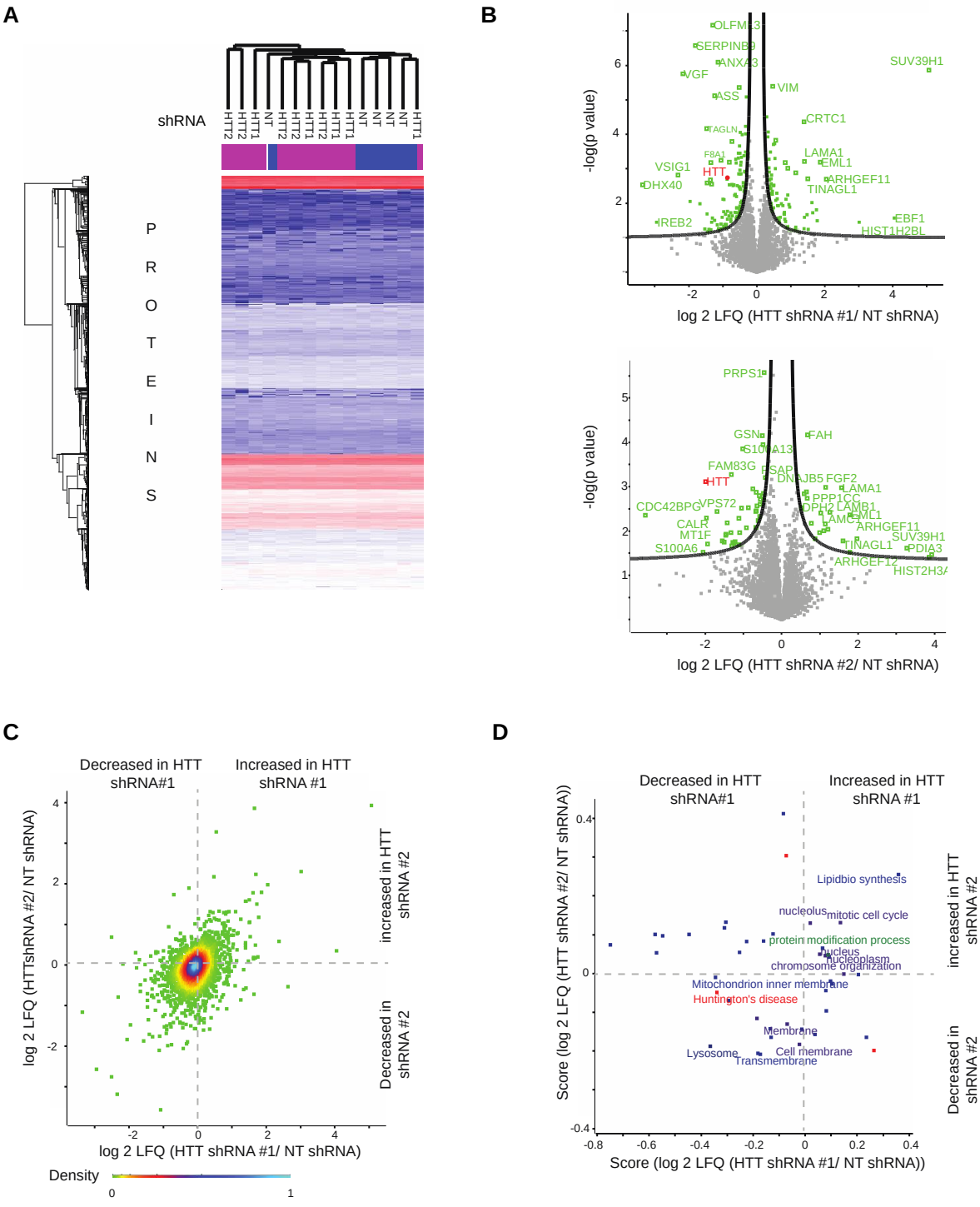

Figure 8. Analysis of the proteome of HTT KD hESCs. A, Label-free quantification (LFQ) of 4820 proteins reveals partial separation of HTT knockdown and control non-targeting (NT) H9 hESCs (n= 5). Proteins (rows) and samples (columns) are clustered according to euclidean distance (red= high, blue= low abundance). B, Volcano plot of LFQ intensities in HTT KD hESC lines (shRNA #1 and #2) as compared to NT shRNA. The significance of a two-tailed t-test is plotted against the log2 fold change of LFQs. Proteins coloured in green are termed significant after correction of multiple testing (FDR= 0.05, s0= 1). C, Comparison of protein expression ratios in HTT shRNA #1 vs HTT shRNA #2 hESCs. Protein changes in both conditions correlated significantly (-log(p)=14, Pearson's correlation). Kernel density is color-coded. D, 2D GO enrichment for GO terms, uniprot key words and KEGG pathways. Significantly altered terms changed in both conditions are labelled with their name (FDR <0.05).

The analysis revealed that proteins related to HD were significantly enriched in the decreased protein population of HTT KD hESCs. Furthermore, the downregulated protein population was also significantly enriched for proteins involved in membrane function and organization (Figure 8 D). Proteins increased on HTT KD hESCs were significantly enriched for proteins involved in lipid biosynthesis, but also transcription, chromatin regulation and extracellular matrix structural constituents (Figure 8 D). Besides HTT, we found that other 14 (9 upregulated, 5 downregulated) proteins were significantly changed in both HTT KD hESC lines (Table 9). Among them, we found an increase in the levels of laminin subunits (*i.e.*, LAMA1, LAMB1 and LAMC1) and nidogen-1, a protein tightly associated to laminin (Table 9).

Gene names	Protein names	T-test difference		-log P-value	
		HTT shRNA #1	HTT shRNA #2	HTT shRNA #1	HTT shRNA #2
SUV39H1	Histone-lysine N-methyltransferase SUV39H1	5.07	3.92	5.87	1.47
ARHGEF11	Rho guanine nucleotide exchange factor 11	2.05	1.97	2.70	1.83
EML1	Echinoderm microtubule-associated protein-like 1	1.87	1.79	3.19	2.36
TINAGL1	Tubulointerstitial nephritis antigen-like	1.51	1.60	2.70	1.77
LAMA1	Laminin subunit alpha-1	1.40	1.57	3.21	2.98
FOXK2	Forkhead box protein K2	0.95	0.88	1.96	1.82
LAMB1	Laminin subunit beta-1	0.82	1.26	1.68	2.43
NID1	Nidogen-1	0.77	0.99	1.93	1.96
LAMC1	Laminin subunit gamma-1	0.73	1.03	1.99	2.41
PRPS1	Ribose-phosphate pyrophosphokinase;Ribose-phosphate pyrophosphokinase 1	-0.51	-0.46	5.36	5.58
HLA-A;MHC class I HLA-A;HLA;HLA-A*0226;HLA-A*02	HLA class I histocompatibility antigen. A-2 alpha chain;HLA class I histocompatibility antigen. A-31 alpha chain;HLA class I histocompatibility antigen. A-29 alpha chain	-0.54	-0.44	3.46	2.71
GRN	Granulins;Acrogranin;Paragranulin;Granulin-1;Granulin-2;Granulin-3;Granulin-4;Granulin-5;Granulin-6;Granulin-7	-0.58	-0.68	1.72	2.00
F8A1	Factor VIII intron 22 protein	-0.81	-1.45	3.19	1.93
HTT;HD	Huntingtin	-0.87	-1.98	2.75	3.11
TAGLN	Transgelin	-1.47	-0.87	4.17	2.53

Table 9. List of proteins significantly changed in both HTT knockdown hESC lines (shRNA #1 and shRNA #2). Means are calculated from the log2 of LFQ values (LFQ HTT shRNA hESCs/Non-targeting shRNA hESCs). Statistical comparisons were made by Student's t-test (n= 5, FDR< 0.05). Red= upregulated, blue = downregulated.

Moreover, both HTT KD hESC lines exhibit a significant increase in SUV39H1, a H3K9 methyltransferase[146,147] that can form multimeric complexes with other H3K9 methylases such as SETDB1[148] and, therefore, could contribute to the aberrant H3K9me3 levels observed in HTT KD hESCs.

Although this proteomic experiment reveals moderate changes induced by loss of HTT in hESCs, it also presents important limitations for our study. For instance, this approach could be not sensitive enough to detect low abundant proteins in hESCs such as transcriptions factors or proteins upregulated during differentiation. We hypothesized that H3K9me3 repressive marks could further decrease the expression of these genes in hESCs or, more importantly, diminish their induction during differentiation. To test this hypothesis, we performed chromatin immunoprecipitation (ChIP) assays of hESCs using an antibody to H3K9me3. We found a >2-fold enrichment for H3K9me3 marks in 2006 regions upon HTT knockdown. Among them, 61 contained coding regions, of which GO biological process term analysis indicated the strongest enrichment for factors involved in transcriptional regulation (Figure 9).

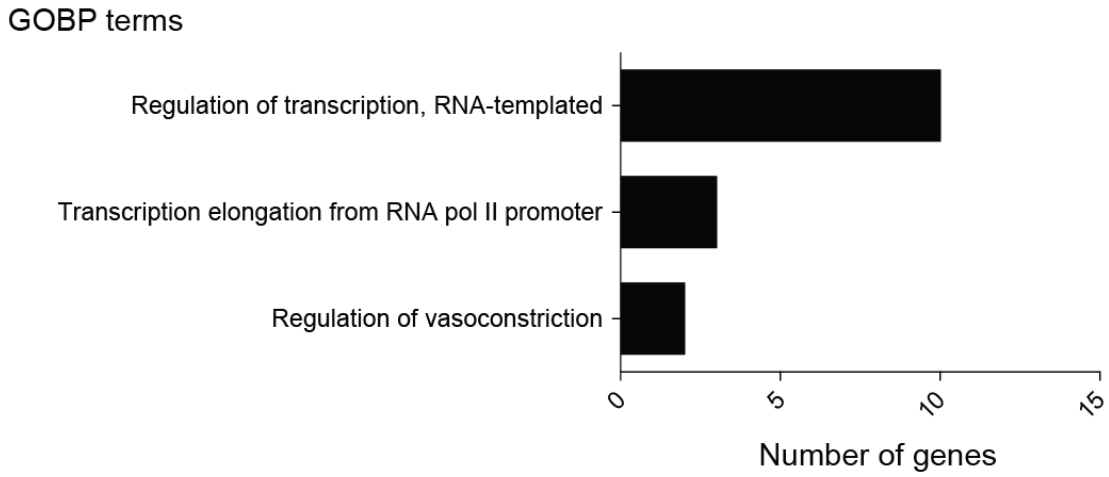

Figure 9. Significantly enriched GO Biological Processes in ChIP experiments with H3K9me3 antibody in HTT KD hESCs. The 61 genes enriched for H3K9me3 in ChIP experiments comparing HTT shRNA #1 and HTT shRNA #2 H9 hESCs with non-targeting shRNA H9 hESCs were analyzed for enriched GO Biological processes (p-value <0.05).

These regulators include 4 zinc finger proteins (ZNF135, ZNF559, ZNF572, ZNF844), 3 transcription elongation factors (TCEB3C, TCEB3CL, TCEB3CL2) and 3 developmental transcriptions (ASCL2, DLX3, GBX1). Besides these transcription factors, we found an enrichment for H3K9me3 in other genes important for nervous system formation, neuronal function, neurotransmission and synapse genesis/stabilization (*i.e.,*

CELSR1, CPEB1[149], SMC1B, ADRA2B, MRGPRX3). Dysfunctions in calcium homeostasis is one of the major alterations observed in HD neurons[150,90]. Interestingly, we have found H3K9me3 enrichment in genes involved in calcium metabolism such as OTOP1, ARPP21 (an inhibitor of calmodulin-dependent enzymes in striatal neurons[151]) and OPRD1, which regulates neurotransmitter release by modulating calcium currents[152]. Prompted by these findings, we asked whether H3K9me3 marks induced by HTT knockdown results in decreased expression of these genes. In particular, we focused on the transcription factors ASCL2 and GBX1 because their important role in neural development. Notably, we did not observe significant changes in the expression of these genes at the hESC stage (Figure 7 E). Given the low expression of these genes in hESCs is triggered upon neural differentiation (Figure 7 F), we hypothesized that H3K9me3 marks impair this induction. Indeed, loss of HTT in hESCs dramatically diminished their ability to induce the expression of ASCL2 and GBX1 during differentiation (Figure 7 F). In addition, we confirmed that HTT knockdown also resulted in diminished expression of other H3K9me3-enriched genes at the NPC stage (*i.e.*, SMC1B, ADGRB1) (Figure 10). Altogether, these results suggest that HTT regulates the expression of distinct neural genes via modulation of H3K9me3.

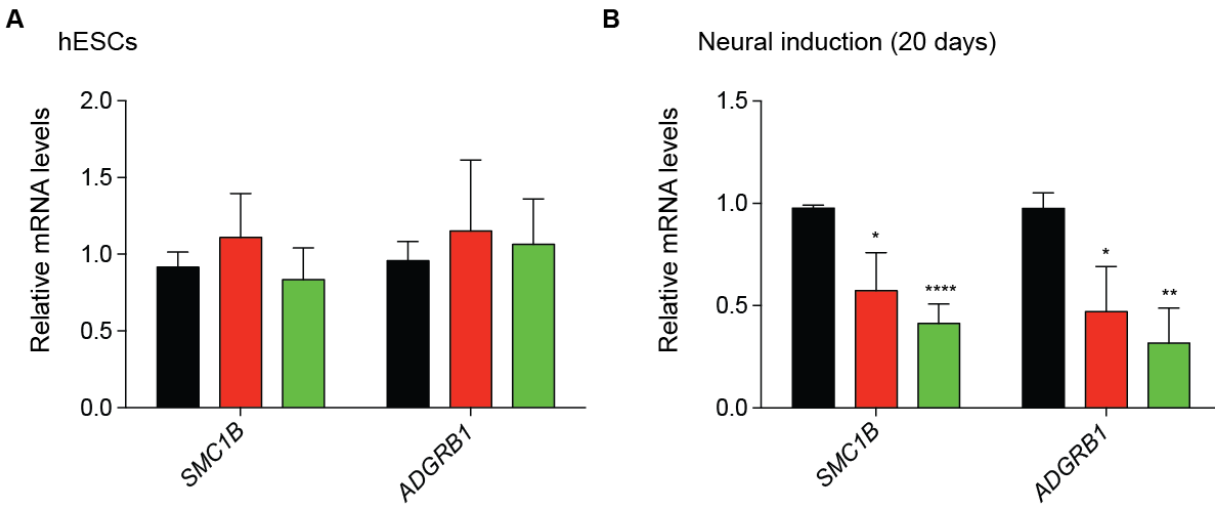

Figure 10. Knockdown of HTT in hESCs affects expression of SMC1B and ADGRB1 in their NPC counterparts. A, qPCR analysis of H9 hESCs. Graph (relative expression to non-targeting (NT) shRNA) represents the mean ± s.e.m. of three independent experiments with two biological replicates. B, qPCR analysis after 20 days of neural induction. Data (relative expression to NT shRNA cells) represent three independent experiments. All the statistical comparisons were made by Student's t-test for unpaired samples. P-value: *(P<0.05), **(P<0.01), **** (P<0.0001).

3.1.4 Knockdown of ATF7IP rescues H3K9me3 changes induced by mHTT

With the increased trimethylation of H3K9 in brain tissues of HD patients and mouse models[111–114], we asked whether HD-iPSCs also exhibit alterations in H3K9me3 levels. Indeed, we found that HD-iPSCs with medium (71) and large (180) polyQ expansions have increased H3K9me3 levels as detected by immunofluorescence (Figure 11 A).

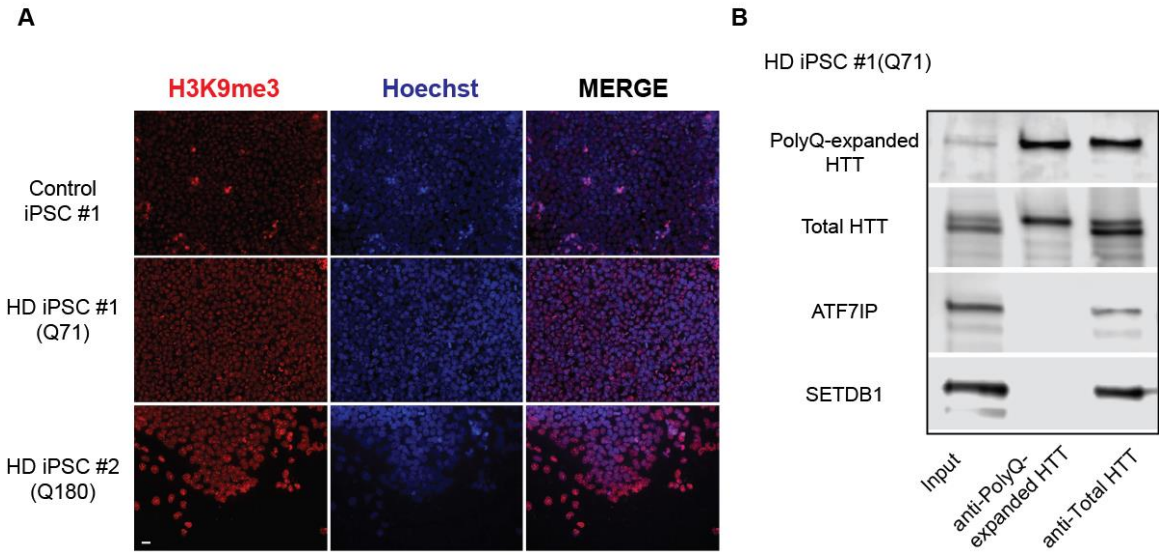

Figure 11. Mutations in HTT reduces its interaction with ATF7IP and induces H3K9me3 levels. A, Immunocytochemistry of control iPSC #1, HD-iPSCs #1 (Q71) and HD-iPSCs #1 (Q180) with antibody to H3K9me3. Hoechst staining was used as a marker of nuclei. Scale bar represents 20 µm. B, Co-immunoprecipitation with PolyQ-expanded HTT and total HTT antibodies in HD iPSC line #1 (Q71) followed by western blot with antibodies to PolyQ-expanded HTT, total HTT, ATF7IP and SETDB1. The images are representative of two independent experiments.

The HD-iPSC lines used in this study express one mutant copy of HTT but also one normal copy (Figure 11 B)[153], allowing us to assess differences in the interaction of ATF7IP with wild-type and mHTT within the same cell. To determine these differences, we performed co-immunoprecipitation experiments using either an antibody against total HTT or polyQ-expanded HTT[59]. After we confirmed the later antibody only immunoprecipitated mHTT, we performed western blot against ATF7IP and SETDB1 (Figure 11 B). Strikingly, we could not detect ATF7IP or SETDB1 in polyQ-expanded HTT pulldowns whereas total HTT pulldown showed interaction with the chromatin factor and the H3K9 methyltransferase (Figure 11 B), indicating that mutations in the polyQ stretch impairs HTT interaction with ATF7IP and SETDB1.

Prompted by these findings, we examined whether loss of ATF7IP diminishes trimethylation of H3K9 in NPCs derived from HD-iPSCs (Figure 12 A). Indeed, we found

that ATF7IP knockdown is sufficient to reduce H3K9me3 levels in HD-NPCs (Figure 12 A). Since differentiation of HD-iPSCs generate NPCs that already present HD-related changes[90,154], one step further was to rescue H3K9me3 levels at the pluripotent state.

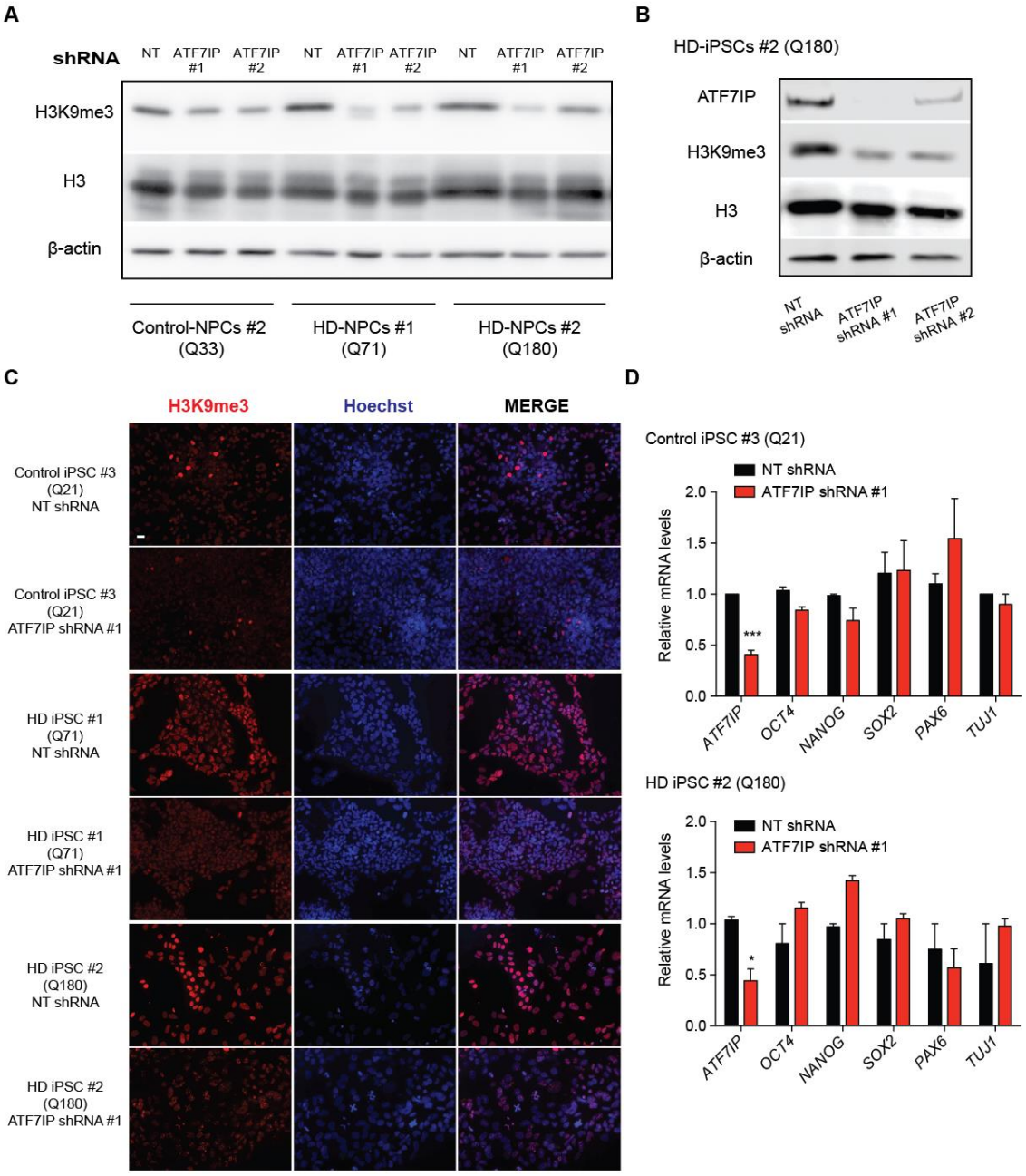

Figure 12. Knockdown of ATF7IP reduces H3K9me3 levels in HD-iPSCs without affecting their ability to differentiate into NPCs. A, 20 days after neural induction, knockdown of ATF7IP in NPCs decreases H3K9me3 levels as assessed by western blot experiments. The images are representative of two independent experiments. B, Western blot analysis of HD-iPSC line #2 (Q180) lysates with antibodies to H3K9me3 and total H3. β-actin is the loading control. C, Immunocytochemistry of control iPSC line #3 (Q21), HD-iPSC line #1 (Q71) and HD-iPSC line #2 (Q180) with antibody to H3K9me3. Hoechst staining was used as a marker of nuclei. Scale bar represents 20 µm. D, qPCR analysis of pluripotency (OCT4, NANOG, SOX2) and neuroectoderm (PAX6, TUBB3) markers in the indicated control and HD iPSC lines upon ATF7IP knockdown. Graphs (relative expression to NT shRNA) represent the mean ± s.e.m. (n= 3-4). All the statistical comparisons were made by Student's t-test for unpaired samples. P-value: *(P<0.05), **(P<0.01), ***(P<0.001), **** (P<0.0001).

Notably, knockdown of ATF7IP diminished H3K9me3 levels in HD-iPSCs (Figure 12 B-C and Figure 13). However, loss of ATF7IP did not affect the expression of distinct pluripotency and neuroectoderm markers in iPSC lines (Figure 12 D). Moreover, ATF7IP knockdown did not impair the ability of HD-iPSCs to differentiate into PAX6-positive cells (Figure 12 E-F). Collectively, these data suggest that modulation of ATF7IP can correct H3K9me3 dysregulation in HD-iPSCs without affecting their ability to generate neural cells.

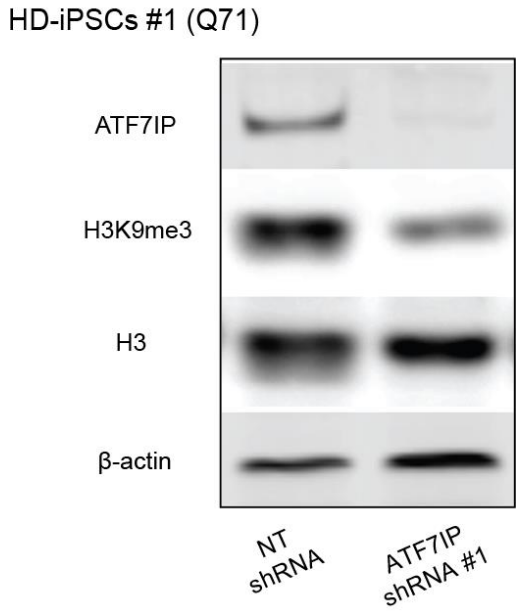

Figure 13. Loss of ATF7IP reduces H3K9me3 levels in HD-iPSCs. Western blot analysis of HD-iPSC line #1 (Q71) lysates with antibodies to H3K9me3 and total H3. β-actin is the loading control. Images are representative of two independent experiments.

3.2 The role of UBE2K in epigenetic control of embryonic stem cell differentiation

3.2.1 Loss of UBE2K impairs neurogenesis from hESCs

Previously, our laboratory has discovered that hESCs have an intrinsic ubiquitin proteasome system when compared to differentiated cells such as neurons. For instance, we observed changes in the expression of multiple E3 enzymes as well as several E2 enzymes (Table 10). Among them, we found increased levels of the E2 enzyme UBE2K. Previous studies reported that HTT interacts with UBE2K. Thus, we asked whether the high levels of UBE2K also participate in the epigenetic regulation of hESCs.

	NPCs		Neurons	
	T-test difference	q-value	T-test difference	q-value
UBE2C	-1.54	<0.0001	-2.47	<0.0001
UBE2G1	-1.15	0.0005	-1.43	0.0001
UBE2K	-1.04	0.0015	-1.03	0.0017
UBE2O	-0.75	0.0241	-1.39	0.0002
UBE2Z	-0.49	0.0164	-0.08	NS
UBE2S	-0.98	NS	-1.71	0.0012
UBE2V1	-0.01	NS	0.44	NS
UBE2V2	0.06	NS	0.40	0.0090
UBE2N	0.09	NS	0.04	NS
UBE2R2	0.14	NS	0.01	NS
UBE2M	0.20	NS	0.39	NS
UBE2Q1/UBE2Q2	0.28	NS	0.81	NS
UBE2I	0.83	0.0007	0.15	NS
UBE2L3	1.26	<0.0001	0.76	<0.0001

Table 10. Quantitative proteomic analysis of E2 enzymes comparing hESCs with their NPC and neuronal counterparts. UBE2K decreases during neural differentiation of hESCs. We used limma's moderated t-test to contrast hESCs (n= 9) versus NPCs (n= 5) and neurons (n= 6). Relative abundance differences are calculated from the log2 of label-free quantification (LFQ) values (LFQ NPCs/hESCs and LFQ Neurons/hESCs). Adjusted p-value (q-value) of <0.05 is considered significant. NS= non-significant.

First, we validated that the levels of UBE2K decrease during neural and terminal differentiation into neurons by western blot (Figure 14 A). The decrease in the protein amount of UBE2K correlated with a downregulation of the mRNA levels during differentiation (Figure 14 B).

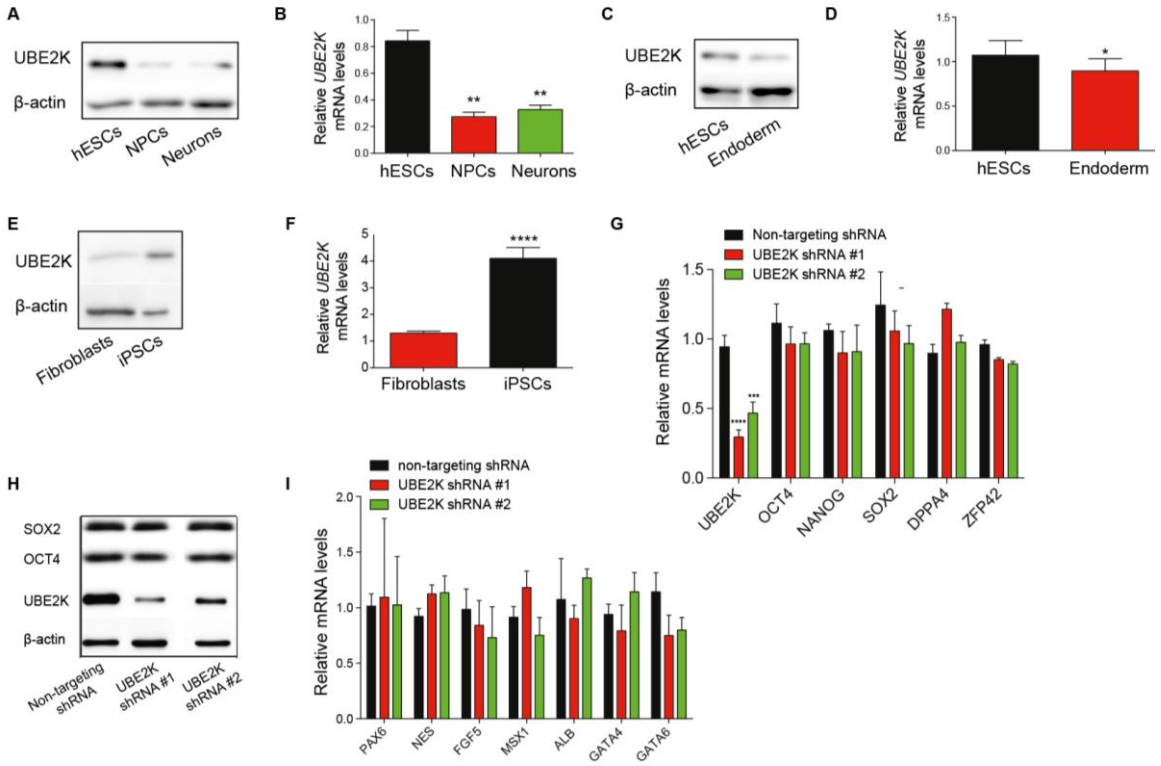

Figure 14. UBE2K is highly expressed in hESCs and iPSCs. A, B and E, Western blot analysis with antibody to UBE2K. β-actin is the loading control. B, UBE2K relative expression in NPCs and neurons compared to H9 hESCs represents the mean ± s.e.m. (n= 3 independent experiments). D, UBE2K relative expression in endoderm compared to H9 hESCs represents the mean ± s.e.m. (n= 5). F, UBE2K relative expression to HFF1 fibroblasts represents the mean ± s.e.m. (n= 6). G, qPCR analysis of UBE2K and pluripotency markers in H9 hESCs. Graph (relative expression to non-targeting shRNA) represents the mean ± s.e.m. of three independent experiments with three biological replicates. H, Western blot analysis with antibodies to UBE2K, SOX2 and OCT4. β-actin is the loading control. I, qPCR analysis of ectodermal (PAX6, NES, FGF5), mesodermal (MSX1) and endodermal (ALB, GATA4, GATA6) germ layer markers. Graph (relative expression to NT shRNA) represents the mean ± s.e.m. of three independent experiments with three biological replicates. All the statistical comparisons were made by Student's t-test for unpaired samples. P-value: *(P<0.05), **(P<0.01), ***(P<0.001), **** (P<0.0001).

Although to a lesser extent, UBE2K also decreased during differentiation into either endoderm or mesoderm (Figure 14 C-D). Moreover, high levels of UBE2K were reprogrammed in iPSCs derived from fibroblasts (Figure 14 E-F). Given the strong correlation between UBE2K expression and pluripotency, we hypothesized that increased levels of UBE2K could be required to maintain the undifferentiated state of hESCs. To assess this hypothesis, we generated stable knockdown hESC lines by using two independent *UBE2K* shRNA (Figure 14 G-H). Loss of UBE2K did not result in significant

differences in pluripotency markers compared to control hESCs (Figure 14 G-H). Moreover, we measured the expression of markers of the distinct germ layers and found no significant changes in endoderm, mesoderm and ectoderm markers (Figure 14 I). Since hESC lines can vary in their characteristics, we examined an independent line and obtained similar results (Figure 15).

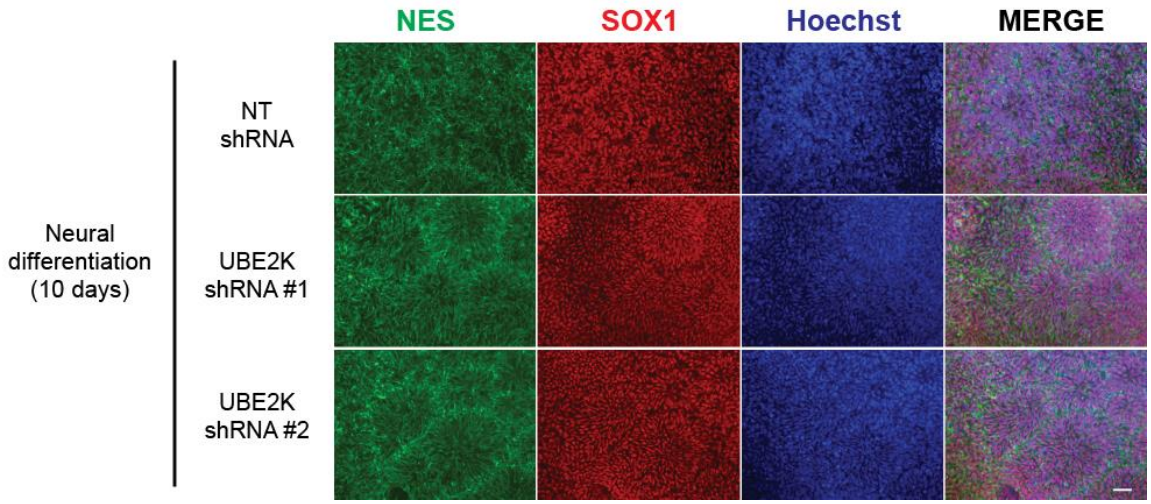

Figure 15. Loss of UBE2K does not impair the induction of NES and SOX1 during the early stages of differentiation into NPCs. After 10 days of neural induction, cells were assessed by immunofluorescence with NES, SOX1, and Hoechst staining. Scale bar represents 20 µm.

Although loss of UBE2K did not significantly alter the levels of pluripotency markers in hESCs, another possibility is that UBE2K determines their ability to differentiate into distinct lineages. Given that UBE2K catalyzes the synthesis of Lys-48-linked polyubiquitin chains targeting proteins for proteasomal degradation [123,155] and increased proteasome activity is required for neurogenesis from hESCs [156,157], we focused on the neural lineage. For this purpose, we performed neural induction and monitored the expression of PAX6, an early marker of neuroectodermal differentiation [91,92]. After 10 days of neural induction, PAX6 levels were triggered at the same extent in both control and UBE2K knockdown (KD) hESCs resulting in cultures of ~100% PAX6-positive cells (Figure 16 A-C). We also analyzed the levels of other neural and neuronal markers and found no significant differences at this stage (Figure 16 C and Figure 15). These results indicate that UBE2K is not required for the commitment of hESCs to a neuroectoderm fate. However, we observed dramatic differences when we further differentiated these cells (20 days on neural induction treatment) to obtain NPCs with the ability to generate terminally differentiated neurons (Figure 16 D-G). At this stage, control NPCs decreased the expression of the early neural marker PAX6 whereas the levels of NPC (*e.g.*, nestin, SOX1) and neuronal markers are upregulated (Figure 16 F-G). In contrast, UBE2K KD cells maintained high levels of PAX6 whereas the levels of neural and neuronal markers are significantly lower compared with control NPCs (Figure 16 D-G). Upon neuronal differentiation treatment, UBE2K KD cells did not develop neuronal extensions (Figure 16 H) and showed a dramatic impairment in the expression of neuronal markers such as MAP2, NEFL and synaptic proteins while retaining high levels of PAX6 expression (Figure 16 H-K). Taken together, these data suggest a critical role of UBE2K in maintaining the ability of hESCs to differentiate into NPCs with intact neurogenic properties.

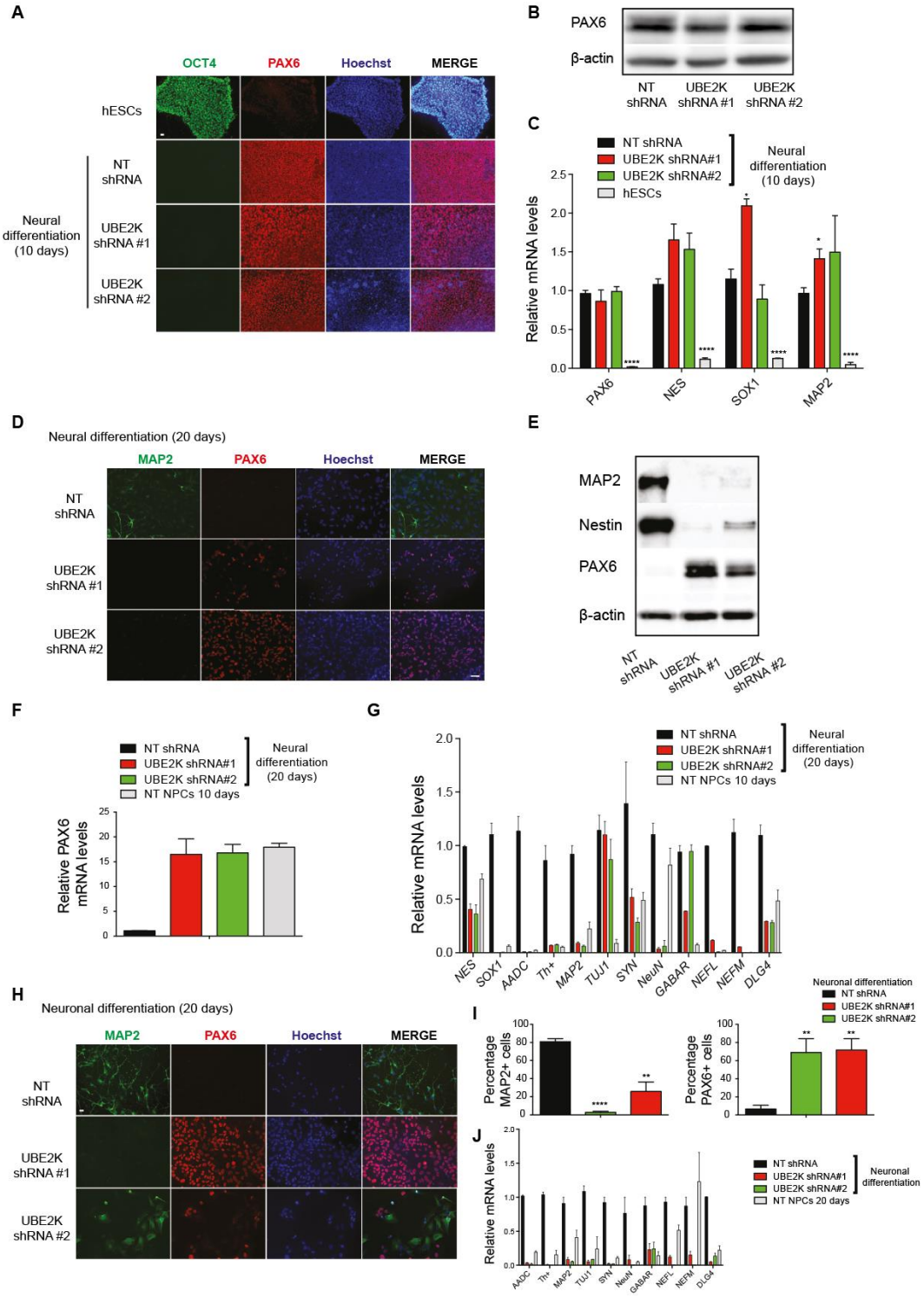

Figure 16. Loss of UBE2K impairs neurogenesis from hESCs. A, After 10 days of neural induction, cells were assessed by immunofluorescence with OCT4, PAX6, and Hoechst staining. Scale bar represents 20 µm. B, Western blot analysis of NPCs after 10 days of neural induction with antibody to PAX6. β-actin is the loading control. C, qPCR analysis after 10 days of neural induction. Graph (relative expression to NT shRNA cells) represents the mean ± s.e.m. of three independent experiments with three biological replicates. D, After 20 days of neural induction, cells were assessed by immunofluorescence with OCT4, PAX6, and Hoechst staining. Scale bar represents 40 µm. E, Western blot analysis of NPCs after 20 days of neural induction with antibodies to MAP2, NES, PAX6 and β-actin. F, G, qPCR analysis after 20 days of neural induction. Graph (relative expression to NT shRNA cells) represents the mean ± s.e.m. of XX independent experiments with three biological replicates. H, After 3 weeks of neuronal induction, cells were assessed by immunofluorescence with MAP2, PAX6, and Hoechst staining. Scale bar represents 20 µm. I, Percentage of MAP2 and PAX6-positive cells/total nuclei after three weeks of neuronal induction (mean ± s.e.m. of two independent experiments, 300-400 total cells per experiment). All the statistical comparisons were made by Student's t-test for unpaired samples. P-value: *(P<0.05), **(P<0.01), ***(P<0.001), **** (P<0.0001).

3.2.2 Knockdown of UBE2K induces trimethylation of H3K9 and impairs induction of neuronal genes

To determine the mechanism(s) by which UBE2K impinges upon hESC function, we performed co-immunoprecipitation experiments followed by a single shot label-free proteomic approach (Table 11).

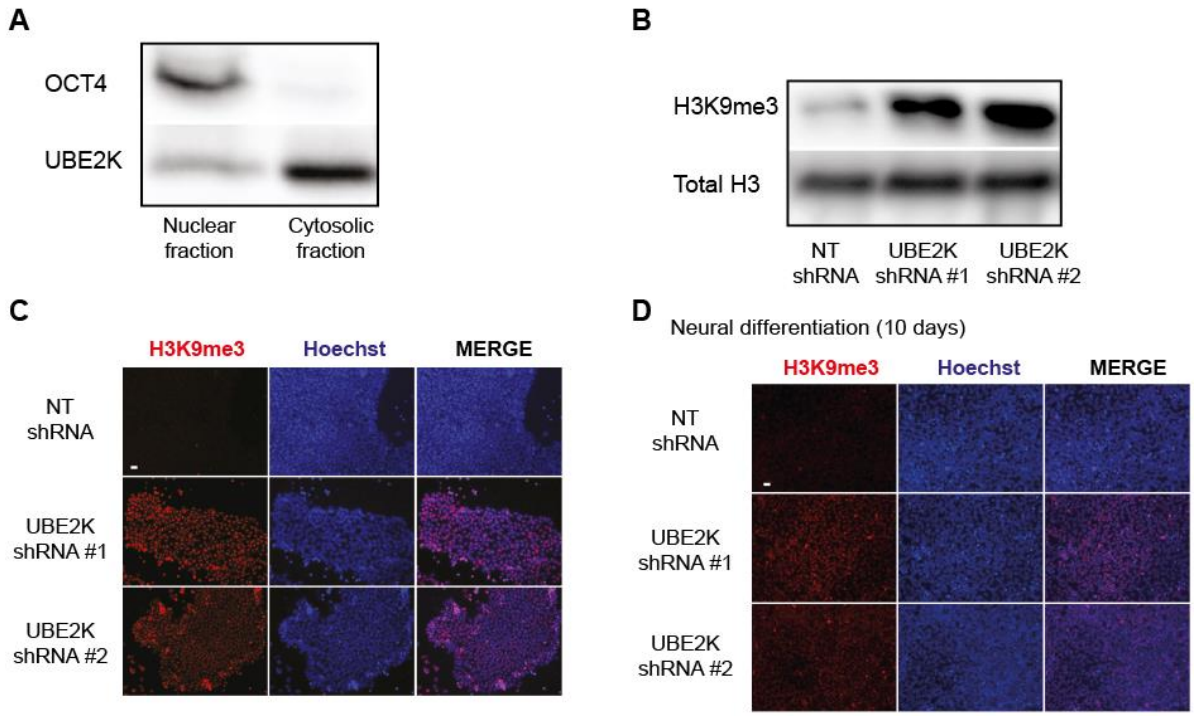

Figure 17. UBE2K regulates trimethylation of H3K9. A, Western blot analysis of nuclear and cytosolic fractions from H9 hESCs with antibodies to OCT4 and UBE2K. B, Western blot analysis of H9 hESCs with antibodies to H3K9me3 and total histones H3. C, Immunocytochemistry of H9 hESC cultures with antibody to H3K9me3 and Hoechst staining. Scale bar represents 20 µm. D, After 3 weeks of neuronal induction, cells were assessed by immunofluorescence with H3K9me3 and Hoechst staining. Scale bar represents 20 µm.

We observed that UBE2K, mitochondrial fission factor (MFF) and the histone H3.3 are the most enriched proteins upon UBE2K co-immunoprecipitation (Table 11). H3.3 is a highly conserved histone that differs from the canonical histones H3.1/H3.2 by only four to five amino acid, respectively. Interestingly, H3.3 is involved in cell differentiation and cell reprogramming[158,159]. In support of a potential role of UBE2K in the nucleus, we detected significant amounts of this E2 enzyme in nuclear fractions of hESCs (Figure 17 A).

Gene names	Protein names	T-test difference	-log P-value
MFF	Mitochondrial fission factor	8.68	3.24
UBE2K	Ubiquitin-conjugating enzyme E2 K	5.29	2.74
H3F3B;H3F3A;H3F3C	Histone H3;Histone H3.3;Histone H3.3C	5.07	1.47
C14orf166	UPF0568 protein C14orf166	4.78	1.66
HCFC1	Host cell factor 1	4.41	2.27
DYNLT1	Dynein light chain Tctex-type 1	3.76	2.23
ATP1A1	Sodium/potassium-transporting ATPase subunit alpha-1	3.71	2.85
PTCD3	Pentatricopeptide repeat domain-containing protein 3, mitochondrial	3.31	2.72
CSNK2A1;CSNK2A3	Casein kinase II subunit alpha;Casein kinase II subunit alpha 3	3.04	2.39
CPNE1	Copine-1	2.99	2.79
PIP4K2A;PIP4K2B	Phosphatidylinositol 5-phosphate 4-kinase type-2 alpha/beta	2.71	2.71
PLCB4	1-phosphatidylinositol 4,5-bisphosphate phosphodiesterase beta-4	2.39	3.34

Table 11. Protein interactors of UBE2K in H9 hESCs. Protein label-free quantification (LFQ) from co-immunoprecipitation (co-IP) experiments with UBE2K antibody compared to control co-IP with FLAG antibody (n=3, Student's t-test, FDR< 0.05 is considered significant).

With the strong interaction between UBE2K and H3.3, we asked whether loss of UBE2K modulates epigenetic marks of pluripotent stem cells. In hESCs, chromatin repressive marks such as H3K9me3 are usually reduced whereas the levels of transcriptional activations marks are globally increased[101,106] Notably, knockdown of UBE2K induced a dramatic increase in the levels of H3K9me3 in two independent hESC lines as well as iPSCs (Figure 17 B-C). Once differentiated into NPCs, UBE2K KD cells maintained high levels of H3K9me3 compared with control cells (Figure 17 D). Taken together, these data indicate that UBE2K regulates the levels of the transcriptional repressive mark H3K9me3 in hESCs and this epigenetic alteration is transmitted to their neural counterparts.

To assess whether increased H3K9me3 levels impair the expression of specific genes, we performed chromatin immunoprecipitation (ChIP) in UBE2K KD hESCs. We found a >2-fold enrichment for H3K9me3 marks in 71 genes upon UBE2K knockdown. Among them, GO biological process term analysis indicated the strongest enrichment for genes involved in transcriptional regulation (Figure 18).

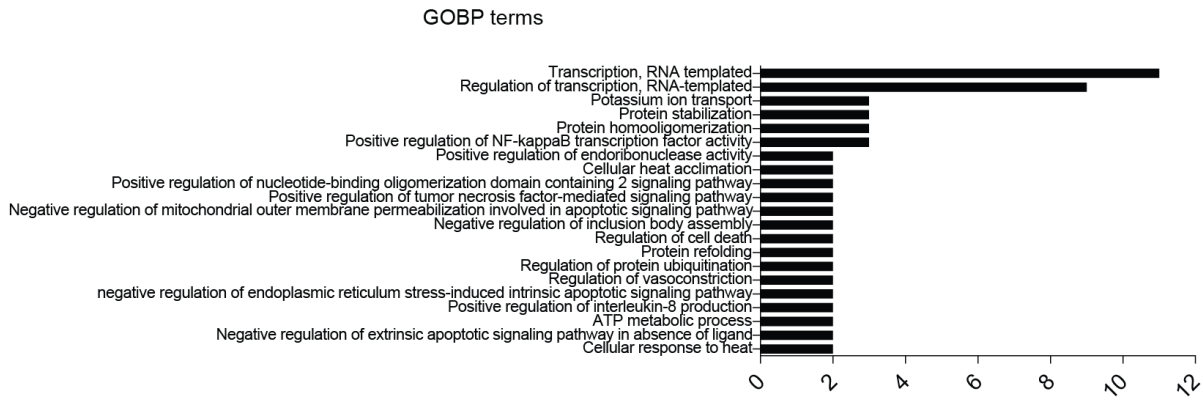

Figure 18. Significantly enriched GO Biological Processes in UBE2K KD hESCs in ChIP experiments with H3K9me3 antibody. The 71 genes enriched for H3K9me3 in ChIP experiments comparing UBE2K shRNA #1 and UBE2K shRNA #2 H9 hESCs with non-targeting shRNA H9 hESCs were analyzed for enriched GO Biological Processes (p-value <0.05 is considered significant).

These regulators include 7 zinc finger proteins (ZNF263, ZNF274, ZNF416, ZNF559, ZNF562, ZNF844, ZNF879), the transcription factor GBX1 and the bHLH transcription cofactor HES6. GBX1 is highly expressed in the neuroectoderm and modulates midbrain/forebrain formation by determining the positioning of the midbrain-hindbrain boundary organizer in the early neural plate[55]. HES6 promotes neuronal differentiation by allowing the transcription factor ASCL1 to induce the expression of genes required for neurogenesis at early stages of development [160]. Besides these transcription factors, loss of UBE2K induced an enrichment for H3K9me3 marks in several genes involved in nervous system formation, neuronal function, establishment of neuronal connections, synapse stabilization, and neurotransmission (*e.g.,* ADRA2B, CELSR1, CPEB1[56], KCNA3, KCNA5, KCNF1, OPRD1[58], PCDHB15, SMC1B, and the GABA receptor subunit GABRR1). Prompted by these findings, we tested whether H3K9me3 modifications result in decreased expression of these pro-neural genes by quantitative analysis of the transcriptome in UBE2K KD hESCs. Integrated analysis of ChIP and transcriptomics data did not show significant downregulated expression of most of the genes enriched for H3K9me3 in UBE2K KD hESCs. Taken together, our data indicate that high levels of UBE2K in hESCs maintain low levels of H3K9me3 marks in key pro-neural and neuronal genes.

3.2.3 UBE2K modulates JARID2 levels

To determine potential targets of UBE2K involved in the trimethylation of H3K9, we performed quantitative proteomics comparing control hESCs with UBE2K KD hESCs (Table 12). Interestingly, loss of UBE2K induced an increase in the levels of the histone methyltransferase regulator JARID2 and also METTL7A, a methyltransferase of unknown function.

List of proteins upregulated upon knockdown of UBE2K in hESCs

Gene names	Protein names	T-test difference		-log P-value	
		UBE2K shRNA 1	UBE2K shRNA 2	UBE2K shRNA 1	UBE2K shRNA 2
PDIA3	Thioredoxin	3.766822433	3.537664413	1.630461609	1.526517826
ACIN1	Apoptotic chromatin condensation inducer in the nucleus	3.113811111	1.800709534	2.16746478	0.799576478
CAMKMT	Calmodulin-lysine N-methyltransferase	1.810609055	1.395643234	3.519090939	2.557966309
PTPRK;DKFZp686C2268	Receptor-type tyrosine-protein phosphatase kappa	1.649758911	1.251145172	1.519857384	1.189812485
CHTF8	Chromosome transmission fidelity protein 8 homolog isoform 2	1.510147858	0.980948257	1.386838829	0.849038968
ITFG3	Protein ITFG3	1.507901764	1.077629471	1.917895863	1.352574137
MTX2	Metaxin-2	1.472535706	1.199636841	1.9143298	2.299868229
		1.15671196	0.963488007	1.337530165	1.669025503
RTN3	Reticulon-3	1.113307571	0.349462128	1.973097302	1.425925157
AKT2	RAC-beta serine/threonine-protein kinase	1.075060272	0.823015213	1.275061416	1.19066161
KRR1	KRR1 small subunit processome component homolog	0.980365753	0.800683975	1.43367122	1.150263958
PEX6	Peroxisome assembly factor 2	0.947927475	0.614145279	1.658016293	1.818815276
HNRPK		0.944860077	0.994746399	2.144466584	3.701768666
PPP1CC	Serine/threonine-protein phosphatase;Serine/threonine-protein phosphatase PP1-gamma catalytic subunit	0.910209656	0.740813446	4.434130041	4.19317083
PRR12	Proline-rich protein 12	0.891211319	0.916115952	1.533050423	1.772712042
METTL7A	**Methyltransferase-like protein 7A**	**0.888065338**	**0.410329056**	**3.705815148**	**1.433225187**
TINAGL1	Tubulointerstitial nephritis antigen-like	0.850399399	1.655990982	1.410828002	1.582731679
LAMTOR2	Ragulator complex protein LAMTOR2	0.794325256	0.680993652	2.23092675	2.226474669
ZNF423	Zinc finger protein 423	0.787024689	0.67005806	1.438159146	0.921969238
TIPIN	TIMELESS-interacting protein	0.693198013	0.903326797	2.01428658	2.025764635
ATG4B	Cysteine protease ATG4B	0.689982224	0.590264511	1.972398067	1.764654486
SRPRB	Signal recognition particle receptor subunit beta	0.670551682	0.735467911	1.910974477	2.170009455
TWF1	Twinfilin-1	0.666596985	0.427342224	3.466383113	2.00576648
PTPRZ1	Receptor-type tyrosine-protein phosphatase zeta	0.65698967	0.482600021	2.316697561	1.575171444
PRIM1	DNA primase;DNA primase small subunit	0.63924942	0.405867386	2.609932771	1.297262912
BANF1	Barrier-to-autointegration factor;Barrier-to-autointegration factor, N-terminally processed	0.63624382	0.40088501	2.816604112	1.731231712
MYO1D;DKFZp686A01173	Unconventional myosin-Id	0.632105637	0.653863525	1.70442979	1.684702669
WRNIP1	ATPase WRNIP1	0.615055847	0.590971756	1.639858688	1.583248395
RPN2	Dolichyl-diphosphooligosaccharide--protein glycosyltransferase subunit 2	0.609716034	0.47336998	1.593784272	1.293983071
AP2S1	AP-2 complex subunit sigma	0.586634827	0.466293335	1.499416999	1.83993129
PPFIA1	Liprin-alpha-1	0.554604721	0.476158905	2.809737533	2.499028144
EHD4	EH domain-containing protein 4	0.54529686	0.284342194	2.78753207	1.887558689
JARID2	**Protein Jumonji**	**0.538499069**	**0.643983459**	**2.415416658**	**2.090819064**
USP47	Ubiquitin carboxyl-terminal hydrolase 47	0.536531067	0.296683121	3.010269694	1.567925445
PDS5B	Sister chromatid cohesion protein PDS5 homolog B	0.511237717	0.460929871	1.775184545	2.458753426
DPH2	Diphthamide biosynthesis protein 2	0.497331238	0.820111465	1.968375602	3.884416406
QTRTD1	Queuine tRNA-ribosyltransferase subunit QTRTD1	0.458888245	0.388759232	2.644654471	1.832552553
RABEP1	Rab GTPase-binding effector protein 1	0.445495987	0.549682617	1.788886809	1.796082833
NAA38;LSM8	N-alpha-acetyltransferase 38, NatC auxiliary subunit	0.39982872	0.551329803	2.235873173	3.890010684
PPP1R14B	Protein phosphatase 1 regulatory subunit 14B	0.38158226	0.381012344	2.195343025	1.719191952
RPRC1;MAP7D1	MAP7 domain-containing protein 1	0.376734161	0.356851196	2.11082335	2.381141628
KIAA1068;NUDCD3	NudC domain-containing protein 3	0.37326622	0.39627533	3.152229659	3.267324489
MASTL	Serine/threonine-protein kinase greatwall	0.364876556	0.264849472	2.200170848	2.276245822
POU2F1;POU2F3;POU2F2	POU domain, class 2, transcription factor 1;POU domain, class 2, transcription factor 3;POU domain, class 2, transcription factor 2	0.349388885	0.288489151	3.30995442	2.093793691
ISOC2	Isochorismatase domain-containing protein 2, mitochondrial	0.348838043	0.475136185	2.388902268	1.892604518

List of proteins downregulated upon knockdown of UBE2K in hESCs

Gene names	Protein names	T-test difference		-log P-value	
		UBE2K shRNA 1	UBE2K shRNA 2	UBE2K shRNA 1	UBE2K shRNA 2
CDC42BPG	Serine/threonine-protein kinase MRCK gamma	-3.308805466	-3.671895218	2.313874392	2.572145401
GUF1	Translation factor GUF1, mitochondrial	-2.985452271	-2.228926849	5.683319128	1.427168378
IREB2	Iron-responsive element-binding protein 2	-2.74932785	-2.22108078	1.486280326	0.961723146
GPD1L	Glycerol-3-phosphate dehydrogenase 1-like protein	-2.642490005	-2.724894333	1.978762322	2.002318405
HNRNPA2B1		-2.283238602	-1.785467529	1.536767217	1.102754473
VSIG1	V-set and immunoglobulin domain-containing protein 1	-2.110469818	-2.415558243	1.521879169	1.718514194
COL1A1	Collagen alpha-1(I) chain	-1.897432709	-1.708493805	3.887163273	1.702390225
ELOF1	Transcription elongation factor 1 homolog	-1.801469803	-1.104278183	1.79999936	0.891784785
CALR		-1.748747635	-1.683153152	1.10158368	1.220123527
ARF3	ADP-ribosylation factor 3	-1.706129074	-1.226445007	2.075322275	0.897027955
EIF4ENIF1	Eukaryotic translation initiation factor 4E transporter	-1.609062195	-0.896789551	1.53116842	1.000597751
EEF1D		-1.547586441	-1.001054382	1.35970928	0.825693509
C1orf52	UPF0690 protein C1orf52	-1.506440353	-1.041460037	1.82405246	1.090503195
AGPAT5	1-acyl-sn-glycerol-3-phosphate acyltransferase epsilon	-1.483044434	-1.491923141	2.202672297	1.222544224
SNRPA	U1 small nuclear ribonucleoprotein A	-1.443012238	-1.914863968	1.216235856	4.165111673
OLFML3	Olfactomedin-like protein 3	-1.423392868	-0.385329437	6.236388008	1.90023741
		-1.379608154	-0.822431564	2.067147219	1.75288053
KRI1	Protein KRI1 homolog	-1.342892838	-0.750530624	2.182094652	0.909809438
SURF2	Surfeit locus protein 2	-1.283132172	-0.97299118	2.910134881	3.963727616
TAGLN	Transgelin	-1.279749298	-1.79088974	2.445198055	4.801074663
ASF1B	Histone chaperone ASF1B	-1.272428131	-1.816962433	1.325590561	1.796750484
NRBF2	Nuclear receptor-binding factor 2	-1.193226242	-1.678313446	1.983198401	3.260019387
		-1.183207321	-0.5986303	3.155417212	1.009639781
APOL2	Apolipoprotein L2	-1.135781479	-0.492294693	1.835699686	2.21891893
APOBEC3B	DNA dC->dU-editing enzyme APOBEC-3B	-1.06306076	-0.392131424	2.282506642	1.196435707
SF3B4	Splicing factor 3B subunit 4	-1.054370117	-1.851135635	1.377491857	1.676088019
MRPL52	39S ribosomal protein L52, mitochondrial	-0.972199631	-1.11235466	1.259933299	1.501125917
UBE2K;HIP2	Ubiquitin-conjugating enzyme E2 K	-0.942032242	-0.235050583	6.052221883	2.122918185
GTSE1	G2 and S phase-expressed protein 1	-0.92220459	-0.633312607	1.963942384	2.022792307
BTF3		-0.90814476	-1.339248657	1.619096575	1.154610138
GRN	Granulins;Acrogranin;Paragranulin;Granulin-1;Granulin-2;Granulin-3;Granulin-4;Granulin-5;Granulin-6;Granulin-7	-0.90234642	-0.581676102	1.9758326	1.215667468
SERPINB9	Serpin B9	-0.89896431	-0.352035522	4.640291608	2.896273366
MRPL30	39S ribosomal protein L30, mitochondrial	-0.885395813	-1.076121902	1.343190499	1.396136452
HMGN1	Non-histone chromosomal protein HMG-14	-0.861757278	-0.705495453	1.38586805	1.63800677
LMCD1	LIM and cysteine-rich domains protein 1	-0.817088699	-0.889386368	3.024417364	0.919913399
GJA1	Gap junction protein;Gap junction alpha-1 protein	-0.814079285	-0.369154358	3.344818885	1.723617457
VIL1	Villin-1	-0.805224991	-0.731871033	2.803879789	2.37242862
RAB5C	Ras-related protein Rab-5C	-0.800119781	-0.295869827	1.9101014	1.479999516
DPYSL3	Dihydropyrimidinase-related protein 3	-0.769957733	-0.644638824	1.574167923	1.350460988
MRPL48	39S ribosomal protein L48, mitochondrial	-0.767944717	-0.817710876	1.331264178	1.169159941
	6-phosphogluconate dehydrogenase, decarboxylating	-0.734509277	-0.657603836	2.06917207	1.556442553
ASS;ASS1	Argininosuccinate synthase	-0.729299545	-0.60763092	2.973673749	2.408142227
SLC7A5;lat1	Large neutral amino acids transporter small subunit 1	-0.704777527	-0.653501511	1.887752441	2.015965765
ANXA3	Annexin A3;Annexin	-0.701567078	-0.751037216	2.773724515	3.916248612
CCDC55;NSRP1	Nuclear speckle splicing regulatory protein 1	-0.629239655	-0.801021957	1.84430775	1.543878202
C19orf43	Uncharacterized protein C19orf43	-0.575564194	-0.444667053	2.310459425	2.376381253
PRKCA	Protein kinase C;Protein kinase C alpha type	-0.573003387	-0.74417305	1.718180754	0.970319574
TPM1		-0.551699829	-0.428111267	3.778522928	1.614132226
LIMD2	LIM domain-containing protein 2	-0.545282745	-0.400942612	1.681931325	1.537445547
MRPS7	28S ribosomal protein S7, mitochondrial	-0.54435997	-0.342670441	1.715134625	1.827136345
DNAJC3	DnaJ homolog subfamily C member 3	-0.522000504	-0.360580444	2.250784455	1.880106024
RPL19	Ribosomal protein L19;60S ribosomal protein L19	-0.513430786	-0.426737213	1.773519636	1.662895384
SF1		-0.513362885	-0.576076126	1.630620442	1.132367133
PC4;SUB1	Activated RNA polymerase II transcriptional coactivator p15	-0.50621376	-0.447818375	3.094400122	3.076523262
GULP1	PTB domain-containing engulfment adapter protein 1	-0.50409317	-0.650629044	2.120089789	2.684650973
LYAR	Cell growth-regulating nucleolar protein	-0.485778046	-0.38442688	2.012341163	1.308440452
RPL26;KRBA2	60S ribosomal protein L26	-0.468328857	-0.380661011	1.94033114	2.190294946
CALD1		-0.465930557	-0.502504349	2.83523892	3.597965113
EIF1AX;EIF1AY	Eukaryotic translation initiation factor 1A, X-chromosomal;Eukaryotic translation initiation factor 1A, Y-chromosomal	-0.419506454	-0.319515991	2.15547511	1.344957833
PSMD9	26S proteasome non-ATPase regulatory subunit 9	-0.413750458	-0.364612961	2.295663822	1.671597156
RPS6	40S ribosomal protein S6	-0.404511261	-0.2632164	2.20789106	1.729197619
TPD52		-0.403290176	-0.440826416	2.288699898	2.470097197
HLA-A	HLA class I histocompatibility antigen	-0.382816315	-0.420048141	2.278680423	2.376543337
GIPC1	PDZ domain-containing protein GIPC1	-0.377431488	-0.373831177	2.241864505	1.547179196
NUDC	Nuclear migration protein nudC	-0.371879196	-0.368219376	3.021408182	1.562156434
PSPH	Phosphoserine phosphatase	-0.348099518	-0.46913414	2.873791518	2.358554325
RPS20	40S ribosomal protein S20	-0.342092133	-0.356018066	2.435034365	2.564622818
EZR;EZR-ROS1	Ezrin;Tyrosine-protein kinase receptor	-0.308622742	-0.210961151	3.806140691	3.632891252

Table 12. Quantitative proteomic analysis of UBE2K KD hESCs. Knockdown of UBE2K induces an increase in the levels of JARID2 and METTL7A. Data represent the Student's t-test difference. Means are calculated from the log2 of label-free quantification (LFQ) values (LFQ UBE2K shRNA hESCs/Non-targeting shRNA hESCs). Statistical comparisons were made by Student's t-test (n=3, FDR< 0.05 is considered significant).

4 Discussion

4.1 HTT

The ubiquitous subcellular localization of HTT does not facilitate the definition of its function. Multiple roles have been described for wild-type HTT such as vesicular transport[51,62,64,161] and mitotic spindle orientation[72]. Furthermore, HTT functions as a scaffolding protein to induce selective autophagy[161]. In addition, HTT modulates gene expression by binding numerous transcription factors and regulators such as the cAMP-response element (CREB)-binding protein (CBP), specificity-protein 1 (SP1), neuroD1, p53 or the nuclear factor-kB (NF-kB)[6]. Loss of transcriptional function of HTT could contribute to explain the transcriptional dysregulation observed in postmortem HD brains and distinct HD mouse models[6,109].

In this study, we identified Activating transcription factor 7-interacting protein 1 (ATF7IP), also known as MBD1-containing chromatin-associated factor 1 (MCAF1) or ATFa-associated modulator (AM), as a new interactor of HTT (Figure 1). In addition, our co-immunoprecipitation experiments followed by western blot indicate that HTT could form a complex together with ATF7IP and SETDB1 (Figure 1 G). ATF7IP regulates chromatin formation by binding and directing transcriptional factors to the general transcriptional machinery. The protein thereby impinges transcriptional regulation. Depending on the subcellular conditions the protein can operate either as an activator or a repressor[116–119]. The mechanism for gene silencing by ATF7IP via methylation is explained in the following paragraphs.

ATF7IP controls methylation based transcriptional repression through interaction with the methyl-CpG binding domain 1 (MBD1) (hence its synonym MCAF1). The multifunctional nuclear protein acts as a transcriptional regulator and transcriptional repression domain. It embodies two conserved domains that interact with MBD1 and transcription factor Sp1. Like ATF7IP, SP1 can activate or repress transcription depending on the context. ATF7IP acts like a co-activator and enables Sp1-guided transcription. By modifying Sp1 on methylated promoter regions ATF7IP blocks transcription activity [116].

Histone methylation is essential for chromatin structure and function. The histone methyltransferase (HMTase) activity of Histone-lysine N-methyltransferase SETDB1 (SETDB1) depends on the assistance of ATF7IP. It triggers the transformation of the dimethyl (H3K9me2) to the trimethyl state (H3K9me3) by increasing the turnover rate of the reaction, both in vitro and in vivo. The functional consequence of H3K9 trimethylation on the promoter region is transcriptional repression[141]. Moreover, ATF7IP aids in the gene expression of the two telomerase enzymes by specificity protein 1 (TERT) and interaction with SP1 in cancer cells. Knockdown of ATF7IP leads also to decreased levels of transcriptionally active RNA polymerase II and the general transcription factor ERCC3 in the TERT promoter and consequently diminished telomerase activity. Interestingly, in naturally occurring abnormal proliferative cancer cells ATF7IP was regularly found to be overexpressed[118].

Notably, although not further studied, previous findings already indicated a link between HD age of onset and genetic variation within the ATF7IP gene: ATF7IP genetic variation correlated with age of onset in HD patients[162]. Together with our data, this suggests that ATF7IP is a potential modifier of the HD chromatin landscape in stem cells that determines the epigenetic changes of the disease: Knockdown of ATF7IP in hESCs decreased nuclear SETDB1 levels as well as trimethylation of H3K9 (Figure 3 A-B), which indicates the ATF7IP also regulates H3K9me3 in these cells. ATF7IP interacts with the H3K9 methyltransferase of SETDB1, facilitating H3K9 trimethylation and heterochromatin formation[116,141]. Moreover, ATF7IP stabilizes SETDB1 in the nucleus of human cell lines[144]. We also found that H3K9me3 levels upon HTT knockdown were drastically increased (Figure 3 D-E) in two independent hESC lines (Figure 4 A-B). Interestingly this effect was also observed when the cells were differentiated into NPCs (Figure 3 F-G).

Among polyQ diseases exhibiting epigenetic imbalances, HD is the one most commonly studied. There are different classes of epigenetic mechanisms. DNA modifications entail methylation and hydroxymethylation, post-translational histone modifications entail acetylation, di- and tri-methylation, phosphorylation, ubiquitylation, SUMOylation and ADP ribosylation and lastly, the exchange of the histone variants H1, H3.3, H2A.Z, H2A.X[109]. Our findings show for the first time that H3K9 is induced by loss of HTT. This is a novel observation that however is in a larger context of broad epigenetic

modulations induced by loss of HTT. The loss of HTT leads to failure of global H3K27 trimethylation in embryoid bodies (EBs) derived from ESCs. However, H3K27 dimethylation was unaffected in HTT null EBs. H3K27 is a site predominantly targeted by PRC2 that has enzymatic activity to assist in gene silencing. Loss of HTT in embryos showed parallel phenotypes to those with lack of PRC2, although they were not as severe as in PRC2 null embryos. This shows that HTT only aids PRC2 in order to stimulate its methyltransferase activity, and does not work as its core component that is directly responsible for methylation. Specifically the polyQ region is interacting with PRC2, leading to more trimethylation of H3K27 with expanding polyQ tract[163]. In contrast, Htt CAG size, though changing histone H3K27me3, is prominently associated with altered histone H3K4me3 at 'active' loci[67].

Via ChIP-Seq we found 61 genes involved in transcriptional regulation (Figure 9) with increased H3K9 trimethylation at promoter sites. H3K9 trimethylation is a mark of transcriptional repression and in the stages of neuronal differentiation we found indeed that HTT knockdown led to reduced expression of ASCL2, GBX1 (Figure 7 D-E) and DLX3 (Figure 10), which all 3 regulate developmental transcription. ASCL2 is a pro-neural factor involved in the determination of neuronal precursors of the nervous system and its transcription is regulated via histone modifications during neural differentiation from hESCs[164]. The homebox protein DLX3 is thought to have a role in the modulating the development of the ventral forebrain[165]. GBX1 is highly expressed in the neuroectoderm and regulates the positioning of the midbrain- hindbrain boundary organizer in the early neural plate, affecting forebrain and midbrain formation[166]. Furthermore, we found reduced expression of SMC1B, a structural maintenance protein involved in chromosome movements (Figure 10). SMC1B is a meiosis-specific cohesin member also has an important role in cellular response to DNA damage. Loss of SMC1B results in impairment of gene expression[167]. Although mutations in SMC1B have been linked to cancer cell formation[167] and sterility in mice[168], there is currently no evidence for its contribution to polyQ diseases. However, these findings provide potential new targets to study transcriptional imbalances in HD. Taken together, our results indicate that HTT is a modulator of H3K9me3 and thereby controls the expression of important neural genes.

Neural cultures derived from HD patient-iPSCs exhibit H3K4me3 and H3K27ac epigenetic alterations, resulting in decreased levels of neurodevelopmental factors

involved in GABA signaling, axonal guidance and calcium influx[90]. Likewise, targeted mutations that expand the CAG stretch in one HTT allele is sufficient to impair H3K4me3 marks in both mouse ESCs and their NPC counterparts[67]. Brain tissues of HD patients exhibit increased H3K9 trimethylation[111–114] which led us to the hypothesis that this epigenetic mark could also be changed in HD-iPSCs. In our study, we indeed found that knockdown of ATF7IP in iPSCs derived from HD patients rescues the hypermethylation of H3K9, which suggests ATF7IP is a potent regulator of the epigenetic landscape. In our results obtained by immunofluorescence, we could observe increased H3K9me3 levels in two mutant HD-iPS cell lines, with either 71 or 180 polyQ repeat expansions (Figure 11 A). Interestingly, we also found that mutations (triplet expansion) in HTT reduces its interaction with ATF7IP and very likely induces H3K9me3 levels (Figure 11 B). As mentioned before, the benefit of using HD-iPSC lines is that each cell expresses one mutant copy of HTT and one normal copy, as it is the case in HD-patients[153]. This enabled us to observe the different mechanisms resulting from interaction of ATF7IP with either the wild-type or mHTT within the same model.

Interestingly, as opposed to the HTT antibody, the polyQ antibody did not immunoprecipitate ATF7IP and SETDB1. This clearly demonstrates that normal HTT function is necessary to promote interaction with ATF7IP and SETDB1 and thereby regulate trimethylation of H3K9. The underlying reason for this could be manifold: One explanation could be that polyQ regions of different lengths can present different conformations[58] and therefore it is likely that the specific epitopes recognizing ATF7IP and SETDB1 are not accessible in mHTT. Furthermore, we already know that mHTT is cleaved by proteases and that its C-terminal part is released into the nucleus, and also that HTT forms inclusion bodies upon which the C-terminal domain changes its conformation. This shows the possibility that interaction between ATF7IP and SETDB1 and HTT takes place on this site, whereas the polyQ antibody binds to the C-terminal domain, occluding the two interactors seen with anti-total HTT. However, this does not contradict our observation that loss of normal HTT supports the interaction between ATF7IP and SETDB1 to increase H3K9me3. Notably, we found that another H3K9 methyltransferase, called SUV39H1, which is known to form a complex with SETDB1, was significantly increased upon loss of HTT in hESCs.

In this study we also demonstrate that ATF7IP knockdown decreases H3K9 trimethylation in HD-IPSCs (Figure 12 B-C and Figure 13) and in HD-NPCs (Figure 12 A). Our data show that ATF7IP knockdown can rescue the H3K9 trimethylation HD-iPSCs. Notably, knockdown of ATF7IP does not influence the neuronal differentiation capacity in these cells. In this study, we did not analyze the effect of HTT on histone acetylation, a major regulator of the epigenetic landscape. Histone acetylation is associated with a relaxed chromatin conformation, which allows access of transcription factors and is regulated by the histone (or lysine) acetyltransferase (KAT) and the histone deacetylase family (HDAC). The CREB-binding protein (CBP) with KAT activity was found in intracellular inclusions in postmortem tissues from HD patients, animal model brains and in vitro and presented the first known histone acetylation dysregulation related to HD[169,170]. Since this initial finding many studies proved dysfunctional histone acetylation in various HD models including neuronal cells from HD Patients[171]. Surprisingly, some studies showed a global decrease in histone acetylation[172,173], while others presented hypoacetylation merely on promoter regions leading to transcriptional downregulation[174,175]. However, despite of more than a decade of research, the exact mechanism of how CBP and histone acetylation contribute to neurodegeneration is unknown[176].

It should be noted that we found 102 significant interactors of HTT in neurons and only 7 proteins in hESCs (Figure 1 C, E and Table 8). Among the 7 interactors NUP205 and U2AF2 were exclusively co-immunoprecipitated in hESCs whereas the other 5 proteins were also detected in neurons (Figure 1 F). NUP205 is involved in nuclear transport[177], whereas U2AF2 is a spliceosome-associated protein controlling RNA polymerase activity[178]. Since these two interactors are located in the nucleus, this indicates that in hESCs the role of HTT is related to nuclear mechanisms and suggests further modes of regulation of HTT on the phenotype in hESCs.

4.2 UBE2K

We performed a neural induction experiment in control and UBE2K knockdown hESCs and found that UBE2K knockdown disables the ability of the cells to differentiate into NPCs with intact neurogenic properties. The dramatic effect started after 20 days of neural induction. In contrast to the control cells, UBE2K KD NPCs showed high levels of

the early neural marker PAX6 and decreased levels of neural and neuronal markers (Figure 16 D-G). Moreover, when differentiated to neurons, UBE2K KD cells did not show neuronal extensions (Figure 16 H). The neuronal markers (MAP2, NEFL) were decreased compared to control neurons and PAX6 levels remained high (Figure 16 H-K).
Co-immunoprecipitation experiments followed by a single shot label-free proteomic approach revealed UBE2K, mitochondrial fission factor (MFF) and the histone H3.3 as most enriched proteins (Table 11). H3.3 is involved in cell differentiation and cell reprogramming[158,159], which suggests a role of UBE2K in the nucleus. In line with this assumption, we found tremendous amounts of UBE2K in nuclear fractions of hESCs (Figure 17 A). Strikingly, upon UBE2K knockdown, we observed also increased H3K9 trimethylation. This effect was consistent in two independent hESC lines as well as iPSCs (Figure 17 B-C). Also, upon differentiation into NPCs, high levels of H3K9me3 were maintained in the UBE2K knockdown cells (Figure 17 D). This indicates that UBE2K regulates the levels of H3K9me3 in hESCs and their neural counterparts, and that loss of UBE2K leads to transcriptional repression of distinct genes. Particularly, the lack of MAP2, NEFL and other genes playing a role in the development and identity of NPCs and neurons (Figure 16 H-K), can be associated with the observed histone modifications. After performing ChIP-seq using UBE2K KD hESCs we found 71 genes presenting H3K9me3 marks with strongest enrichment for genes involved in transcriptional regulation (Figure 18).

Remarkably, many genes with high enrichment for H3K9me3 marks were involved neuronal processes such as the formation of the nervous system, neuronal function and establishment of neuronal connections, supporting our results with disturbed differentiation into NPCs and neurons. These genes include ADRA2B, CELSR1, SMC1B, and the GABA receptor subunit GABRR1. In conclusion, our data indicate that loss of UBE2K induces changes in the H3K9me3 landscape of hESCs impairing the induction of key neuronal factors.

When we compared control hESCs with UBE2K KD hESCs via quantitative proteomics we found increased levels of the histone methyltransferase regulator JARID2 and also METTL7A, a methyltransferase of unknown function in UBE2K knockdown cells (Table 12). Jarid2 is required for differentiation of mouse ESCs and its inhibition leads to a reduction of H3K27me3 by regulating the PRC2 complex[108]. Furthermore, Jarid2

activates trimethylation of H3K9 via specific interaction with the histone H3K9 methyltransferase SETDB1 during heart development[179]. This suggests that further interplay of epigenetic and non-epigenetic mechanisms, is potentially modified by Ube2k. This requires further studies and is currently under investigation.

4.3 Conclusion and the missing link between HTT and UBE2K

In this study, we analyzed the effect of HTT and UBE2K knockdown on the epigenetic landscape of hESCs and HD-patient derived IPSCs. Consistent with previous studies, we discovered a strong modulation of the epigenetic landscape in these cells upon knockdown of both HTT and UBE2K. Particularly, promoter sites showed increased methylation by H3K9me3, representing transcriptional repression of these genes.

For the first time, we identified ATF7IP as a novel interactor of HTT and found increased trimethylation of H3K9 induced upon loss of HTT in hESCs and HD-IPSCs and their neuronally differentiated counterparts. Markedly, the genes most affected were involved in neuronal functions, particularly important for the correct differentiation into NPCs and neurons.

Moreover, the H3K9 methyltransferase SETDB1, a known interactor of ATF7IP, was decreased upon ATF7IP knockdown in hESCs. This indicates that ATF7IP is indeed a modulator of the chromatin landscape in hESCs and HD-IPSCs and thereby maintains proper transcriptional induction of genes. Since loss of HTT promotes the interaction of ATF7IP with SETDB1, HTT very likely regulates the interaction of SETDB1 with its activator ATF7IP to control trimethylation of H3K9.

Among the transcriptional regulators that we identified via ChIP-seq in UBE2K KD cells, we found the bHLH transcription cofactor HES6. As mentioned in the results, HES6 facilitates the transcription factor ASCL1 to induce the expression of important genes for neurogenesis at the early stages of development[160]. Remarkably, we found ASCL1 not only exhibiting enriched H3K9me3 marks on its promoter in HTT KD cells, but could also verify its decreased expression in NPCs on mRNA level.

Although previously found and confirmed as HTT interactor, we were not able to copurify UBE2K together with HTT: This could suggest that the interaction could be transient and could be associated with direct degradation of the HTT protein by UBE2K and associated E3 ligases. Also, it might play a role only in specific cell types, organelles or settings of hESCs. A study showed for example that the polyQ domain of normal HTT can present different conformations depending on its subcellular location[58].

The phenotype of UBE2K knockdown of neural differentiation is much more prominent as compared to HTT, and could be mediated by an increase of the histone methyltransferase regulator JARID2, which in turn regulates PRC2 in mice ESCs and promotes H3K9 trimethylation via interaction with methyltransferase SETDB1. As mentioned before, HTT facilitates PRC2 to stimulate its methyltransferase activity. Therefore, UBE2K and HTT are responsible for balancing epigenetic function and determining hESC fate, and PRC2 could be a common node between the two proteins that requires further investigation. These studies are currently underway. Interference with these mechanisms and the further characterization in models of disease may help to find novel therapies for human neurodegenerative diseases.

References

1. Vonsattel, J. P. G. & Difiglia, M. Huntington Disease. *J. Neuropathol. Exp. Neurol.* **57,** 369–384 (1998).
2. Roos, R. A. Huntington's disease: a clinical review. *Orphanet J. Rare Dis.* **5,** 40 (2010).
3. Walker, F. O. Huntington's disease. *Lancet Lond. Engl.* **369,** 218–228 (2007).
4. MacDonald, M. E. *et al.* A novel gene containing a trinucleotide repeat that is expanded and unstable on Huntington's disease chromosomes. *Cell* **72,** 971–983 (1993).
5. Cattaneo, E., Zuccato, C. & Tartari, M. Normal huntingtin function: an alternative approach to Huntington's disease. *Nat. Rev. Neurosci.* **6,** 919–930 (2005).
6. Saudou, F. & Humbert, S. The Biology of Huntingtin. *Neuron* **89,** 910–26 (2016).
7. Vonsattel, J. P. G., Keller, C. & Pilar Amaya, M. del. Neuropathology of Huntington's Disease. **89,** 599–618 (2008).
8. Ikeda, H. *et al.* Expanded polyglutamine in the Machado–Joseph disease protein induces cell death in vitro and in vivo. *Nat. Genet.* **13,** 196–202 (1996).
9. Finkbeiner, S. Huntington's Disease. *Cold Spring Harb Perspect Biol* **3,** (2011).
10. Ehrlich, M. E. *et al.* ST14A cells have properties of a medium-size spiny neuron. *Exp. Neurol.* **167,** 215–226 (2001).
11. Dragatsis, I., Levine, M. S. & Zeitlin, S. Inactivation of Hdh in the brain and testis results in progressive neurodegeneration and sterility in mice. *Nat. Genet.* **26,** 300–306 (2000).
12. Gauthier, L. R. *et al.* Huntingtin Controls Neurotrophic Support and Survival of Neurons by Enhancing BDNF Vesicular Transport along Microtubules. *Cell* **118,** 127–138 (2004).
13. Gunawardena, S. *et al.* Disruption of axonal transport by loss of huntingtin or expression of pathogenic polyQ proteins in Drosophila. *Neuron* **40,** 25–40 (2003).
14. O'Kusky, J. R., Nasir, J., Cicchetti, F., Parent, A. & Hayden, M. R. Neuronal degeneration in the basal ganglia and loss of pallido-subthalamic synapses in mice with targeted disruption of the Huntington's disease gene. *Brain Res.* **818,** 468–479 (1999).
15. Trushina, E. *et al.* Mutant huntingtin impairs axonal trafficking in mammalian neurons in vivo and in vitro. *Mol. Cell. Biol.* **24,** 8195–8209 (2004).
16. Ho, L. W., Brown, R., Maxwell, M., Wyttenbach, A. & Rubinsztein, D. C. Wild type Huntingtin reduces the cellular toxicity of mutant Huntingtin in mammalian cell models of Huntington's disease. *J. Med. Genet.* **38,** 450–452 (2001).
17. Leavitt, B. R. *et al.* Wild-type huntingtin reduces the cellular toxicity of mutant huntingtin in vivo. *Am. J. Hum. Genet.* **68,** 313–324 (2001).
18. Leavitt, B. R. *et al.* Wild-type huntingtin protects neurons from excitotoxicity. *J. Neurochem.* **96,** 1121–1129 (2006).
19. Rigamonti, D. *et al.* Wild-type huntingtin protects from apoptosis upstream of caspase-3. *J. Neurosci. Off. J. Soc. Neurosci.* **20,** 3705–3713 (2000).
20. Sun, Y., Savanenin, A., Reddy, P. H. & Liu, Y. F. Polyglutamine-expanded huntingtin promotes sensitization of N-methyl-D-aspartate receptors via post-synaptic density 95. *J. Biol. Chem.* **276,** 24713–24718 (2001).
21. Zuccato, C. *et al.* Loss of huntingtin-mediated BDNF gene transcription in Huntington's disease. *Science* **293,** 493–498 (2001).
22. Zuccato, C. *et al.* Huntingtin interacts with REST/NRSF to modulate the transcription of NRSE-controlled neuronal genes. *Nat. Genet.* **35,** 76–83 (2003).
23. Everett, C. M. & Wood, N. W. Trinucleotide repeats and neurodegenerative disease. *Brain* **127,** 2385–2405 (2004).

24. Perutz, M. F., Johnson, T., Suzuki, M. & Finch, J. T. Glutamine Repeats as Polar Zippers: Their Possible Role in Inherited Neurodegenerative Diseases. *Proc. Natl. Acad. Sci. U. S. A.* **91,** 5355–5358 (1994).
25. Steffan, J. S. *et al.* SUMO Modification of Huntingtin and Huntington's Disease Pathology. *Science* **304,** 100–104 (2004).
26. Neuwald, A. F. & Hirano, T. HEAT Repeats Associated with Condensins, Cohesins, and Other Complexes Involved in Chromosome-Related Functions. *Genome Res.* **10,** 1445–1452 (2000).
27. Andrade, M. A. & Bork, P. HEAT repeats in the Huntington's disease protein. *Nat. Genet.* **11,** 115–116 (1995).
28. MacDonald, M. E. Huntingtin: alive and well and working in middle management. *Sci. STKE Signal Transduct. Knowl. Environ.* **2003,** pe48–pe48 (2003).
29. Xia, J., Lee, D. H., Taylor, J., Vandelft, M. & Truant, R. Huntingtin contains a highly conserved nuclear export signal. *Hum. Mol. Genet.* **12,** 1393–1403 (2003).
30. Cornett, J. *et al.* Polyglutamine expansion of huntingtin impairs its nuclear export. *Nat. Genet.* **37,** 198–204 (2005).
31. Goldberg, Y. P. *et al.* Cleavage of huntingtin by apopain, a proapoptotic cysteine protease, is modulated by the polyglutamine tract. *Nat. Genet.* **13,** 442–449 (1996).
32. Wellington, C. L. *et al.* Caspase cleavage of gene products associated with triplet expansion disorders generates truncated fragments containing the polyglutamine tract. *J. Biol. Chem.* **273,** 9158–9167 (1998).
33. Wellington, C. L. *et al.* Inhibiting caspase cleavage of huntingtin reduces toxicity and aggregate formation in neuronal and nonneuronal cells. *J. Biol. Chem.* **275,** 19831–19838 (2000).
34. Davies, S. W. *et al.* Formation of neuronal intranuclear inclusions underlies the neurological dysfunction in mice transgenic for the HD mutation. *Cell* **90,** 537–548 (1997).
35. DiFiglia, M. *et al.* Aggregation of huntingtin in neuronal intranuclear inclusions and dystrophic neurites in brain. *Science* **277,** 1990–1993 (1997).
36. Kim, Y. J. *et al.* Caspase 3-cleaved N-terminal fragments of wild-type and mutant huntingtin are present in normal and Huntington's disease brains, associate with membranes, and undergo calpain-dependent proteolysis. *Proc. Natl. Acad. Sci. U. S. A.* **98,** 12784–12789 (2001).
37. Lunkes, A. *et al.* Proteases acting on mutant huntingtin generate cleaved products that differentially build up cytoplasmic and nuclear inclusions. *Mol. Cell* **10,** 259–269 (2002).
38. Wellington, C. L. *et al.* Caspase cleavage of mutant huntingtin precedes neurodegeneration in Huntington's disease. *J. Neurosci. Off. J. Soc. Neurosci.* **22,** 7862–7872 (2002).
39. Gafni, J. *et al.* Inhibition of calpain cleavage of huntingtin reduces toxicity: accumulation of calpain/caspase fragments in the nucleus. *J. Biol. Chem.* **279,** 20211–20220 (2004).
40. Gafni, J. & Ellerby, L. M. Calpain Activation in Huntington's Disease. *J. Neurosci.* **22,** 4842–4849 (2002).
41. Wang, K. K. Calpain and caspase: can you tell the difference? *Trends Neurosci.* **23,** 20–26 (2000).
42. Sepers, M. & Raymond, L. Mechanisms of synaptic dysfunction and excitotoxicity in Huntington's disease. *Drug Discov. Today* **19,** 990–996 (2014).
43. Ellis, H. M. & Horvitz, H. R. Genetic control of programmed cell death in the nematode C. elegans. *Cell* **44,** 817–829 (1986).

44. Ona, V. O. *et al.* Inhibition of caspase-1 slows disease progression in a mouse model of Huntington's disease. *Nature* **399,** 263–267 (1999).
45. Kalchman, M. A. *et al.* Huntingtin is ubiquitinated and interacts with a specific ubiquitin-conjugating enzyme. *J. Biol. Chem.* **271,** 19385–19394 (1996).
46. Hackam, A. S. *et al.* Huntingtin interacting protein 1 induces apoptosis via a novel caspase-dependent death effector domain. *J. Biol. Chem.* **275,** 41299–41308 (2000).
47. Humbert, S. *et al.* The IGF-1/Akt pathway is neuroprotective in Huntington's disease and involves Huntingtin phosphorylation by Akt. *Dev. Cell* **2,** 831–837 (2002).
48. Warby, S. C. *et al.* Huntingtin phosphorylation on serine 421 is significantly reduced in the striatum and by polyglutamine expansion in vivo. *Hum. Mol. Genet.* **14,** 1569–1577 (2005).
49. Luo, S., Vacher, C., Davies, J. E. & Rubinsztein, D. C. Cdk5 phosphorylation of huntingtin reduces its cleavage by caspases: implications for mutant huntingtin toxicity. *J. Cell Biol.* **169,** 647–656 (2005).
50. Huang, K. *et al.* Huntingtin-interacting protein HIP14 is a palmitoyl transferase involved in palmitoylation and trafficking of multiple neuronal proteins. *Neuron* **44,** 977–986 (2004).
51. Difiglia, M. *et al.* Huntingtin Is a Cytoplasmic Protein Associated with Vesicles in Human and Rat-Brain Neurons. *Neuron* **14,** 1075–1081 (1995).
52. Harjes, P. & Wanker, E. E. The hunt for huntingtin function: interaction partners tell many different stories. *Trends Biochem. Sci.* **28,** 425–433 (2003).
53. Li, S.-H. & Li, X.-J. Huntingtin-protein interactions and the pathogenesis of Huntington's disease. *Trends Genet. TIG* **20,** 146–154 (2004).
54. Sipione, S. & Cattaneo, E. Modeling Huntington's disease in cells, flies, and mice. *Mol. Neurobiol.* **23,** 21–51 (2001).
55. Goehler, H. *et al.* A protein interaction network links GIT1, an enhancer of huntingtin aggregation, to Huntington's disease. *Mol. Cell* **15,** 853–865 (2004).
56. Marcora, E., Gowan, K. & Lee, J. E. Stimulation of NeuroD activity by huntingtin and huntingtin-associated proteins HAP1 and MLK2. *Proc. Natl. Acad. Sci. U. S. A.* **100,** 9578–9583 (2003).
57. Trettel, F. *et al.* Dominant phenotypes produced by the HD mutation in STHdh(Q111) striatal cells. *Hum. Mol. Genet.* **9,** 2799–2809 (2000).
58. Ko, J., Ou, S. & Patterson, P. H. New anti-huntingtin monoclonal antibodies: implications for huntingtin conformation and its binding proteins. *Brain Res. Bull.* **56,** 319–329 (2001).
59. Trottier, Y. *et al.* Polyglutamine expansion as a pathological epitope in Huntington's disease and four dominant cerebellar ataxias. *Nature* **378,** 403–406 (1995).
60. Ferrante, R. J. *et al.* Heterogeneous topographic and cellular distribution of huntingtin expression in the normal human neostriatum. *J. Neurosci. Off. J. Soc. Neurosci.* **17,** 3052–3063 (1997).
61. Fusco, F. R. *et al.* Cellular localization of huntingtin in striatal and cortical neurons in rats: lack of correlation with neuronal vulnerability in Huntington's disease. *J. Neurosci. Off. J. Soc. Neurosci.* **19,** 1189–1202 (1999).
62. Velier, J. *et al.* Wild-Type and Mutant Huntingtins Function in Vesicle Trafficking in the Secretory and Endocytic Pathways. *Exp. Neurol.* **152,** 34–40 (1998).
63. Hilditch-Maguire, P. *et al.* Huntingtin: an iron-regulated protein essential for normal nuclear and perinuclear organelles. *Hum. Mol. Genet.* **9,** 2789–2797 (2000).
64. Hoffner, G., Kahlem, P. & Djian, P. Perinuclear localization of huntingtin as a consequence of its binding to microtubules through an interaction with β-tubulin:

relevance to Huntington's disease. *J. Cell Sci.* **115,** 941–948 (2002).
65. Kegel, K. B. *et al.* Huntingtin is present in the nucleus, interacts with the transcriptional corepressor C-terminal binding protein, and represses transcription. *J. Biol. Chem.* **277,** 7466–7476 (2002).
66. Li, J.-Y., Plomann, M. & Brundin, P. Huntington's disease: a synaptopathy? *Trends Mol. Med.* **9,** 414–420 (2003).
67. Biagioli, M. *et al.* Htt CAG repeat expansion confers pleiotropic gains of mutant huntingtin function in chromatin regulation. *Hum Mol Genet* **24,** 2442–57 (2015).
68. Duyao, M. P. *et al.* Inactivation of the mouse Huntington's disease gene homolog Hdh. *Science* **269,** 407–410 (1995).
69. Nasir, J. *et al.* Targeted disruption of the Huntington's disease gene results in embryonic lethality and behavioral and morphological changes in heterozygotes. *Cell* **81,** 811–823 (1995).
70. Zeitlin, S., Liu, J. P., Chapman, D. L., Papaioannou, V. E. & Efstratiadis, A. Increased apoptosis and early embryonic lethality in mice nullizygous for the Huntington's disease gene homologue. *Nat. Genet.* **11,** 155–163 (1995).
71. White, J. K. *et al.* Huntingtin is required for neurogenesis and is not impaired by the Huntington's disease CAG expansion. *Nat. Genet.* **17,** 404–410 (1997).
72. Godin, J. D. *et al.* Huntingtin Is Required for Mitotic Spindle Orientation and Mammalian Neurogenesis. *Neuron* **67,** 392–406 (2010).
73. Conforti, P. *et al.* Lack of huntingtin promotes neural stem cells differentiation into glial cells while neurons expressing huntingtin with expanded polyglutamine tracts undergo cell death. *Neurobiol Dis* **50,** 160–70 (2013).
74. Nguyen, G. D., Gokhan, S., Molero, A. E. & Mehler, M. F. Selective roles of normal and mutant huntingtin in neural induction and early neurogenesis. *PloS One* **8,** e64368 (2013).
75. Myers, R. H. *et al.* Homozygote for Huntington disease. *Am. J. Hum. Genet.* **45,** 615–618 (1989).
76. Wexler, N. S. *et al.* Homozygotes for Huntington's disease. *Nature* **326,** 194–197 (1987).
77. Batista, C. M. C. *et al.* A progressive and cell non-autonomous increase in striatal neural stem cells in the Huntington's disease R6/2 mouse. *J. Neurosci. Off. J. Soc. Neurosci.* **26,** 10452–10460 (2006).
78. Curtis, M. A. *et al.* Increased cell proliferation and neurogenesis in the adult human Huntington's disease brain. *Proc. Natl. Acad. Sci. U. S. A.* **100,** 9023–9027 (2003).
79. Curtis, M. A. *et al.* The distribution of progenitor cells in the subependymal layer of the lateral ventricle in the normal and Huntington's disease human brain. *Neuroscience* **132,** 777–788 (2005).
80. Molero, A. E. *et al.* Impairment of developmental stem cell-mediated striatal neurogenesis and pluripotency genes in a knock-in model of Huntington's disease. *Proc. Natl. Acad. Sci. U. S. A.* **106,** 21900–21905 (2009).
81. Brandt, J., Shpritz, B., Codori, A. M., Margolis, R. & Rosenblatt, A. Neuropsychological manifestations of the genetic mutation for Huntington's disease in presymptomatic individuals. *J. Int. Neuropsychol. Soc. JINS* **8,** 918–924 (2002).
82. Joshi, P. R. *et al.* Age-dependent alterations of corticostriatal activity in the YAC128 mouse model of Huntington disease. *J. Neurosci. Off. J. Soc. Neurosci.* **29,** 2414–2427 (2009).
83. Milnerwood, A. J. & Raymond, L. A. Early synaptic pathophysiology in neurodegeneration: insights from Huntington's disease. *Trends Neurosci.* **33,** 513–523 (2010).

84. Murphy, K. P. *et al.* Abnormal synaptic plasticity and impaired spatial cognition in mice transgenic for exon 1 of the human Huntington's disease mutation. *J. Neurosci. Off. J. Soc. Neurosci.* **20,** 5115–5123 (2000).
85. Paulsen, J. S. *et al.* Detection of Huntington's disease decades before diagnosis: the Predict-HD study. *J. Neurol. Neurosurg. Psychiatry* **79,** 874–880 (2008).
86. Paulsen, J. S. *et al.* Brain structure in preclinical Huntington's disease. *Biol. Psychiatry* **59,** 57–63 (2006).
87. Schippling, S. *et al.* Abnormal motor cortex excitability in preclinical and very early Huntington's disease. *Biol. Psychiatry* **65,** 959–965 (2009).
88. Zhang Yu *et al.* Depletion of wild‐type huntingtin in mouse models of neurologic diseases. *J. Neurochem.* **87,** 101–106 (2003).
89. Rigamonti, D. *et al.* Huntingtin's neuroprotective activity occurs via inhibition of procaspase-9 processing. *J. Biol. Chem.* **276,** 14545–14548 (2001).
90. Consortium, H. D. iPSC. Induced pluripotent stem cells from patients with Huntington's disease show CAG-repeat-expansion-associated phenotypes. *Cell Stem Cell* **11,** 264–78 (2012).
91. Evans, M. J. & Kaufman, M. H. Establishment in culture of pluripotential cells from mouse embryos. *Nature* **292,** 154–156 (1981).
92. Thomson, J. A. *et al.* Embryonic stem cell lines derived from human blastocysts. *Science* **282,** 1145–1147 (1998).
93. Hershko, A. & Ciechanover, A. The ubiquitin system. *Annu. Rev. Biochem.* **67,** 425–479 (1998).
94. Hochstrasser, M. Ubiquitin-dependent protein degradation. *Annu. Rev. Genet.* **30,** 405–439 (1996).
95. Okita, Y. & Nakayama, K. I. UPS delivers pluripotency. *Cell Stem Cell* **11,** 728–30 (2012).
96. Goldberg, A. L. Functions of the proteasome: the lysis at the end of the tunnel. *Science* **268,** 522–523 (1995).
97. David, Y., Ziv, T., Admon, A. & Navon, A. The E2 Ubiquitin-conjugating Enzymes Direct Polyubiquitination to Preferred Lysines. *J. Biol. Chem.* **285,** 8595–8604 (2010).
98. Young, R. A. Control of the Embryonic Stem Cell State. *Cell* **144,** 940–954 (2011).
99. Hu, X.-L., Wang, Y. & Shen, Q. Epigenetic control on cell fate choice in neural stem cells. *Protein Cell* **3,** 278–290 (2012).
100. Watanabe, A., Yamada, Y. & Yamanaka, S. Epigenetic regulation in pluripotent stem cells: a key to breaking the epigenetic barrier. *Philos. Trans. R. Soc. Lond. B. Biol. Sci.* **368,** 20120292 (2013).
101. Meshorer, E. *et al.* Hyperdynamic plasticity of chromatin proteins in pluripotent embryonic stem cells. *Dev. Cell* **10,** 105–116 (2006).
102. Loh, Y.-H. *et al.* Genomic approaches to deconstruct pluripotency. *Annu. Rev. Genomics Hum. Genet.* **12,** 165–185 (2011).
103. Bibikova, M. *et al.* Human embryonic stem cells have a unique epigenetic signature. *Genome Res.* **16,** 1075–1083 (2006).
104. Gan, Q., Yoshida, T., McDonald, O. G. & Owens, G. K. Concise review: epigenetic mechanisms contribute to pluripotency and cell lineage determination of embryonic stem cells. *Stem Cells Dayt. Ohio* **25,** 2–9 (2007).
105. Bernstein, B. E. *et al.* A bivalent chromatin structure marks key developmental genes in embryonic stem cells. *Cell* **125,** 315–326 (2006).
106. Hawkins, R. D. *et al.* Distinct epigenomic landscapes of pluripotent and lineage-committed human cells. *Cell Stem Cell* **6,** 479–491 (2010).
107. Meshorer, E. & Misteli, T. Chromatin in pluripotent embryonic stem cells and

differentiation. *Nat. Rev. Mol. Cell Biol.* **7,** 540–546 (2006).
108. Pasini, D. *et al.* JARID2 regulates binding of the Polycomb repressive complex 2 to target genes in ES cells. *Nature* **464,** 306–310 (2010).
109. Valor, L. M. Transcription, epigenetics and ameliorative strategies in Huntington's Disease: a genome-wide perspective. *Mol. Neurobiol.* **51,** 406–423 (2015).
110. Glajch, K. E. & Sadri-Vakili, G. Epigenetic Mechanisms Involved in Huntington's Disease Pathogenesis. *J. Huntingt. Dis.* **4,** 1–15 (2015).
111. Ferrante, R. J. *et al.* Chemotherapy for the Brain: The Antitumor Antibiotic Mithramycin Prolongs Survival in a Mouse Model of Huntington's Disease. *J. Neurosci. Off. J. Soc. Neurosci.* **24,** 10335–10342 (2004).
112. Gardian, G. *et al.* Neuroprotective Effects of Phenylbutyrate in the N171-82Q Transgenic Mouse Model of Huntington's Disease. *J. Biol. Chem.* **280,** 556–563 (2005).
113. Ryu, H. *et al.* ESET/SETDB1 gene expression and histone H3 (K9) trimethylation in Huntington's disease. *Proc. Natl. Acad. Sci. U. S. A.* **103,** 19176–19181 (2006).
114. Stack, E. C. *et al.* Modulation of nucleosome dynamics in Huntington's disease. *Hum. Mol. Genet.* **16,** 1164–1175 (2007).
115. Becker, J. S., Nicetto, D. & Zaret, K. S. H3K9me3-Dependent Heterochromatin: Barrier to Cell Fate Changes. *Trends Genet. TIG* **32,** 29–41 (2016).
116. Fujita, N. *et al.* MCAF mediates MBD1-dependent transcriptional repression. *Mol. Cell. Biol.* **23,** 2834–2843 (2003).
117. Ichimura, T. *et al.* Transcriptional Repression and Heterochromatin Formation by MBD1 and MCAF/AM Family Proteins. *J. Biol. Chem.* **280,** 13928–13935 (2005).
118. Liu, L. *et al.* MCAF1/AM is involved in Sp1-mediated maintenance of cancer-associated telomerase activity. *J. Biol. Chem.* **284,** 5165–5174 (2009).
119. Sasai, N., Saitoh, N., Saitoh, H. & Nakao, M. The Transcriptional Cofactor MCAF1/ATF7IP Is Involved in Histone Gene Expression and Cellular Senescence. *PLOS ONE* **8,** e68478 (2013).
120. Li, W., Tu, D., Brunger, A. T. & Ye, Y. A ubiquitin ligase transfers preformed polyubiquitin chains from a conjugating enzyme to a substrate. *Nature* **446,** 333–337 (2007).
121. Bae, Y., Choi, D., Rhim, H. & Kang, S. Hip2 interacts with cyclin B1 and promotes its degradation through the ubiquitin proteasome pathway. *FEBS Lett.* **584,** 4505–4510 (2010).
122. Tanno, Y. *et al.* Localization of huntingtin-interacting protein-2 (Hip-2) mRNA in the developing mouse brain. *J. Chem. Neuroanat.* **17,** 99–107 (1999).
123. Christensen, D. E., Brzovic, P. S. & Klevit, R. E. E2–BRCA1 RING interactions dictate synthesis of mono- or specific polyubiquitin chain linkages. *Nat. Struct. Mol. Biol.* **14,** 941–948 (2007).
124. Song, S. *et al.* Essential Role of E2-25K/Hip-2 in Mediating Amyloid-β Neurotoxicity. *Mol. Cell* **12,** 553–563 (2003).
125. Howard, R. A. *et al.* Ubiquitin conjugating enzymes participate in polyglutamine protein aggregation. *BMC Cell Biol.* **8,** 32 (2007).
126. de Pril, R., Fischer, D. F., Roos, R. A. C. & van Leeuwen, F. W. Ubiquitin-conjugating enzyme E2-25K increases aggregate formation and cell death in polyglutamine diseases. *Mol. Cell. Neurosci.* **34,** 10–19 (2007).
127. Kikuchi, J. *et al.* Induction of ubiquitin-conjugating enzyme by aggregated low density lipoprotein in human macrophages and its implications for atherosclerosis. *Arterioscler. Thromb. Vasc. Biol.* **20,** 128–134 (2000).
128. Park, I.-H. *et al.* Reprogramming of human somatic cells to pluripotency with defined factors. *Nature* **451,** 141–146 (2008).

129. Park, I.-H. *et al.* Disease-specific induced pluripotent stem cells. *Cell* **134,** 877–886 (2008).
130. Chambers, S. M. *et al.* Highly efficient neural conversion of human ES and iPS cells by dual inhibition of SMAD signaling. *Nat. Biotechnol.* **27,** 275–280 (2009).
131. Rappsilber, J., Ishihama, Y. & Mann, M. Stop and go extraction tips for matrix-assisted laser desorption/ionization, nanoelectrospray, and LC/MS sample pretreatment in proteomics. *Anal. Chem.* **75,** 663–670 (2003).
132. Cox, J. *et al.* Accurate proteome-wide label-free quantification by delayed normalization and maximal peptide ratio extraction, termed MaxLFQ. *Mol. Cell. Proteomics MCP* **13,** 2513–2526 (2014).
133. Cox, J. & Mann, M. 1D and 2D annotation enrichment: a statistical method integrating quantitative proteomics with complementary high-throughput data. *BMC Bioinformatics* **13,** S12 (2012).
134. Dobin, A. *et al.* STAR: ultrafast universal RNA-seq aligner. *Bioinforma. Oxf. Engl.* **29,** 15–21 (2013).
135. Trapnell, C. *et al.* Differential gene and transcript expression analysis of RNA-seq experiments with TopHat and Cufflinks. *Nat. Protoc.* **7,** 562–578 (2012).
136. Li, H. *et al.* The Sequence Alignment/Map format and SAMtools. *Bioinforma. Oxf. Engl.* **25,** 2078–2079 (2009).
137. Feng, J., Liu, T., Qin, B., Zhang, Y. & Liu, X. S. Identifying ChIP-seq enrichment using MACS. *Nat. Protoc.* **7,** 1728–1740 (2012).
138. Machanick, P. & Bailey, T. L. MEME-ChIP: motif analysis of large DNA datasets. *Bioinforma. Oxf. Engl.* **27,** 1696–1697 (2011).
139. Peters, M. F. & Ross, C. A. Isolation of a 40-kDa Huntingtin-associated Protein. *J. Biol. Chem.* **276,** 3188–3194 (2001).
140. Fujita, K. *et al.* A functional deficiency of TERA/VCP/p97 contributes to impaired DNA repair in multiple polyglutamine diseases. *Nat. Commun.* **4,** 1816 (2013).
141. Wang, H. *et al.* mAM Facilitates Conversion by ESET of Dimethyl to Trimethyl Lysine 9 of Histone H3 to Cause Transcriptional Repression. *Mol. Cell* **12,** 475–487 (2003).
142. Ichimura, T. *et al.* Transcriptional Repression and Heterochromatin Formation by MBD1 and MCAF/AM Family Proteins. *J. Biol. Chem.* **280,** 13928–13935 (2005).
143. Minkovsky, A. *et al.* The Mbd1-Atf7ip-Setdb1 pathway contributes to the maintenance of X chromosome inactivation. *Epigenetics Chromatin* **7,** 12 (2014).
144. Timms, R. T., Tchasovnikarova, I. A., Antrobus, R., Dougan, G. & Lehner, P. J. ATF7IP-Mediated Stabilization of the Histone Methyltransferase SETDB1 Is Essential for Heterochromatin Formation by the HUSH Complex. *Cell Rep.* **17,** 653–659 (2016).
145. Patrick Callaerts, Georg Halder & Gehring, and W. J. Pax-6 in Development and Evolution. *Annu. Rev. Neurosci.* **20,** 483–532 (1997).
146. Peters, A. H. F. M. *et al.* Partitioning and Plasticity of Repressive Histone Methylation States in Mammalian Chromatin. *Mol. Cell* **12,** 1577–1589 (2003).
147. Rea, S. *et al.* Regulation of chromatin structure by site-specific histone H3 methyltransferases. *Nature* **406,** 593–599 (2000).
148. Fritsch, L. *et al.* A subset of the histone H3 lysine 9 methyltransferases Suv39h1, G9a, GLP, and SETDB1 participate in a multimeric complex. *Mol. Cell* **37,** 46–56 (2010).
149. Bestman, J. E. & Cline, H. T. The RNA binding protein CPEB regulates dendrite morphogenesis and neuronal circuit assembly in vivo. *Proc. Natl. Acad. Sci. U. S. A.* **105,** 20494–20499 (2008).
150. Bezprozvanny, I. & Hayden, M. R. Deranged neuronal calcium signaling and Huntington disease. *Biochem. Biophys. Res. Commun.* **322,** 1310–1317 (2004).

151. Nair, A. G., Bhalla, U. S. & Hellgren Kotaleski, J. Role of DARPP-32 and ARPP-21 in the Emergence of Temporal Constraints on Striatal Calcium and Dopamine Integration. *PLoS Comput. Biol.* **12,** (2016).
152. Bardoni, R. *et al.* Delta Opioid Receptors Presynaptically Regulate Cutaneous Mechanosensory Neuron Input to the Spinal Cord Dorsal Horn. *Neuron* **81,** 1443 (2014).
153. Noormohammadi, A. *et al.* Mechanisms of protein homeostasis (proteostasis) maintain stem cell identity in mammalian pluripotent stem cells. *Cell. Mol. Life Sci.* **75,** 275–290 (2018).
154. The HD iPSC Consortium *et al.* Developmental alterations in Huntington's disease neural cells and pharmacological rescue in cells and mice. *Nat. Neurosci.* **20,** 648–660 (2017).
155. Araki, K. & Nagata, K. Protein Folding and Quality Control in the ER. *Cold Spring Harb. Perspect. Biol.* **3,** a007526 (2011).
156. Vilchez, D. *et al.* FOXO4 is necessary for neural differentiation of human embryonic stem cells. *Aging Cell* **12,** 518–522 (2013).
157. Vilchez, D. *et al.* Increased proteasome activity in human embryonic stem cells is regulated by PSMD11. *Nature* **489,** 304–8 (2012).
158. Harada, A. *et al.* Chd2 interacts with H3.3 to determine myogenic cell fate. *EMBO J.* **31,** 2994–3007 (2012).
159. Wen, D. *et al.* Histone variant H3.3 is an essential maternal factor for oocyte reprogramming. *Proc. Natl. Acad. Sci. U. S. A.* **111,** 7325–7330 (2014).
160. Bae, S., Bessho, Y., Hojo, M. & Kageyama, R. The bHLH gene Hes6, an inhibitor of Hes1, promotes neuronal differentiation. *Development* **127,** 2933–2943 (2000).
161. Rui, Y.-N. *et al.* Huntingtin functions as a scaffold for selective macroautophagy. *Nat. Cell Biol.* **17,** 262–275 (2015).
162. Valcárcel-Ocete, L. *et al.* Exploring Genetic Factors Involved in Huntington Disease Age of Onset: E2F2 as a New Potential Modifier Gene. *PLoS ONE* **10,** (2015).
163. Seong, I. S. *et al.* Huntingtin facilitates polycomb repressive complex 2. *Hum. Mol. Genet.* **19,** 573–583 (2010).
164. Ziller, M. J. *et al.* Dissecting neural differentiation regulatory networks through epigenetic footprinting. *Nature* **518,** 355–359 (2015).
165. Zhu, H. & Bendall, A. J. Dlx3 is expressed in the ventral forebrain of chicken embryos: implications for the evolution of the Dlx gene family. *Int. J. Dev. Biol.* **50,** 71–75 (2006).
166. Rhinn, M., Lun, K., Ahrendt, R., Geffarth, M. & Brand, M. Zebrafish gbx1 refines the Midbrain-Hindbrain Boundary border and mediates the Wnt8 posteriorization signal. *Neural Develop.* **4,** 12 (2009).
167. Mannini, L. *et al.* SMC1B is present in mammalian somatic cells and interacts with mitotic cohesin proteins. *Sci. Rep.* **5,** 18472 (2015).
168. Takabayashi, S., Yamauchi, Y., Tsume, M., Noguchi, M. & Katoh, H. A spontaneous smc1b mutation causes cohesin protein dysfunction and sterility in mice. *Exp. Biol. Med. Maywood NJ* **234,** 994–1001 (2009).
169. Kazantsev, A., Preisinger, E., Dranovsky, A., Goldgaber, D. & Housman, D. Insoluble detergent-resistant aggregates form between pathological and nonpathological lengths of polyglutamine in mammalian cells. *Proc. Natl. Acad. Sci.* **96,** 11404–11409 (1999).
170. Steffan, J. S. *et al.* Histone deacetylase inhibitors arrest polyglutamine-dependent neurodegeneration in *Drosophila*. *Nature* **413,** 739–743 (2001).
171. Yeh, H. H. *et al.* Histone deacetylase class II and acetylated core histone immunohistochemistry in human brains with Huntington's disease. *Brain Res.* **1504,** 16–24 (2013).

172. Lim, S. *et al.* D-β-Hydroxybutyrate Is Protective in Mouse Models of Huntington's Disease. *PLOS ONE* **6,** e24620 (2011).
173. Giralt, A. *et al.* Long-term memory deficits in Huntington's disease are associated with reduced CBP histone acetylase activity. *Hum. Mol. Genet.* **21,** 1203–1216 (2012).
174. McFarland, K. N. *et al.* Genome-Wide Histone Acetylation Is Altered in a Transgenic Mouse Model of Huntington's Disease. *PLOS ONE* **7,** e41423 (2012).
175. Valor, L. M., Guiretti, D., Lopez-Atalaya, J. P. & Barco, A. Genomic Landscape of Transcriptional and Epigenetic Dysregulation in Early Onset Polyglutamine Disease. *J. Neurosci.* **33,** 10471–10482 (2013).
176. Valor, L. M. & Guiretti, D. What's wrong with epigenetics in Huntington's disease? *Neuropharmacology* **80,** 103–14 (2014).
177. Galy, V., Mattaj, I. W. & Askjaer, P. Caenorhabditis elegans Nucleoporins Nup93 and Nup205 Determine the Limit of Nuclear Pore Complex Size Exclusion In Vivo. *Mol. Biol. Cell* **14,** 5104–5115 (2003).
178. Lin, C.-L. *et al.* RNA structure replaces the need for U2AF2 in splicing. *Genome Res.* **26,** 12–23 (2016).
179. Mysliwiec, M. R. *et al.* Jarid2 (Jumonji, AT Rich Interactive Domain 2) Regulates NOTCH1 Expression via Histone Modification in the Developing Heart. *J. Biol. Chem.* **287,** 1235–1241 (2012).

Erklärung

Ich versichere, dass ich die von mir vorgelegte Dissertation selbständig angefertigt, die benutzten Quellen und Hilfsmittel vollständig angegeben und die Stellen der Arbeit, einschließlich Tabellen, Karten und Abbildungen, die anderen Werken im Wortlaut oder dem Sinn nach entnommen sind, in jedem Einzelfall als Entlehnung kenntlich gemacht habe; dass diese Dissertation noch keiner anderen Fakultät oder Universität zur Prüfung vorgelegen hat; dass sie -abgesehen von unten angegebenen Teilpublikationen- noch nicht veröffentlicht worden ist sowie, dass ich eine solche Veröffentlichung vor Abschluss des Promotionsverfahrens nicht vornehmen werde.

Die Bestimmungen der Promotionsordnung sind mir bekannt. Die von mir vorgelegte Dissertation ist von Dr. David Vilchez betreut worden.

Köln, den 18.04.2018

(Dilber Irmak)